

Topological phase transitions, invariants and enriched bulk-edge correspondences in fermionic gapless systems with extended Fermi surface

Fadi Sun^{1,2} and Jinwu Ye^{1,2,3}

¹ *The School of Science, Great Bay University, Dongguan 523000, Guangdong, China*

² *Institute for Theoretical Sciences, Westlake University, Hangzhou 310024, Zhejiang, China*

³ *Department of Physics and Astronomy, Mississippi State University, MS 39762, USA*

(Dated: March 14, 2023)

Topological phases and topological phase transitions (TPT) are among the most fantastic phenomena in Nature. Here we show that injecting a current may lead to new topological phases, especially new gapless topological metallic phases with extended Fermi surfaces (FSs) through novel class of TPTs in the bulk or the boundary. Specifically, we study the quantum anomalous Hall (QAH) system in a square lattice under various forms of injecting currents. In addition to the previously known Chern insulator (which will be called even Chern insulator here), band insulator and band metal (BM), we find three new topological phases we name as: the gapped odd Chern insulator (Odd CI), the gapless odd Chern metal (Odd CM) and even Chern metal (Even CM). The Chern number may not be effective anymore in characterizing the topological gapless phases with extended FS. It is the Hall conductance which acts as the new topological invariant in such gapless systems. Its jump is a universal integer or non-integer across the even CM/BM or odd CM/BM TPT respectively where there is also a corresponding TPT in the Longitudinal (L-) edge modes. The Odd/even CM to BM transition is a novel class of TPT without any non-analyticity in the ground state energy density. This presents the first example of a TPT which is not a quantum phase transition (QPT). The original bulk-edge correspondence is enriched into bulk/Longitudinal (L-)/Transverse (T-) edge correspondence. The L- edge reconstruction may happen earlier, later or at the same time as the bulk TPT respectively in the even CI/odd CI/odd CM sequence with the edge dynamic exponent $z_L = 3$, in the even CI/even CM/odd CM sequence with $z_L = 2$ or a direct even CI/odd CM with a flat edge. The disappearance of the T- edge always happen at the same time as the bulk TPT with a universal edge critical behaviour. We classify all the possible bulk and edge TPTs and also evaluate the thermodynamic quantities such as the density of states, specific heat, compressibility and the Wilson ratio in all the phases and also their quantum scaling forms near all these TPTs. The methods may be applied to explore new topological phases of other Hamiltonians in any lattice in any dimension in any forms of injecting current. Doing various experiments by injecting different sorts of currents may become an effective way to drive various topological phases to new topological gapped or gapless metallic phases through novel bulk or edge TPTs.

I. INTRODUCTION

The Anomalous Hall Effect (AHE) due to the Berry phase of itinerant electrons in a quantum Ferromagnet in real space [1] or in momentum space [2, 3] has been under intense investigations since more than 20 years ago. It involves the spin-orbit coupling which couples the orbital motion of electrons to the spin polarization [4]. The AHE in a metallic Ferromagnet is in general, not quantized, so can take any value. However, it can be quantized in an insulator, called Quantum Anomalous Hall (QAH) effect. The original QAH was proposed [5] even earlier in a honeycomb lattice model soon after the discovery of integer and fractional quantum Hall effects (FQHE). Since the first experimental realization of the quantum anomalous Hall (QAH) effect in Cr doped $\text{Bi}(\text{Sb})_2\text{Te}_3$ thin films [8, 9], it has also been observed in many other materials such as both Cr doped and V doped $(\text{Bi},\text{Sb})_2\text{Te}_3$ films [10]. More recently, it was also discovered in the twisted bilayer graphene [11]. It was realized with cold atoms with the fermions ^{40}K in [12]. The bosonic version of QAH was also implemented with spinor bosons ^{87}Rb in [13]. The connections between the non-interacting fermionic QAH and the interacting bosonic version of

QAH and various quantum or topological phase transitions in interacting bosonic systems were explored in [28].

It turns out that the FQHE and QAH are just two early members of the vast number of topological quantum matter [14–17]. The topological quantum matter is one of the main themes in condensed matter physics, lattice gauge theories and topological quantum field theories [14–17]. It not only contain new physical concepts, rich and profound phenomena with deep mathematical structures, but may also have some potential industry applications such as dissipationless transmissions, quantum communications and topological quantum computing.

There have been flurries of classifications of both gapped and gapless topological phases [14–17]. In the known non-interacting gapless case, the gapless source comes from the Dirac fermions, Weyl fermions and various line/ring nodes in the bulk. We call this class of bulk gapless system with Fermi points or lines, linear dispersion $\omega \sim k$ and vanishing density of states (DOS) $D(\omega) \sim \omega$ as having the dynamic exponent $z = 1$. There are still little works on how to characterizing a bulk topological gapless system with extended Fermi surface (FS), neither much work on topological phase transitions (TPT) between various topological phases. Furthermore,

how to define topological invariants to characterize a bulk gapless system with extended FS and what are the associated edge modes remain outstanding problems. Because these extended FS originates from point-like Fermi points with quadratic band touching $\omega \sim k^2$ and constant DOS $D(\omega) \sim \text{const.}$ at a TPT, we call such class of gapless systems as having the bulk dynamic exponent $z = 2$ which are the main focus of the present work.

There are two complementary approaches to address these outstanding problems. One way is to use SPT or SET to classify by various mathematical tools such as Co-homology, K-theory (for non-interacting fermions), Co-bordisms and tensor categories or its higher order versions [16, 17]. Another is to start from a concrete parent Hamiltonian hosting various topological phases, then explore its topological phases and TPTs under various deformations breaking different symmetries [5, 16, 18–22]. Here we take the second approach, but limit to non-interacting fermionic systems[5]. We focus on the simplest and widely experimentally realized topological phase: the quantum anomalous Hall (QAH) phase [5, 8–10, 12, 28] and also establish its connection to the un-quantized AHE. Specifically, we start from a QAH Hamiltonian which hosts some known gapped topological phases such as Chern insulator and band insulator and see how a Parity (P-) breaking injecting current Fig.1a,b or a P-persevering chemical potential or energy dispersion drives the parent QAH Hamiltonian into new topological gapped or gapless phases through new classes of topological phase transitions (TPT). We also define the new "topological bulk invariants" of these $z = 2$ topological gapless phase, investigate the associated new edge state structure, explore enriched bulk-edge correspondence and new longitudinal/transverse edge-edge correspondence. During this establishment, we propose a classification of the QAH insulators and AHE metals in Fig.2.

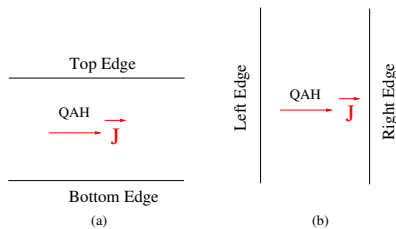


FIG. 1. New topological phases and bulk or edge TPTs are generated by (a) Injecting a longitudinal current into the QAH sample in a strip geometry. (b) Injecting a transverse current into the QAH sample in a strip geometry.

This work contains 3 parts. In part I, under an injecting current (Fig.1a,b), we evaluate the Hall conductivity at both zero and finite temperatures. Then we study the non-analytical behaviours of the ground state energy and map out the global phase diagram in the Zeeman field/injecting current plane Fig.3. The 2 old phase turn into 4 phases: the old (even) Chern insulator with the Chern number $\text{Ch}_- = \pm 1$ and quantized Hall conductivity

$\sigma_{xy} = \pm 1 \times e^2/h$ when $c < v$, a new $z = 2$ Odd Chern metal (OCM) phase with $\text{Ch}_- = \pm 1$, extended Fermi surfaces (FS) and un-quantized universal Hall conductivity $|\sigma_{xy}| = v/c < 1$ (in the unit of e^2/h) when $c > v$. The emergence of the particle and hole FS in the Odd Chern metal phase is responsible for the reduced Hall conductivity which is still independent of h/t and many other microscopic details of the Hamiltonian. The old band insulator with $\text{Ch}_- = 0, \sigma_{xy} = 0$ and a new band metal phase with $\text{Ch}_- = 0, \sigma_{xy} = 0$ with extended FSs. The TPT from the Chern insulator to the band insulator is a 3rd order with the dynamic exponent $z = 1$, while both the Chern insulator to Odd Chern metal, and the band insulator to band metal are second order ones with $z = 2$. Strikingly, the TPT from the Odd Chern metal to the band metal is novel: it has no non-analyticity to infinite order in the ground state energy, but the Chern number of the band jumps $\Delta \text{Ch}_- = \pm 1$ and the Hall conductivity has a universal non-integer jump $\Delta \sigma_{xy} = v/c$. This presents the first example of a TPT from both bulk and associated edge properties, but not a QPT in conventional wisdom [24, 29, 30]. We also evaluate various thermodynamic quantities such as the density of states, specific heat, compressibility and Wilson ratio at a finite T in all the 4 phases and also their quantum scaling forms near all these bulk TPTs.

Then we study the edge states in a strip geometry when the injecting current is either parallel (longitudinal) or transverse to the edge, from both the lattice model and from the effective low energy theory. During the bulk TPT from the even Chern insulator to the Odd Chern metal, the edge in a parallel injection also undergoes very unusual edge TPT: Inside the Chern insulator $c < v$ before the TPT, the two edge modes on the two opposite sides of the sample (Fig.1c) flow along the opposite directions $v_L > 0, v_R < 0$, but one side flow slower than the other side $|v_R| < |v_L|$. Only the edge mode contributes to $\sigma_H = \pm 1$. At the TPT $c = v$, one edge mode becomes completely flat with zero velocity $v_R = 0$ which can be viewed as a fine tuning to a multi-critical point (Fig.2). Inside the odd Chern metal after the TPT $c > v$, the two opposite sides of the sample start to flow along the *same* direction $v_L > 0, v_R > 0$, but one side flows much slower than the other side $|v_R| \ll |v_L|$. Both bulk and edge contribute to the transport. However, in a transverse boost, the edge mode velocity behaves as $\sqrt{v^2 - c^2}$ before the TPT $c < v$, but were squeezed out after the TPT $c > v$, so no T-edge modes in the Odd Chern metal anymore. Only the bulk contributes to the transport. So the $z = 2$ Odd Chern metal has the exotic edge modes with $v_L v_R > 0$ in a parallel injection (Fig.1a), but not in a transverse injection (Fig.1b). We may call this new phenomenon a new longitudinal (L-) /transverse (T-) edge correspondence under the current injection. As alerted in the last paragraph, the novel bulk TPT from Odd Chern metal to band metal can also be viewed from the edge in a parallel boost: the former has one edge mode with $v_L v_R > 0$, the latter none. Obviously, the Odd Chern

remains the same universal number as the $n = 1$ case. So does the jump from the odd Chern metal to its T-reversal odd Chern number partner which is twice as that from the OCM to the BM. This could be a universal salient feature of the odd Chern metal (Fig.2) ! This fact establish the Hall conductivity jump as the new "topological invariants" characterizing the gapless topological phases with extended FS. (4) Due to the $n = 2$ NNN feature, the Doppler shift in the 4 nodes become the same sign. This is contrast to the $n = 1$ NN injecting current case where the 4 nodes have 2+ and 2- Doppler shifts.

As a byproduct, taking some results from [23], for the QAH or AHE due to the artificially generated SOC which is a non-relativistic effect, we find that a Galileo boost v on a lattice leads to the $n = 1$ NN gauge-invariant current and $n = 2$ NNN current. So the results achieved in Sec.V and Sec.VI can also be applied to a moving sample. So if an insulator is band or Chern type may depend on if the observer is moving relative to the lattice. Then after absorbing the $n = 1$ NN gauge-invariant current into the QAH Hamiltonian by a unitary transformation, the NNN current term in the transformed basis changes sign after some critical boost velocity $v_c \sim 1cm/s$ solely determined by the Wannier functions. So does the Doppler shift near the four nodes. All these new features are subject to the scattering measurements in the moving frame in Fig.34.

In terms of the SPT language, despite the original QAH Hamiltonian breaks the time-reversal symmetry explicitly, it still has a charge (C-) conjugation symmetry and also a parity (P-) symmetry. An injecting current or a moving sample breaks P-symmetry, but keeps the C-symmetry. Because it is a non-interacting system, the C-symmetry is never broken during the evolution, so it is the C-symmetry protected topological phases and TPTs driven by the $n = 1$ and $n = 2$ current.

In part III, we study the P-preserving deformation such as an energy dispersion. It leads to a even Chern metal phase which has the same bulk properties as the odd Chern metal. But the Universal Hall conductance jump from the even CM to the band metal is an integer number. It also has a dramatically different L-edge mode properties than the odd CM: the L-edge mode satisfies the conventional $v_L v_R < 0$ instead of the exotic $v_L v_R > 0$. A real material contains both P-breaking and P-persevering components and is examined in Sec. VIII. We find that as the parameter changes, the generic AHE will be either in even-like Chern metal or odd-like Chern metal: there is a edge reconstruction between the two with a L- edge exponent $z_l = 2$. We propose a complete classification of AHE metals leading to un-quantized QAH effect as the Band metal (BM), odd Chern metal and even Chern metal, while the gapped phases leading to quantized QAH effect as BI, CI and odd CI (Fig.2). The BM is nothing but the previously well studied one contributing to the un-quantized AHE [2, 3]. While the itinerant metal contributing the AHE due to the Berry phase acquired by electrons moving in the non-coplanar spin texture in the real space in a Ferromagnet

does not fall into this non-interacting classification [1].

Experimentalists got used to apply magnetic field, electric field, or strain, pressure, neutron scattering, muon spin rotation, etc. Here, we show that injecting various forms of currents may be an effective way to bring out a lot of information on the topological phases, also drive them to new phases through novel TPTs. Alternatively, for SOC which is a non-relativistic effect, putting the sample in a strip shape to move in a trail, then perform various scattering experiments such as neutron, X-ray scattering or ARPES may also be helpful for artificially generated QAH systems.

The rest of the paper is organized as follows: we will first study the QAH under a P-breaking injecting current (Fig.1a,b). We will study the bulk properties of both systems via lattice theory and continuum effective theory in the thermodynamic limit, then investigate the corresponding edge properties in a strip geometry in both longitudinal and transverse edge via also both lattice theory and the continuum effective theory. Then in the first two appendices, we investigate the QAH under a P-preserving chemical potential or energy dispersion by the similar approaches. The P-breaking and P-preserving Hamiltonian are two different kinds of deformations leading to different bulk phases and topological phase transitions, also different edge properties. A real material contains both and will be examined in Sec.VIII. In Sec.IX, we summarize "Topological invariants" and the enriched bulk/L-edge/T-edge correspondence in gapless fermionic systems with extended Fermi surface. The experimental detections are analyzed in Sec.X.

II. THE BULK PROPERTIES: THE MICROSCOPIC LATTICE THEORY

The quantum anomalous Hall model on a square lattice takes the form

$$H_{QAH} = - \sum_i [c_i^\dagger (t\sigma_z - it_s\sigma_x)c_{i+x} + c_i^\dagger (t\sigma_z - it_s\sigma_y)c_{i+y} + h.c.] - h \sum_i (n_{i\uparrow} - n_{i\downarrow}) + U \sum_i n_i^2 - \mu \sum_i n_i. \quad (1)$$

Without loss of generality, we assume that $t > 0$ and $t_s > 0$. In this work, we focus on the non-interacting limit $U = 0$, but the chemical potential can be zero or non-zero.

Under an injecting current (for its motivation from a Galileo transformation, see appendix E), one obtains the injected Hamiltonian:

$$H_{inj} = H_{QAH} + \sum_i (it_{b,x}c_i^\dagger c_{i+x} + it_{b,y}c_i^\dagger c_{i+y} + h.c.) \quad (2)$$

The non-injected Hamiltonian Eq.1 has the Charge conjugation C-symmetry and the parity P-symmetry $k_x \rightarrow -k_x, k_y \rightarrow -k_y; \sigma_x \rightarrow -\sigma_x, \sigma_y \rightarrow -\sigma_y$. but

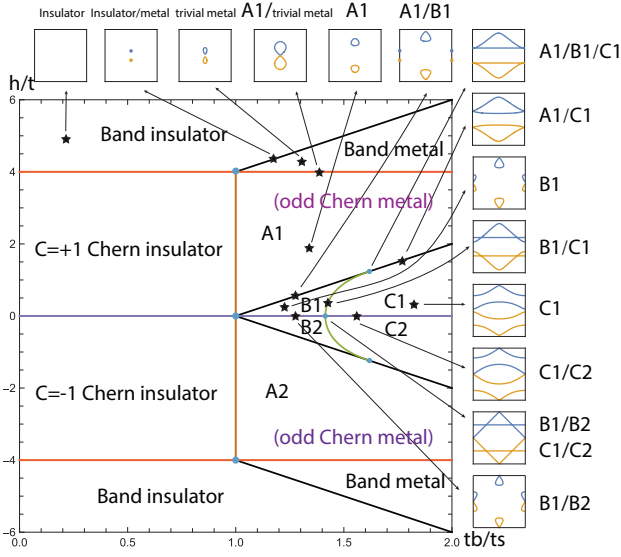


FIG. 3. The global Phase diagram of the Lattice Hamiltonian Eq.2 with a fixed $t_s/t = 1$. The phase diagram does depend on the ratio t_s/t . For simplicity, we take $t_s/t = 1$ in this figure only. Then the black phase boundary is a straight line. But t_s/t is taken as any value in the continuum effective actions. The topological metal phases are named as A1, A2, B1, B2, C1, C2. Green means the Particle (P-) FS, the yellow Hole (H-) FS. The inserts plot the Fermi surface of different metal phases within the 1st Brillouin Zone, where we use the notation A1/B1 for the phase boundary between A1 and B1, etc. The first box stands for the band insulator where there is no FS, the second is the metal-insulator transition where there are two Fermi points (one P-, one H-) emerging with the quadratic band touchings (so the dynamic exponent $z = 2$), they evolve into two (one P-, one H-) Fermi pockets in the band metal. Then they touch quadratically at $(0, 0)$ in the A1-CM/BM QCP with *not* any non-analyticity. A1 corresponds to Fig.9d, A1/B1 to Fig.13d. The P- FS expands to A1/C1, the bottom part of the FS becomes straight in A1/B1/C1. B1 corresponds to Fig.13e. The collision of the two P- FS from B1 leads to B1/C1. B1/B2 differs from B1 by the conic touching of P- and H- Fermi pocket at $(0, \pi)$ and $(\pi, 0)$ with *not* any non-analyticity. Then the split between the P- and H- FS from C1/C2 leads to C1. See also Fig.12, 13 and Fig.16, 17 near $h/t = \pm 4$ and $h/t = 0$ respectively in the continuum calculation. See also Fig.23 for higher order $n = 2$ boost.

no Time Reversal T-symmetry. The injected Hamiltonian Eq.2 breaks the P-symmetry, still respects the C-symmetry: $\sigma_x \mathcal{K} (\mathcal{K}$ denotes the complex conjugate),

$$(\sigma_x \mathcal{K}) H(\mathbf{k}) (\sigma_x \mathcal{K}) = -H(-\mathbf{k}) \quad (3)$$

The C-symmetry guarantees a relation between upper band and lower band $E_+(\mathbf{k}) = -E_-(-\mathbf{k})$, and the Berry curvature $\Omega_+(\mathbf{k}) = -\Omega_-(-\mathbf{k})$. We also have $\Omega_{\pm}(\mathbf{k}) = \Omega_{\pm}(-\mathbf{k})$. Note that the QAH belongs to the Class A, but still with the particle number conserved. Because

this C-symmetry does not conserve the particle number, so it can not be understood as the existence of an anticommutating symmetry operators, otherwise the system would belong to the Class D instead of the Class A [16].

For simplicity, we study the injection along the y direction, thus $t_{b,x} = 0$ and $t_{b,y} = t_b$. It can be easily generalized to any injection direction. In momentum space, the Hamiltonian becomes

$$H_{\text{inj}} = \sum_k c_k^\dagger \{ -[h + 2t(\cos k_x + \cos k_y)]\sigma_z + 2t_s \sin k_x \sigma_x + 2t_s \sin k_y \sigma_y - 2t_b \sin k_y \sigma_0 \} c_k \quad (4)$$

The Diagonalization of Eq.(4) leads to the two bands

$$E_{\pm}(\mathbf{k}) = -2t_b \sin k_y \pm \sqrt{[h + 2t(\cos k_x + \cos k_y)]^2 + 4t_s^2(\sin^2 k_x + \sin^2 k_y)} \quad (5)$$

Since $E_+(\mathbf{k}) \geq E_-(\mathbf{k})$ always holds for a fixed \mathbf{k} , we will call the E_+ the upper band and the E_- the lower band. When t_b is sufficiently small, it is in a insulating phase; When t_b/t_s is sufficiently large, it is in a metallic phase, with hole surface is given by $E_-(\mathbf{k}) = 0$ and electronic surface given by $E_+(\mathbf{k}) = 0$.

The critical t_b are determined by the minimization problem $\min_k E_+(\mathbf{k}; t_b) = 0$. In the full range of t_b/t_s , the Fermi surfaces (FS) can be rather complicated, see Fig.3.

When $4t > h > 0$, it is in the Chern insulator phase. At the critical $t_b/t_s = 1$ and the Fermi points are located at $(\pi, \arccos(\frac{2t-h}{2t}))$, it moves into the A1 Odd Chern metal phase, then as t_b increases further to $t_b = \sqrt{t_s^2 + h(h+4t)}/4$, the previous Fermi points grow-up into a Fermi surface with the emergence of the other Fermi point at $(0, \arccos[\frac{-t(2t+h)}{2(t^2+t_b^2-t_s^2)}])$ (See A1/B1), it moves into the B1 Odd Chern metal phase. When $t > t_b$ increases further, these two Fermi surfaces can collide at B1/C1 to move into the C1 phase.

When $h > 4t$, it is in the band insulator phase. At the critical $t_b = \sqrt{t_s^2 + h(h-4t)}/4$, the Fermi points are located at $(0, \arccos(\frac{2t}{h-2t}))$, it moves into the band metal phase.

The TPTs in Fig.3 can be classified into 4 classes: (1) The linear band touching due to the Dirac points are 3rd TPT with $z = 1$. In the $t_b = 0$, it is a Dirac point with emergent Lorentz invariance. The $t_b \neq 0$ drives it into a boosted Dirac point. (2) The emergency of the P- or H- Fermi point in insulator/metal, A1/B1 are quadratic band touching 2nd order TPT with the dynamic exponent $z = 2$. (3) Band metal/A1, B1/B2, C1/C2, even the M point B1/B2 (C1/C2) can be understood as the the conic band touching between the P- and the H- FS. They do *not* have any non-analyticity in the ground state energy. (4) The P-/P- FS (equivalently H-/H- FS) collision in A1/C1, B1/C1 are TPT with universal sub-leading scalings [30, 36].

TABLE I. The classification of bulk QPT or TPT.

4 classes TPTs	CI-BI	CI-OCM	OCM-BM	P-FS/P-FS collision
Dynamic exponent	$z = 1$	$z = 2$	No	saddle point cone
Order	3rd	2nd	Infinite order	3rd, 5th..
Scaling	Yes	Yes	No	sub-leading
$R_W = T\kappa_u/C_v$	$\frac{2\ln 2}{9\zeta(3)}$	$\frac{3}{\pi^2}$	$\frac{3}{\pi^2}$	sub-leading

where we only list one representative of CI-BI, CI-CI in the second column, CI-OCM, BI-BM, OCM-OCM in the 3rd column, OCM-BM, OCM-OCM in the 4th column, H-FS/H-FS in the 5th column. The Odd CM can also be replaced by the Even CM except the ECM-ECM transition does not exist as demonstrated in Sec.VII and VIII (See Fig.29 and Fig.37). The Wilson ratio (WR) was evaluated in the lattice in Sec.II-C-3 and in the continuum effective theories in Sec.III-A-3c and III-B-3c. The WR for all the gapped phases (CI and BI) $R_W = (T/\tilde{\Delta})^2$ (See Eq.19) is not listed in the Table. In fact, $R_W = \frac{3}{\pi^2}$ also holds inside the all the gapless phases (CM and BM), because the OCM to the BM transition has no analyticity anyway. We did not list the edge reconstruction transition from the CI to odd CI in Fig.23 and even CM to odd CM in Fig.29 with the longitudinal dynamic exponent $z_L = 3$ and $z_L = 2$ respectively. For the bulk or edge properties of these phases, see Table II.

In fact, as elucidated in Fig.3, if one look at $B1 \rightarrow B1/C1 \rightarrow C1$, the B1/C1 QCP is reached by the collision of the two P- FS (or equivalently, the two H-FS) from B1, so this class of TPT can be similarly investigated by the method developed in [30], universal *subleading* scalings can be derived. One can also similarly study the TPT from $A1 \rightarrow A1/C1 \rightarrow C1$. In the following, we are mainly interested in the experimentally most relevant case t_b/t_s is not too large, so focus on A1,A2,B1,B2 phases and class-1 and class-2 TPTs, but do not discuss C1 and C2 phase and the class-3 TPT in any details. The A1,A2,B1,B2 phases can be distinguished by σ_{xy} and Fermi surfaces (FS) topology: The A1 phase has $0 < \sigma_{xy} < 1$ and the FS is just one part, the B1 phase has $0 < \sigma_{xy} < 1$ and the FS consists of two disconnected parts. A2(B2) have the same FSs as A1(B1), but with opposite sign of σ_{xy} .

A. The quantum Hall response at zero and finite temperature: Topological phase transitions (TPT).

In order to calculate Berry connections \mathbf{A} and Berry curvatures Ω , it is convenient to rewrite the boosted QAH

Hamiltonian Eq.(2) in terms of (d_0, \vec{d}) vectors:

$$\begin{aligned}
H(\mathbf{k}) &= d_0(k)\sigma_0 + d_x(k)\sigma_x + d_y(k)\sigma_y + d_z(k)\sigma_z, \\
d_0(k) &= -2t_b \sin k_y, \quad \mathbf{d} = (d_x, d_y, d_z) \\
d_x(k) &= 2t_s \sin k_x, \quad d_y(k) = 2t_s \sin k_y, \\
d_z(k) &= -[h + 2t(\cos k_x + \cos k_y)]
\end{aligned} \tag{6}$$

Then the Berry Connections and Berry curvatures can be evaluated as:

$$\begin{aligned}
A_{\pm,i}(\mathbf{k}) &= i\langle \pm, \mathbf{k} | \partial_{k_i} | \pm, \mathbf{k} \rangle = \frac{(d_y \partial_{k_i} d_x - d_x \partial_{k_i} d_y)}{2|\mathbf{d}|(|\mathbf{d}| \pm d_z)} \\
\Omega_{\pm,xy}(\mathbf{k}) &= \partial_{k_x} A_{\pm,y} - \partial_{k_y} A_{\pm,x} = \mp \frac{1}{2|\mathbf{d}|^3} \mathbf{d} \cdot \partial_x \mathbf{d} \times \partial_y \mathbf{d}
\end{aligned} \tag{7}$$

Since the t_b term is proportional to the unit matrix σ^0 , so it does not affect the eigenvectors, then the Berry connections and Berry curvatures are exactly the same as $t_b = 0$ case. Note that σ_{xy} is related to $\Omega_{\pm,xy}$ and $\sigma_{yx} = -\sigma_{xy}$ is related to $\Omega_{\pm,yx}$. For later calculations on Hall response, we will only consider σ_{xy} and drop subscript xy in Ω .

1. Zero temperature Hall conductance and TPT

As long as $h \neq 0, \pm 4t$, the upper band and the lower band are well separated, thus one can calculate the Chern number of the lower band via integrating the Berry curvature $\Omega_-(\mathbf{k})$ over the entire Brillouin zone (BZ) which is a torus \mathbb{T}^2 :

$$\text{Ch}_- = \frac{1}{2\pi} \int_{\mathbb{T}^2} d^2\mathbf{k} \Omega_-(\mathbf{k}) = \begin{cases} 0, & |h/t| > 4; \\ +1, & 4 > h/|t| > 0; \\ -1, & 0 > h/|t| > -4; \end{cases} \tag{8}$$

In the insulating phase, only the lower band is full occupied, thus the Chern number is the zero temperature Hall conductance in unit e^2/h , that is $\sigma_H = \text{Ch}_-$. In the metallic phase, both band are partially filled, thus the zero temperature Hall conductance reduces to $\sigma_H = \text{Ch}_- \times |t_s/t_b|$.

In any case, the zero temperature Hall conductance can be expressed as

$$\begin{aligned}
\sigma_H &= \frac{1}{2\pi} \int_{\mathbb{T}^2} d^2\mathbf{k} \sum_{s=\pm} \Omega_s(\mathbf{k}) \Theta(-E_s(\mathbf{k})) \\
&= \text{Ch}_- \times \min(1, |t_s/t_b|).
\end{aligned} \tag{9}$$

As shown in Fig.4, the Hall conductivity show plateau structure during the scanning of h : it is zero for band insulator and band metal, show a plateau with value $-t_s/t_b$ for A2 phase and B2 phase, show a plateau with value t_s/t_b for A1 phase and B1 phase, becomes zero again for band insulator and band metal.

We conclude that the zero temperature Hall conductance in the metallic phase is reduced by a factor $|t_s/t_b| < 1$ relative to its quantized value in the Chern insulator phase (Fig.4). In both the insulating phase and metallic phase, they are not that sensitive to the microscope details. As to be shown in the following sections, they can all be reproduced via the analytical evaluations of relevant integrals in the continuum theory.

2. Finite temperature Hall conductance

At finite temperature, one only need to replace the step function in Eq.9 by the Fermi distribution function

$$\begin{aligned}\sigma_H(T) &= \frac{1}{2\pi} \int_{\mathbb{T}^2} d^2\mathbf{k} \sum_{s=\pm} \Omega_s(\mathbf{k}) f(E_s(\mathbf{k})) \\ &= \frac{1}{2\pi} \int_{\mathbb{T}^2} d^2\mathbf{k} \Omega_-(\mathbf{k}) [f(E_-(\mathbf{k})) - f(E_+(\mathbf{k}))] \\ &= Ch_- + \frac{1}{\pi} \int_{\mathbb{T}^2} d^2\mathbf{k} \Omega_+(\mathbf{k}) f(E_+(\mathbf{k}))\end{aligned}\quad (10)$$

where $f(E) = 1/[\exp(E/T) + 1]$. The finite T Hall conductances as varying parameters of h/t or t_b/t_s are plotted in Fig.5

B. The ground-state energy and Quantum phase transitions (QPT)

We are interested in the non-analytical behaviours in the ground-state energy density on the lattice which can be numerically calculated via

$$E_{\text{GS}}^{(\text{lat})} = \int_{\mathbb{T}^2} \frac{d^2\mathbf{k}}{(2\pi)^2} [E_+(\mathbf{k})\Theta(-E_+(\mathbf{k})) + E_-(\mathbf{k})\Theta(-E_-(\mathbf{k}))]\quad (11)$$

The quantum phase transitions can be driven either by tuning by the Zeeman field h/t or the boost t_b/t .

1. QPTs driven by the boost t_b/t

In the insulating phase, the lower band is full occupied, the ground-state energy density is

$$E_{\text{GS}}^{(\text{lat})} = \int_{\mathbb{T}^2} \frac{d^2\mathbf{k}}{(2\pi)^2} E_-(\mathbf{k}; t_b) = \int_{\mathbb{T}^2} \frac{d^2\mathbf{k}}{(2\pi)^2} E_-(\mathbf{k}; t_b=0)\quad (12)$$

where the last equality is due to that the t_b -dependent part in Eq.5 is odd in \vec{k} , so vanishes after integration

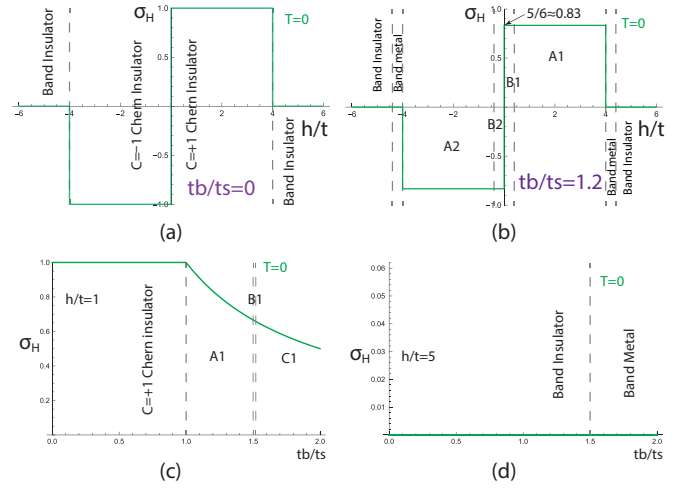


FIG. 4. The zero temperature $T = 0$ Hall conductance σ_H as a function of h/t for fixed $t_b/t_s = 0, 1.2$ in (a) Across the 3rd order TPT with $z = 1$ from BI/CI, CI/CI, CI/BI, the $\sigma_H(T = 0)$ has an integer jump $\Delta\sigma_H = -1, 2, 1$ respectively, (b) As shown in Fig.9, there is no non-analytical behaviours (infinite order) for the BM/A2, B1/B2, A1/BM TPTs, but $\sigma_H(T = 0)$ still has a universal non-integer jump $\Delta\sigma_H = -t_s/t_b = -1/1.2 = -5/6, 2 \times 5/6, 5/6$ respectively, independent of any other microscopic details. When across the 2nd order TPT with $z = 2$ from the BI/BM, A2/B2, and A1/B1, $\sigma_H(T = 0)$ has no changes. In a generic case, the BM should contribute to a un-quantized AHE (See Fig.24 and Table 1), but it vanishes in this particular $n = 1$ case due to some fine tuning. As a function of t_b/t_s for fixed $h/t = 1, 5$ in (c) a 2nd order QPT with $z = 2$ and (d) $\sigma_H = 0$ in both the BI and BM. We expect the class-3 TPT of B1/C1 and A1/C1 [30] has no changes in $\sigma_H(T = 0)$ either. See also Fig.14 and Fig.18 near $h/t = \pm 4$ and $h/t = 0$ respectively in the continuum calculations.

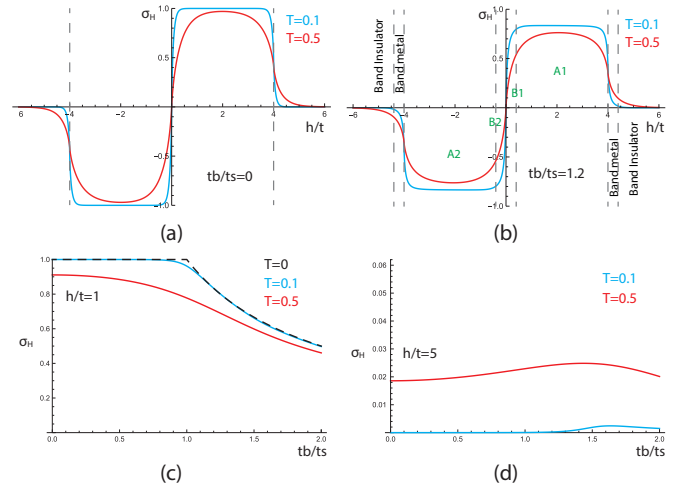


FIG. 5. The finite temperature $T > 0$ Hall conductance σ_H as a function of h for fixed $t_b/t_s = 0, 1.2$ in (a) and (b) and as function of t_b/t_s for fixed $h/t = 1, 5$ in (c) and (d), where we also choose $t = t_s = 1$, thus $T = 0.1$ means $k_B T/t = 0.1$.

over entire Brillouin zone (BZ). Thus the $E_{GS}^{(\text{lat})}$ is independent of t_b in the insulating phase. However, in the metallic phase, due to the partial filling of the upper and lower bands, the $E_{GS}^{(\text{lat})}$ does depend on t_b . Thus near the insulating-metallic transition driven by t_b at some critical value $t_{b,c}$, the ground-state energy density $E_{GS,I}^{(\text{lat})} = \text{const}$ in the insulating side ($t_b < t_{b,c}$), $E_{GS,M}^{(\text{lat})} \propto (t_b - t_{b,c})^\alpha$ in the metallic side ($t_b > t_{b,c}$). The index $\alpha > 0$ indicates the order of the phase transition is $\lceil \alpha \rceil$. For example, if $\alpha \leq 1$, then is the first order transition with a cusp at $t_b = t_{b,c}$; if $1 < \alpha \leq 2$, then is the second order QPT shown in Fig.6,7.

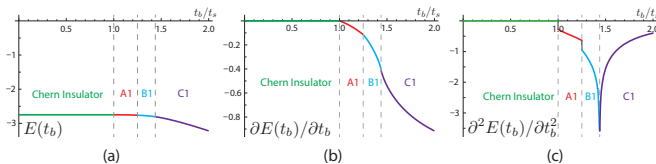


FIG. 6. The ground-state energy density $E_{GS}^{(\text{lat})}$ as the function of t_b/t , with fixed $t = t_s = 1$ and $h = 0.5$ in Fig.3. From (a),(b),(c) are $E_{GS}^{(\text{lat})}$'s zeroth-/first-/second-order derivative with respect to t_b . The vertical dashed lines correspond to the critical t_b , which separate the Chern insulator, A1,B1 and C1. An obvious second order QPT discontinuity is shown at $t_b = 1.0, 1.25$ both with $z = 2$, the cusp at $t_b = 1.44$ shows a third order one in the class-3 [30] respectively. See also table I.

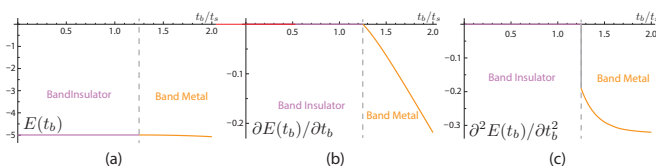


FIG. 7. The same as Fig.6, but with $h = 4.5$ in Fig.3. The only vertical dashed line corresponds to the critical t_b which separates the band insulator from the band metal. An obvious second order QPT discontinuity with $z = 2$ is shown at $t_b = 1.25$.

Because any phase transitions are independent of how they are approached or scanned, so scanning t_b/t or h/t should research consistent results. That is indeed the case as shown in the following section.

2. QPTs driven by h/t

We first study the TPT between band insulator and Chern Insulator. Because E_{GS} is t_b independent in the insulating phases, so the TPTs are the same as the no-boost $t_b = 0$ case. In Fig.8 we numerically evaluate the ground-state energy Eq.(12) as a function of scanning $-6 < h/t < 6$ with fixed $t_b = 0$ which is identical to

the $t_b/t < 1$ case. An obvious third order discontinuity is shown between the band insulator and the Chern insulator.

Now we study TPTs between metals where E_{GS} becomes t_b independent. Scanning $-6 < h/t < 6$ with fixed $t_b > t_s$, we meet consecutively band insulator, band metal, A2 Odd Chern metal, B2 Odd Chern metal, B1, A1, band metal, band insulator. In the Fig.9, a clear second order discontinuity appears between band insulator/band metal A2/B2 phase, and A1/B1 phase. However, no any order discontinuity is found The band metal/A2, B2/B1, A1/band metal transitions, so they could be just infinite-order TPT. But they can still be distinguished by the Hall conductance shown in Fig.4.

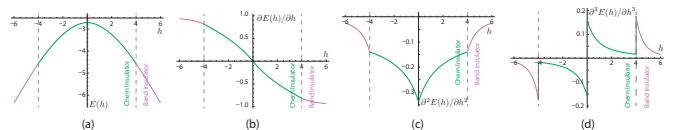


FIG. 8. The ground-state energy density E_{GS} as function of h , with fixed $t = t_s = 1$, $t_b = 0$. From left to right are E_{GS} 's 0th-/1st-/2nd-/3rd-order derivative with respect to h . The vertical dashed lines correspond to the critical h , which separate band insulator, Chern insulator (-1), Chern insulator (+1), band insulator. An obvious 3rd order QPT discontinuity with $z = 1$ is shown at $h/t = -4, 0, +4$.

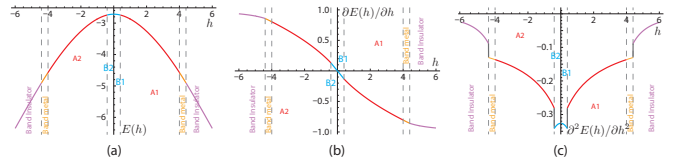


FIG. 9. The ground-state energy density E_{GS} as function of h , with fixed $t = t_s = 1$, $t_b = 1.2$. From left to right are E_{GS} 's 0th-/1st-/2nd-/3rd-order derivative with respect to h . The vertical dashed lines correspond to the critical h , which separate band insulator, tribal metal, A2, B2, B1, A1, band metal, band insulator. A clear 2nd order QPT discontinuity with $z = 2$ is obtained between band insulator/band metal A2/B2, A1/B1 phase. However, no non-analytical behaviours are found for the BM/A2, B2/B1, A1/BM transitions, even in the third-order derivatives and beyond. The underlying physical mechanisms for these infinite order TPT are explored from the continuum effective theory in Sec.III-A and III-B.

C. Thermodynamic Quantities

We will first discuss the density of states (DOS), then use it to compute several experimentally measurable quantities.

1. The density of states (DOS)

From the Hamiltonian (6), one can find the Matsubara Green's function

$$\begin{aligned} G(\mathbf{k}, i\omega_n) &= [i\omega_n - H(\mathbf{k})]^{-1} \\ &= \frac{P_+(\mathbf{k})}{i\omega_n - E_+(\mathbf{k})} + \frac{P_-(\mathbf{k})}{i\omega_n - E_-(\mathbf{k})} \end{aligned} \quad (13)$$

where $P_{\pm} = \frac{1}{2}[1 \pm \mathbf{d} \cdot \boldsymbol{\sigma} / |\mathbf{d}|]$ are the projection operators onto the $s = \pm$ upper/lower bands and $P_+ + P_- = 1$.

The total DOS $D(\omega) = D_+(\omega) + D_-(\omega)$ is

$$\begin{aligned} D(\omega) &= -\frac{1}{\pi} \int \frac{d^2\mathbf{k}}{(2\pi)^2} \Im \text{Tr}[G_R(\mathbf{k}, \omega)] \\ &= \int \frac{d^2\mathbf{k}}{(2\pi)^2} [\delta(\omega - E_+(\mathbf{k})) + \delta(\omega - E_-(\mathbf{k}))] \end{aligned} \quad (14)$$

It should be convenient to introduce the DOS for each band

$$D_{\pm}(\omega) = \int \frac{d^2\mathbf{k}}{4\pi^2} \delta(\omega - E_{\pm}(\mathbf{k})), \quad (15)$$

The DOS on a lattice contain some van-Hove singularities when ω far away from 0, which makes numerical calculation on DOS time consuming. The lattice DOS is plotted in Fig.10. For $\omega \sim 0$, in a metallic phase where $t_b/t > 1$, the DOS is nearly, but not exactly a constant.

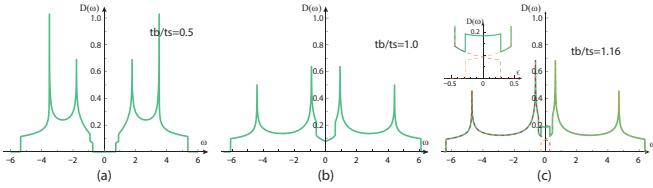


FIG. 10. At fixed $t = t_s = 1$ and $h = 1$, the density of states (DOS) of Eq.(4) at different t_b/t_s values: (a) $t_b/t_s = 0.5$ in Chern insulator, (b) $t_b/t_s = 1.0$ on the QCP between Chern Insulator and A1 Odd Chern metal with $z = 2$, (c) $t_b/t_s = 1.16$ inside the A1 Odd Chern metal. The cusps are Van-Hove singularities. Note that (c) inset is showing the total density of states is nearly, but not exactly flat near $\omega = 0$. Compare to Fig.15 and Fig.19 near $h/t = \pm 4$ and $h/t = 0$ respectively in the continuum calculation.

2. The specific heat and compressibility

Here, we will make use of the DOS to evaluate the two conserved quantities, then compute the Wilson ratio. The Helmholtz free energy density

$$\begin{aligned} F(T) &= -T \int \frac{d^2\mathbf{k}}{(2\pi)^2} \ln[2(1 + \cosh(E_+(\mathbf{k})/T))] \\ &= E_{\text{GS}} + \int \frac{d^2\mathbf{k}}{(2\pi)^2} (|E_+(\mathbf{k})| - T \ln[2(1 + \cosh \frac{E_+(\mathbf{k})}{T})]) \end{aligned} \quad (16)$$

where the zero temperature part of $F(T)$ is nothing but the ground-state energy density E_{GS} in Eq.11.

The specific heat (at a constant volume) $C_v(T) = -T \frac{\partial^2 F}{\partial T^2}$:

$$\begin{aligned} C_v(T) &= \int \frac{d^2\mathbf{k}}{(2\pi)^2} \frac{[E_+(\mathbf{k})]^2}{T^2 [1 + \cosh(E_+(\mathbf{k})/T)]} \\ &= \int \frac{d\omega \omega^2 D_+(\omega)}{T^2 [1 + \cosh(\omega/T)]} = \int \frac{d\omega \omega^2 D(\omega)}{2T^2 [1 + \cosh(\omega/T)]} \end{aligned} \quad (17)$$

The (isothermal) uniform compressibility $\kappa_u(T) = \sum_{s=\pm} \int \frac{d^2\mathbf{k}}{(2\pi)^2} \frac{\partial f(E_{s,\mathbf{k}})}{\partial E_{s,\mathbf{k}}}$ is

$$\begin{aligned} \kappa_u(T) &= \int \frac{d^2\mathbf{k}}{(2\pi)^2} \frac{[E_+(\mathbf{k})]^2}{T^2 [1 + \cosh(E_+(\mathbf{k})/T)]} \\ &= \int \frac{d\omega D(\omega)}{2T [1 + \cosh(\omega/T)]} = \int \frac{d\omega D_+(\omega)}{T [1 + \cosh(\omega/T)]} \end{aligned} \quad (18)$$

Below we discuss their low temperature behaviours.

In the gapped phases, i.e. Chern insulator or band insulator, we denote the gap as

$$\tilde{\Delta} = \min_k E_+(k) > 0, \quad (19)$$

then $D(\omega) = 0$ for entire $-\tilde{\Delta} < \omega < \tilde{\Delta}$ and $D(\tilde{\Delta}) = D_2 > 0$ at the gap edge (Fig.10a), thus $C_v(T) = 2D_2 \tilde{\Delta}^2 T^{-1} e^{-\tilde{\Delta}/T}$. Similarly, $\kappa_u(T) = 2D_2 T e^{-\tilde{\Delta}/T}$. Both are exponentially suppressed in T .

In the gapless phases, i.e. A or B Odd Chern metal phase or band metal phase, we have $\tilde{\Delta} = \min_k E_+(k) < 0$ and $D(0) = D_0 > 0$ (Fig.10c), thus $C_v(T) = \frac{\pi^2}{3} D_0 T$, linear in T . Similarly, $\kappa_u(T) = D_0 + \dots$ where the sub-leading T dependence \dots can be best evaluated in the continuum theory to be evaluated in Sec.III.

For the 3rd order QCPs with $h = 0, \pm 4t$ and $t_b/t < 1$, we have $\tilde{\Delta} = \min_k E_+(k) = 0$ and $D(\omega) = D_1 \omega$ for small ω just like a Dirac fermion, thus $C_v(T) = 9\zeta(3) D_1 T^2$ where $\zeta(3) \approx 1.2021$ is the Riemann Zeta function:

$$\zeta(s) = \sum_{n=1}^{\infty} 1/n^s = \frac{1}{\Gamma(s)} \int_0^{\infty} \frac{x^{s-1}}{e^x - 1} dx \quad (20)$$

Similarly, $\kappa_u(T) = 2 \ln 2 D_1 T$ where $\ln(2) \approx 0.6931$.

For the other QCPs which are 2nd order, i.e. $\tilde{\Delta} = 0$ and $t_b/t_s > 1$, or at the boundary between A1 and B1, we always have non-zero $D(0) = D_0 > 0$ (Fig.10b), thus $C_v(T) = \frac{\pi^2}{3} D_0 T$. Similarly, $\kappa_u(T) = D_0 + \dots$ where again the sub-leading T dependence \dots can also be best evaluated in the continuum theory to be evaluated in Sec.III.

3. The Wilson ratio

The Wilson ratio is defined as the ratio of the two conserved quantities $R_W = T \kappa_u / C_v$ which has the following low temperature behaviours.

In the gapped phases, i.e. Chern insulator phase or band insulator phase, $R_W = (T/\tilde{\Delta})^2$ where $\tilde{\Delta}$ is given in Eq.19.

In the gapless phases, i.e. A or B Odd Chern metal phase or band metal phase, $R_W = \frac{3}{\pi^2} \approx 0.3040$.

For the 3rd order QCP with $z = 1$ near $h = 0, \pm 4t$ and $t_b/t_s < 1$, $R_W = \frac{2 \ln 2}{9\zeta(3)} \approx 0.1281$.

For the other QCP which are 2nd order with $z = 2$, $R_W = \frac{3}{\pi^2} \approx 0.3040$.

These results will also be confirmed by the analytic calculations from the continuum theory in Sec.III-A-3(c) near $h/t = \pm 4$ and III-B-3(c) near $h/t = 0$ respectively. They are also listed in the last line of the Table-I.

So we conclude the Wilson ratio can be used to distinguish all the gapped, gapless and QCPs. However, one need Ch_- or σ_H , especially the longitudinal/transverse edge to be discussed in Sec.V and VI to distinguish the topology.

D. QPT versus TPT

Quantum phase transition (QPT) is characterized by the change of the ground state energy as shown in Sec.II-B. One diagnose the QPT by the non-analytical behaviours of ground state energy density: namely, by taking consecutive derivatives on the ground state energy density at $T = 0$ with respect to the tuning parameter such as the injection/boost or the Zeeman field until hitting the singularity [24, 29, 30]. The number of derivatives needed to reach the singularity gives the 1st, 2nd, or higher order QPT. The DOS and the dynamic exponent z can also be extracted. Then at a finite T near the QPT, various physical quantities such as the specific heat, compressibility and Wilson ratio satisfy the corresponding scaling functions or sub-leading scalings [30].

While Topological phase transition (TPT) is characterized by the change of topological invariants such as the Chern number Ch_- and quantum Hall conductance as shown in Sec.II-A. For the non-interacting Fermi system [29–31], there is also the corresponding changes in the Fermi surface topology as shown in Fig.3.

QPT, especially in interacting bosonic or quantum spin system may not necessarily be a TPT. For example, the QPT from the BI-BM in Fig.12 is a pure 2nd order QPT with $z = 2$ which is not a TPT. Of course, the well known SF-Mott QPT, AFM to VBS, etc are not TPT [24]. However, the QPT from CI to OCM is also a 2nd order one with $z = 2$, but despite there is no change in the Chern number Ch_- , there is also a corresponding changes in both longitudinal and transverse edge modes. So it is also a TPT. However, in general, a TPT must be also a QPT. For example, the TPT from the CI to BI is a TPT where the Chern number Ch_- and the Hall conductance σ_H changes by ± 1 . Of course, there is also a corresponding changes in the edge modes due to the conventional bulk-edge correspondence. At the same time, it is also a 3rd order QPT with $z = 1$. Of course, the

well-known TPT from FQH to insulator transition [23] is also a QPT with $z = 1$. However, for the very first time, we discover a counter-example to this general believe: the TPT from the OCM to the BM is not a QPT! This maybe the very first example of a TPT which is NOT a QPT. Similar classifications also apply to Fig.16. See also Table I and Table II. See also Sec.VIII-C for more concrete discussions.

III. THE BULK EFFECTIVE THEORY IN THE CONTINUUM LIMIT

In the momentum space, Eq.2 becomes:

$$H(\mathbf{k}) = -[h + 2t(\cos k_x + \cos k_y)]\sigma_z + 2t_s \sin k_x \sigma_x + 2t_s \sin k_y \sigma_y - 2t_b \sin k_y \sigma_0 \quad (21)$$

When $h \sim 4t$, there are low-energy excitations near $\mathbf{K}_3 = (\pi, \pi)$, it reduces to

$$H_3(\mathbf{K}_3 + \mathbf{k}) = -[h - 4t + t(k_x^2 + k_y^2)]\sigma_z - 2t_s k_x \sigma_x - 2t_s k_y \sigma_y + 2t_b k_y \sigma_0 \quad (22)$$

When $h \sim 0$, there are low-energy excitations near both $\mathbf{K}_1 = (\pi, 0)$ and $\mathbf{K}_2 = (0, \pi)$, it reduces to

$$\begin{aligned} H_1(\mathbf{K}_1 + \mathbf{k}) &= -[h + t(k_x^2 - k_y^2)]\sigma_z - 2t_s k_x \sigma_x + 2t_s k_y \sigma_y - 2t_b k_y \sigma_0 \\ H_2(\mathbf{K}_2 + \mathbf{k}) &= -[h - t(k_x^2 - k_y^2)]\sigma_z + 2t_s k_x \sigma_x - 2t_s k_y \sigma_y + 2t_b k_y \sigma_0 \end{aligned} \quad (23)$$

When $h \sim -4t$, there are low-energy excitations near $\mathbf{K}_0 = (0, 0)$, it reduces to

$$H_0(\mathbf{k}) = -[h + 4t - t(k_x^2 + k_y^2)]\sigma_z + 2t_s k_x \sigma_x + 2t_s k_y \sigma_y - 2t_b k_y \sigma_0 \quad (24)$$

The low-energy physics near all the 4 Dirac points can be written in a generic form

$$H(\mathbf{k}) = (\Delta + \alpha_x k_x^2 + \alpha_y k_y^2)\sigma_z + v_x k_x \sigma_x + v_y k_y \sigma_y - c k_y \sigma_0 \quad (25)$$

where the velocities $v_{x,y}$ and “mass” $\alpha_{x,y}$ must be non-zero. In this work, all the above equations correspond to the isotropic case $|v_x| = |v_y|$ and $|\alpha_x| = |\alpha_y|$. As stressed below Eq.2, both the C-symmetry (charge symmetry) and P-symmetry (parity symmetry) exist at $c = 0$, and P-symmetry is broken at $c \neq 0$, but the C-symmetry still holds at $c \neq 0$.

Diagonalization of the effective Hamiltonian leads to the energy dispersion

$$\epsilon_{\pm}(\mathbf{k}) = \pm \sqrt{(\Delta + \alpha_x k_x^2 + \alpha_y k_y^2)^2 + v_x^2 k_x^2 + v_y^2 k_y^2} - c k_y \quad (26)$$

The half-filling condition and C-symmetry ensure the Fermi energy is always zero. By examining the minima

of upper band $\min_{\mathbf{k}} \epsilon_+(\mathbf{k})$, there exists a critical velocity c_0 and $c < c_0$ the ϵ_+ is empty and the system is in an insulating phase; and $c > c_0$ the ϵ_+ is partially filled and the system is in a metallic phase; When $\alpha_y \Delta > 0$, the critical velocity is $c_0 = \sqrt{v_y^2 + 4\alpha_y \Delta}$; when $\alpha_y \Delta < 0$, the critical velocity is $c_0 = |v_y|$. See Fig.11 for a geometric interpretation of the critical velocity in the two cases.

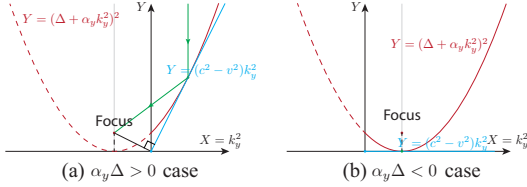


FIG. 11. Geometric determination of the critical velocity (a) $\alpha\Delta > 0$ and (b) $\alpha\Delta < 0$. The condition $0 = \min_{\mathbf{k}} \epsilon_+(\mathbf{k})$ is equivalent to $0 = \min_{\mathbf{k}} [(\Delta + \alpha_y k_y^2)^2 - (c^2 - v^2)k_x^2]$. The symmetry axis of the parabola is $k_y^2 = -\Delta/\alpha$. In both cases, the two Fermi points are located at momentum $\pm\sqrt{|\Delta/\alpha|}$ shown in Fig.13. It may be contrasted the Geometric determination of the critical velocities inside a superfluid with or without a roton minimum [23].

When re-write the continuum Hamiltonian Eq.25 in the form of Eq.6:

$$\begin{aligned} H(k) &= d_0(k)\sigma_0 + d_x(k)\sigma_x + d_y(k)\sigma_y + d_z(k)\sigma_z, \\ d_0(k) &= -ck_y, \quad \mathbf{d} = (d_x, d_y, d_z) \\ d_x(k) &= v_x k_x, \quad d_y(k) = v_y k_y, \\ d_z(k) &= \Delta + \alpha_x k_x^2 + \alpha_y k_y^2 \end{aligned} \quad (27)$$

and then the Berry Connections and Berry curvatures stay the same form as in Eq.7:

$$\begin{aligned} A_{\pm, i}(\mathbf{k}) &= \frac{(d_y \partial_{k_i} d_x - d_x \partial_{k_i} d_y)}{2|\mathbf{d}|(|\mathbf{d}| \pm d_z)} \\ \Omega_{\pm, xy}(\mathbf{k}) &= \mp \frac{1}{2|\mathbf{d}|^3} \mathbf{d} \cdot \partial_x \mathbf{d} \times \partial_y \mathbf{d} \end{aligned} \quad (28)$$

which takes the identical form as Eq.7. But it is integrated over R^2 here, while it is over a Torus \mathbb{T}^2 there.

It can be written in an explicit form

$$\begin{aligned} A_{\pm}(\mathbf{k}) &= \frac{v_x v_y (k_y, -k_x)}{2\sqrt{A^2 + \bar{k}^2} [\sqrt{A^2 + \bar{k}^2} \pm A]} \\ \Omega_{\pm, xy}(\mathbf{k}) &= \mp \frac{v_x v_y (\Delta - \alpha_x k_x^2 - \alpha_y k_y^2)}{2[A^2 + \bar{k}^2]^{3/2}} \end{aligned} \quad (29)$$

where $A = \Delta + \alpha_x k_x^2 + \alpha_y k_y^2$, $\bar{k}^2 = v_x^2 k_x^2 + v_y^2 k_y^2$.

Since the c boost term does not affect the eigenvectors, the Berry connections and Berry curvatures are exactly the same as $c = 0$ case.

Because the upper band and lower band are always separated either directly or indirectly, thus a Chern number of lower band, independent of its filling, can always

be evaluated via the integral $\text{Ch}_- = \frac{1}{2\pi} \int_{\mathbb{R}^2} \Omega_-(\mathbf{k}) d^2\mathbf{k}$, which gives

$$\text{Ch}_- = \text{sgn}(v_x v_y) [2 \text{sgn}(\Delta) - \text{sgn}(\alpha_x) - \text{sgn}(\alpha_y)] / 4, \quad (30)$$

where $\text{sgn}()$ denotes the sign function [26].

The band Chern number, which is independent of the filling, is closely related to the zero temperature Hall conductance which does depend on the filling. The linear response theory gives the intrinsic Hall conductance [25] in the unit e^2/h as

$$\sigma_H = \frac{1}{2\pi} \int_{\mathbb{R}^2} \sum_{s=\pm} \Omega_s(\mathbf{k}) \Theta(-\epsilon_s(\mathbf{k})) d^2\mathbf{k} \quad (31)$$

where the unit step function $\Theta(\epsilon) = 1$ when $\epsilon > 0$ and $= 0$, when $\epsilon \leq 0$. it just replaces the \mathbb{T}^2 in a lattice Eq.9 by R^2 in the continuum.

Due to the C-symmetry, the intrinsic Hall conductance can be separated into two parts

$$\begin{aligned} \sigma_H &= \frac{1}{2\pi} \int_{\mathbb{R}^2} \Omega_-(\mathbf{k}) d^2\mathbf{k} + \frac{1}{\pi} \int_{\mathbb{R}^2} \Omega_+(\mathbf{k}) \Theta(-\epsilon_+(\mathbf{k})) d^2\mathbf{k} \\ &= \text{Ch}_- + \nu_b \end{aligned} \quad (32)$$

whose interpretation in terms of the edge states in a strip geometry will be given in Sec.IV-A-1.

When $\max \epsilon_-(\mathbf{k}) < 0 < \min \epsilon_+(\mathbf{k})$, $\nu_b = 0$ and $\sigma_H = \text{Ch}_-$. However, when $\min \epsilon_+(\mathbf{k}) < 0 < \max \epsilon_-(\mathbf{k})$, the evaluation of the second integral in Eq.(32) gives

$$\nu_b = \text{sgn}(\text{Ch}_-) \frac{\text{sgn}(\alpha_y \Delta) - 1}{2} \frac{c - |v_y|}{c} \quad (33)$$

which indicates that ν_b and Ch_- always have opposite sign. So $|\sigma_H|$ is always smaller than $|\text{Ch}_-|$.

Using Eq.(30), one can reproduce the correct Chern number calculated from the lattice Hamiltonian Eq.6.

I) When $h \sim 4t$, $\Delta = 4t - h$, $\alpha_x = \alpha_y = -t$, $v_x = v_y = -2t_s$, thus $\text{Ch}_- = [\text{sgn}(4t - h) + \text{sgn}(t)]/2$;

If $t > 0$, $\text{Ch}_- = +1$ when $h < 4t$ (aka $h/|t| < 4$), 0 otherwise;

If $t < 0$, $\text{Ch}_- = -1$ when $h > 4t$ (aka $h/|t| > -4$), 0 otherwise.

II) When $h \sim 0$, $\Delta_1 = \Delta_2 = -h$, $\alpha_{1x} = -\alpha_{1y} = -\alpha_{2x} = \alpha_{2y} = t$, $v_{1x} = -v_{1y} = -v_{2x} = v_{2y} = 2t_s$, thus $\text{Ch}_- = \text{Ch}_{1-} + \text{Ch}_{2-} = -\text{sgn}(-h) = \text{sgn}(h)$;

III) When $h \sim -4t$, $\Delta = -4t - h$, $\alpha_x = \alpha_y = t$, $v_x = v_y = 2t_s$, thus $\text{Ch}_- = [\text{sgn}(-4t - h) - \text{sgn}(t)]/2$;

If $t > 0$, $\text{Ch}_- = -1$ when $h > -4t$ (aka $h/|t| > -4$), 0 otherwise;

If $t < 0$, $\text{Ch}_- = +1$ when $h < -4t$ (aka $h/|t| < -4$), 0 otherwise.

These I),II),III) are indeed consistent with Eq.(8) achieved on a lattice. Notice that Ch_- , if it is not zero, only depends on $\text{sgn}(h)$, but independent of $\text{sgn}(t)$ and $\text{sgn}(t_s)$.

The $\alpha_x\alpha_y > 0$ case corresponding to $|h/t| \sim 4$ transition, and $\alpha_x\alpha_y < 0$ case corresponding to $|h/t| \sim 0$ transition. Since the sign of $\alpha_x\alpha_y$ makes the topological property dramatically different, in the following, we will discuss $\alpha_x\alpha_y > 0$ and $\alpha_x\alpha_y < 0$ separately.

A. The bulk topological transitions near $|h/t| = 4$ (the $\alpha_x\alpha_y > 0$ case)

Without loss of generality, we consider $h/t \sim -4$ and near $\mathbf{K}_0 = (0, 0)$ case, which belongs to the $\alpha_x\alpha_y > 0$ case,

$$H_0(\mathbf{k}) = [\Delta + \alpha(k_x^2 + k_y^2)]\sigma_z + vk_x\sigma_x + vk_y\sigma_y - ck_y\sigma_0 \quad (34)$$

where $\Delta = -(h + 4t)$, $\alpha = t$, $v = 2t_s$, $c = 2t_b$. Diagonalization of Eq.(34) leads to two bands

$$\epsilon_{\pm}(\mathbf{k}) = \pm\sqrt{v^2k^2 + (\Delta + \alpha k^2)^2} - ck_y \quad (35)$$

As shown in Fig.11, when $\alpha\Delta > 0$, the critical velocity $c_0 = \sqrt{v^2 + 4\alpha\Delta}$. When $\alpha\Delta < 0$, the critical velocity $c_0 = |v|$. The phase diagram of Eq.(34) is given in Fig.12.

At a fixed Δ , when $c \rightarrow c_0$, energy bands overlap. There is an electron pocket near $\mathbf{k} = (0, \sqrt{|\Delta/\alpha|})$ with $z = 2$ in the $k_y > 0$ regime and the corresponding hole pocket near $\mathbf{k} = (0, -\sqrt{|\Delta/\alpha|})$ with $z = 2$ in the $k_y < 0$ regime. When $|c - c_0| \ll v$, the gap in Eq.19 vanishes linearly as $c \rightarrow c_0$ with

$$\tilde{\Delta} = \min_k \epsilon_+(k) = \sqrt{|\Delta/\alpha|}(c - c_0) + \dots \quad (36)$$

At a fixed $c < v$, when $\Delta \rightarrow 0$, then the upper band and lower band conic touch at $k = 0$ with $z = 1$. When $|\Delta| \ll v^2/\alpha$, the gap vanishes also linearly as $\Delta \rightarrow 0$ with

$$\tilde{\Delta} = \min_k \epsilon_+(k) = \sqrt{1 - c^2/v^2}|\Delta| + \dots \quad (37)$$

Both Eq.36 and Eq.37 will be used in evaluating various thermodynamic quantities in Sec.III-A-3.

1. Hall conductance at zero and finite temperatures

We will also evaluate the Hall conductance at zero and finite T respectively.

(a). Zero temperature Hall conductance

When $c < c_0$, the $T = 0$ intrinsic Hall conductance in unit e^2/h can be evaluated as $\sigma_H = \frac{1}{2\pi} \int_{\mathbb{R}^2} \Omega_-(\mathbf{k}) d^2\mathbf{k}$

$$\begin{aligned} \sigma_H &= Ch_- = [\text{sgn}(\Delta) - \text{sgn}(\alpha)]/2 \\ &= \text{sgn}(\Delta)[1 - \text{sgn}(\alpha\Delta)]/2 \end{aligned} \quad (38)$$

which can be obtained by just setting $\text{sgn}(\alpha_x) = \text{sgn}(\alpha_y)$ in Eq.30. It suggests that $\sigma_H = -1$ for $h < -4t$ and $\sigma_{xy} = 0$ for $h > -4t$ If choosing $t > 0$, this is consistent with calculation on lattice scale.

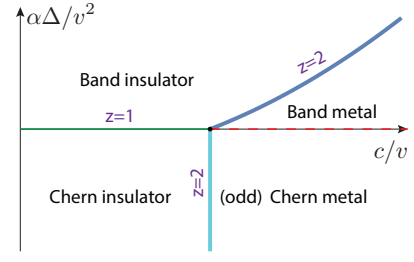


FIG. 12. The phase diagram of Eq.(34). It is the part near $h/t \sim \pm 4$ in the global phase diagram in Fig.3 where the Odd Chern metal is the A1 phase. Thick/thin/dashed line are 2nd/3rd/infinite order Topological phase transitions (TPTs) respectively. The Chern insulator with $Ch_- = 1, \sigma_H = 1$ to the insulator with $Ch_- = 0, \sigma_H = 0$ is 3rd order TPT due to the linear band touching of the Dirac fermion with $z = 1$. The Dirac fermion at $c/v = 0$ has the emergent Lorentz invariance which is broken by any $0 < c/v < 1$. The Chern insulator to the Odd Chern metal with $Ch_- = 1, \sigma_H < 1$ and $z = 2$ transition can be read from Fig.13. The band insulator to the band metal transition with $z = 2$ can be read from the first 3 boxes in Fig.3. The dashed line from the Odd Chern metal to the band metal with $Ch_- = 0, \sigma_H = 0$ due to the conic band touching between the P- and the H- FS is infinite order and can be read from the 3rd to the 5th boxes in Fig.3.

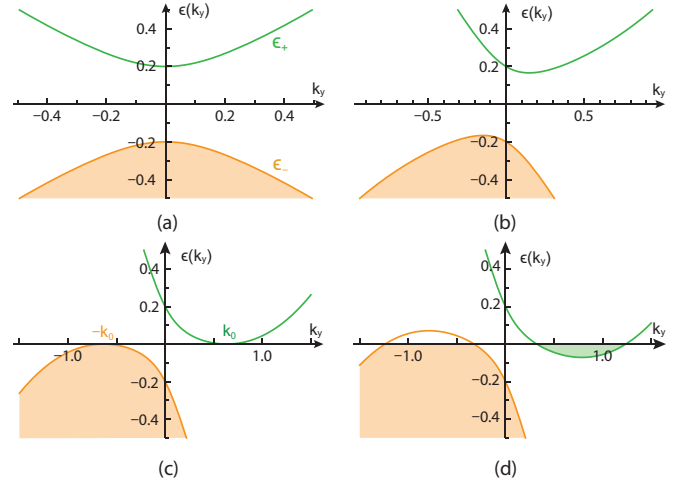


FIG. 13. The dispersion $\epsilon_{\pm}(k)$ as function of k_y with fixed $k_x = 0$ and $v = 1$, $\Delta = 1/5$, $\alpha = -1/2$, $c = 0, 0.5, 1.0, 1.1$. (a) it has a direct gap at $k_y = 0$, (b) it has an indirect gap at $k_y \neq 0$, (c) it becomes gapless and shows Fermi points at $k_y = \pm k_0$ with the quadratic band touching and $z = 2$, (d) it becomes gapless and show finite Fermi pockets. It is the A1 phase in Fig.3.

When $c > c_0$, there is an electron pocket near $\mathbf{k} = (0, \sqrt{|\Delta/\alpha|})$ in the $k_y > 0$ regime, and a hole pocket near $\mathbf{k} = (0, -\sqrt{|\Delta/\alpha|})$ in the $k_y < 0$ regime (Fig.13). Both $+/-$ band contribute to the Hall conductance as

shown in Eq.32.

$$\sigma_H = \frac{1}{2\pi} \int_{\mathbb{R}^2} \Omega_-(\mathbf{k}) d^2\mathbf{k} + \frac{1}{\pi} \int_{\mathbb{R}^2} \Omega_+(\mathbf{k}) \Theta(-\epsilon_+(\mathbf{k})) d^2\mathbf{k} \quad (39)$$

Because the electron FS is a simple closed loop, Eq.39 can be expressed as the Berry phase for an adiabatic path around the FS [3]

$$\sigma_H = \text{Ch}_- + \frac{1}{\pi} \oint d\mathbf{k}_F \cdot \mathbf{A}_+(\mathbf{k}_F) = \text{Ch}_- + \frac{\phi_+}{\pi}. \quad (40)$$

Evaluation of the integral Eq.39 or Eq.(40) leads to the same result

$$\begin{aligned} \sigma_H &= \text{Ch}_- \left[1 + \frac{c-v}{c} \Theta(c-v) \Theta(-\alpha\Delta) \right] \\ &= \text{sgn}(\Delta) \times \min(1, v/c) \quad \text{if } \alpha\Delta < 0 \end{aligned} \quad (41)$$

otherwise 0. The Hall conductance developed a cusp at the critical velocity $c = v$ as shown in Fig.14.

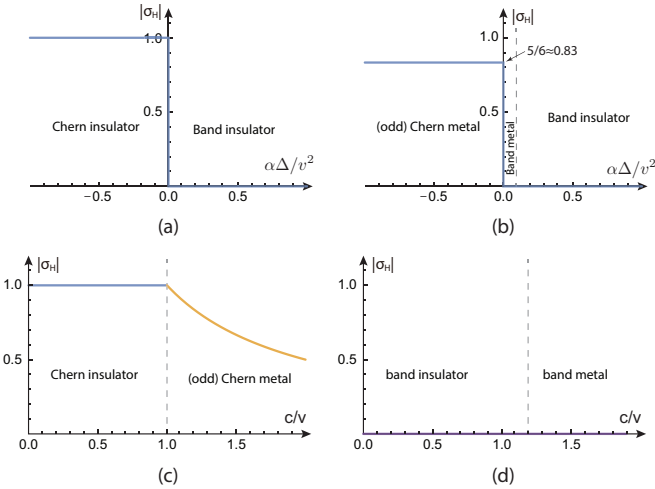


FIG. 14. The Hall conductance of Eq.(34) at different $\alpha\Delta/v^2$ or c/v values: Varying $\alpha\Delta/v^2$ in (a) and (b): (a) fixing $c/v = 0.5$, (b) fixing $c/v = 1.2$. There is a jump from Odd Chern metal to the band metal with the magnitude $v/c = 5/6$. However, as indicated in Fig.12, it is infinite order. Varying c/v in (c) and (d): (c) fixing $\alpha\Delta/v^2 = -0.1$, (d) fixing $\alpha\Delta/v^2 = +0.1$. Again, as already alerted in Fig.4d, in a generic case, the BM should contribute to a un-quantized AHE (See Fig.24 and Table 1). But it vanishes in this particular $n = 1$ case due to the fine tuning. They match all the TPTs achieved on the lattice shown in Fig.4, so the captions of Fig.4 on the universality classes of the TPTs also apply here.

(b). Finite temperature Hall conductance

When $c < c_0$, the intrinsic Hall conductance [25] in unit e^2/h can be evaluated as

$$\sigma_H(T) = \frac{1}{2\pi} \sum_{s=\pm} \int_{\mathbb{R}^2} d^2\mathbf{k} \Omega_s(\mathbf{k}) f(\epsilon_s(k)) \quad (42)$$

which is just replacing T^2 in Eq.10 by R^2 .

Due to the C-symmetry, the finite temperature Hall conductance can be expressed as

$$\begin{aligned} \sigma_H(T) &= \text{Ch}_- + \frac{1}{\pi} \int_{\mathbb{R}^2} d^2\mathbf{k} \Omega_+(\mathbf{k}) f(\epsilon_+(\mathbf{k})) \\ &= \text{Ch}_- + \nu(T) \end{aligned} \quad (43)$$

which is also just replacing T^2 in Eq.10 by R^2 .

The $\nu(T = 0)$ and Ch_- has been evaluated in Eq.30 and Eq.33 respectively. At low temperature T where T is the lowest energy scale, one can get a low temperature expansion of $\nu(T)$. By keeping the leading low T dependence, assuming $|\alpha\Delta/v^2| \ll 1/2$, we have

1) When $\alpha\Delta > 0$ in the band insulating phase, $\nu(T) - \nu(T = 0) \propto -\text{sgn}(\Delta) T e^{-|\Delta|/T}$; $-\text{sgn}(\Delta) T^2$; $-\text{sgn}(\Delta) T^2$ at $c < c_0$, $c = c_0$, $c > c_0$ respectively.

2) When $\alpha\Delta < 0$ in the Chern insulating phase, $\nu(T) - \nu(T = 0) \propto -\text{sgn}(\Delta) T e^{-|\Delta|/T}$; $-\text{sgn}(\Delta) T$; $-\text{sgn}(\Delta) T^2$ at $c < c_0$, $c = c_0$, $c > c_0$ respectively.

2. Ground-state energy density and topological phase transitions

When $c < c_0$, $\min \epsilon_+ \geq 0 \geq \max \epsilon_-$, the lower band is full occupied and the upper band is complete empty, thus the ground-state energy density is $E_{\text{GS}} = (4\pi^2)^{-1} \int_{\mathbb{R}^2} d^2\mathbf{k} \epsilon_-(\mathbf{k})$. The integral is divergent in R^2 , we need a cut-off Λ for k . Due to its odd property, the ck_y part in Eq.35 drops off, one obtain

$$E_0 = -\frac{|\Delta|^3}{6\pi v^2} + E_\Lambda \quad (44)$$

where E_Λ is Λ , $\alpha\Delta$ and v dependent function which is differentiable up to 3 degrees of differentiation, but may contain higher order non-analyticity.

When $c > c_0$, $\min \epsilon_+ < 0 < \max \epsilon_-$, both the lower band and the upper band are only partially occupied, thus the ground-state energy density becomes $E_{\text{GS}} = (4\pi^2)^{-1} \sum_{s=\pm} \int_{\mathbb{R}^2} d^2\mathbf{k} \epsilon_s(\mathbf{k}) \Theta(-\epsilon_s(\mathbf{k}))$. Due to the C-symmetry, it can be expressed as $E_{\text{GS}} = E_0 + E_1 \Theta(c - c_0)$, where the c -dependent part is $E_1 = (2\pi^2)^{-1} \int_{\mathbb{R}^2} d^2\mathbf{k} \epsilon_+(\mathbf{k}) \Theta(-\epsilon_+(\mathbf{k}))$. The integral is convergent, we obtain

$$\begin{aligned} E_1 &= -\frac{1}{16\pi\alpha^3} \left[\frac{1}{4} (c^2 - c_0^2) (c^2 + c_0^2 - 4v^2 - 8\alpha\Delta) \right. \\ &\quad \left. + v^2 (v^2 + 4\alpha\Delta) \ln(c/c_0) \right] \end{aligned} \quad (45)$$

In the following, we study the possible TPT encoded in the ground state energy density.

(a). Band insulator to Chern insulator transition

In the range $c < v$ and tuned by Δ , one only have the E_0 part. It is easy to see a third-order non-analytical behaviour at $\Delta = 0$,

$$E_{\text{GS}} = -\frac{|\Delta|^3}{6\pi v^2} + \dots \quad (46)$$

which has the dynamic exponent $z = 1$.

(b). *Band metal to Odd Chern metal transition:*

In the range $c > v$ and tuned by Δ , one need both E_0 and E_1 part. It is easy to see the third-order non-analytical behaviour at $\Delta = 0$ in the two parts gets canceled:

$$E_{\text{GS}} = -\frac{|\Delta|^3}{6\pi v^2} + \frac{|\Delta|^3}{6\pi v^2} + \dots \quad (47)$$

Carefully treating the exact results $E_{\text{GS}} = E_0 + E_1\Theta(c - c_0)$ tells E_{GS} is smooth at $\Delta = 0$, which is consistent with numerical result's infinite order differentiable. This fact explains why the 3rd order TPT across the green line changes to infinite order across the red dashed line in Fig.12. Even so, as shown in Fig.13b, there is still a universal jump $\Delta\sigma_H = v/c$, so it is still a TPT.

(c). *Band insulator to band metal transition:*

In the range $\alpha\Delta > 0$ and tuned by either Δ or c . It is easy to tell a second-order non-analytical behaviour at $\Delta = (c^2 - v^2)/(4\alpha)$ when tuning Δ ,

$$E_{\text{GS}} = E_0 - \frac{c^2 - v^2}{4\pi c^2} \left(\Delta - \frac{c^2 - v^2}{4\alpha}\right)^2 \Theta(c^2 - v^2 - 4\alpha\Delta) \quad (48)$$

and also a second-order non-analytical behaviour at $c = \sqrt{v^2 + 4\alpha\Delta}$ when tuning c ,

$$E_{\text{GS}} = E_0 - \frac{\Delta}{4\pi\alpha^2} (c - \sqrt{v^2 + 4\alpha\Delta})^2 \Theta(c^2 - v^2 - 4\alpha\Delta) \quad (49)$$

which has the dynamic exponent $z = 2$.

(d). *Chern insulator to Odd Chern metal transition*

In the range $\alpha\Delta < 0$ and tuned by c . It is easy to see a second-order non-analytical behaviour at $c = v$,

$$E_{\text{GS}} = E_0 + \frac{\alpha\Delta}{4\pi|\alpha|^3} (c - v)^2 \Theta(c^2 - v^2) + \dots \quad (50)$$

which has the dynamic exponent $z = 2$.

In summary, transitions (c) and (d) are second-order QPT with $z = 2$; (a) is third-order QPT with $z = 1$. (b) is infinite-order without any non-analyticity. These are consistent with the results achieved in a lattice in Sec.II-B.

3. Thermodynamic Quantities

(a). *The density of states*

From the Hamiltonian (25), the Matsubara Green's function

$$G(\mathbf{k}, i\omega_n) = \frac{P_+(\mathbf{k})}{i\omega_n - \epsilon_+(\mathbf{k})} + \frac{P_-(\mathbf{k})}{i\omega_n - \epsilon_-(\mathbf{k})} \quad (51)$$

where P_s are the projection operators onto $s = \pm$ bands and $P_+ + P_- = 1$.

The total DOS is

$$D(\omega) = \int \frac{d^2q}{(2\pi)^2} [\delta(\omega - \epsilon_+(k)) + \delta(\omega - \epsilon_-(k))] \quad (52)$$

It would be convenient to introduce the DOS for each band $D(\omega) = D_+(\omega) + D_-(\omega)$:

$$D_{\pm}(\omega) = \int \frac{d^2\mathbf{k}}{4\pi^2} \delta(\omega - \epsilon_{\pm}(\mathbf{k})), \quad (53)$$

Due to the C-symmetry, $D_+(\omega) = D_-(-\omega)$.

$$D_+(\omega) = \frac{1}{4\pi|\alpha|} [1 + \rho(\omega)] \Theta(\omega - \min \epsilon_+) \quad (54)$$

For some reason related to the C-symmetry, $\rho(\epsilon) = -\rho(-\epsilon)$ is an odd function. The odd property leads to flat feature of the total DOS near $\omega = 0$ when $\min \epsilon_+ < 0 < \max \epsilon_-$,

$$D(\omega) = \frac{1}{2\pi|\alpha|}, \text{ if } \min \epsilon_+ < \omega < \max \epsilon_- \quad (55)$$

The DOS is plotted in Fig.15.

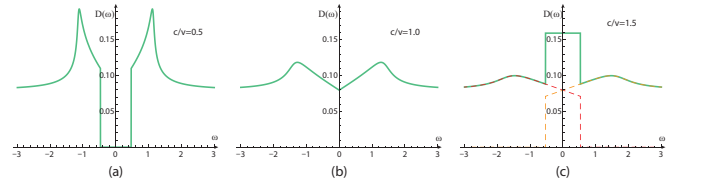


FIG. 15. Density of states (DOS) of Eq.(34) at different c/v values: (a) $c/v = 0.5$ in Chern Insulator, (b) $c/v = 1.0$ on the QCP between Chern insulator and Odd Chern metal, (c) $c/v = 1.5$ in Odd Chern metal. Here, we fixed $v = 1$, $\alpha = -1$, $\Delta = 1$ in Fig.12. Note that $\epsilon_{\pm}(k)$ is quadratic in k at the band minimum in Fig.13, which leads to a finite DOS at the band edge and $z = 2$. So the DOS at $\omega = 0$ in (b) is finite. The flat feature of total DOS near $\omega = 0$ is a result of truncation of $H(k)$ at the k^2 order. Indeed, the lattice calculations on DOS in Fig.10 shows that it is not a constant anymore. It matches Fig.10 very well near the low energy $\omega \sim 0$.

(b). *The specific heat and Compressibility*

Here, we will make use of the DOS to evaluate the two conserved quantities, then compute the Wilson ratio. The Helmholtz free energy density (taking $k_B = 1$)

$$F(T) = -T \int \frac{d^2\mathbf{k}}{(2\pi)^2} \ln[2(1 + \cosh(\epsilon_+(\mathbf{k})/T))] \quad (56)$$

where the zero temperature part of $F(T)$ is nothing but the ground-state energy density E_{GS} calculated in Sec.III-A-2. The specific heat (at constant volume) is given by

$$C_v(T) = \int \frac{d^2\mathbf{k}}{(2\pi)^2} \frac{[\epsilon_+(\mathbf{k})]^2}{T^2 [1 + \cosh(\epsilon_+(\mathbf{k})/T)]} \quad (57)$$

The dynamic density-density response function is

$$\chi^{00}(q, i\omega_n) = -T \sum_{iv_m, k} \text{Tr}[G(i\omega_n + iv_m, k + q)G(iv_m, k)] \quad (58)$$

Taking the $\omega_n \rightarrow 0$, then $q \rightarrow 0$ limit in $\chi^{00}(q, i\omega_n)$ gives the (isothermal) uniform compressibility

$$\kappa_u(T) = \sum_{s=\pm} \int \frac{d^2k}{(2\pi)^2} \frac{\partial f(\epsilon_{s,k})}{\partial \epsilon_{s,k}} = \int \frac{d\omega D_+(\omega)}{T[1 + \cosh(\omega/T)]} \quad (59)$$

and the zero temperature limit $\frac{\partial f(\epsilon)}{\partial \epsilon} = \delta(\epsilon)$ recovery the well-known relation between compressibility and DOS $\kappa_u(T) = D(0)$.

At low temperature $T \ll |\Delta|, v^2/|\alpha|, c^2/|\alpha|, |(c^2 - v^2)/\alpha|$, one can get a low temperature expansion of $C_v(T)$ and $\kappa_u(T)$ [38]. We do not need to distinguish $\alpha\Delta > 0$ or $\alpha\Delta < 0$, but need to care if $\Delta = 0$ or not. By keeping the leading low T dependence, assuming $|\alpha\Delta/v^2| < 1/2$ to simplify the technical calculations [37], we have

$\Delta \neq 0$ case in Fig.12

At $c < c_0$, we have $\tilde{\Delta} = \min_k \epsilon_+(k) > 0$ and $D(\omega) = 0$ for $|\omega| < \tilde{\Delta}$ and $D(\tilde{\Delta}) > 0$ at the gap edge (Fig.15a), thus $C_v(T) = 2D(\tilde{\Delta})\tilde{\Delta}^2 T^{-1} e^{-\tilde{\Delta}/T}$. Similarly, $\kappa_u(T) = 2D(\tilde{\Delta})T e^{-|\tilde{\Delta}|/T}$.

At $c = c_0$, we have $\tilde{\Delta} = \min_k \epsilon_+(k) = 0$ and $D(\omega) = D(0) + D'(0^+)|\omega|$ for small $|\omega|$ (Fig.15b), thus $C_v(T) = \frac{\pi^2}{3} D(0)T$. Here $D'(0^+)$ means the right derivatives of $D(\omega)$ at 0. Similarly, $\kappa_u(T) = D(0) + 2 \ln 2D'(0^+)T$;

At $c > c_0$, we have $\tilde{\Delta} = \min_k \epsilon_+(k) < 0$ and $D(\omega) = \frac{1}{2\pi|\alpha|}$ for $|\omega| < |\tilde{\Delta}|$ in Eq.55 and $D(\tilde{\Delta}) > 0$ (Fig.15c), thus $C_v(T) = \frac{\pi^2}{3} D(0)T$. Similarly, $\kappa_u(T) = D(0) + 2[D(\tilde{\Delta}) - D(0)]T e^{-|\tilde{\Delta}|/T}$.

$\Delta = 0$ case in Fig.12

At $c < c_0$, we have $\tilde{\Delta} = \min_k \epsilon_+(k) = 0$ and $D(\omega) = D'(0^+)|\omega|$ for small ω , thus $C_v(T) = 9\zeta(3)D'(0^+)T^2$ where $\zeta(3) \approx 1.2021$. Similarly, $\kappa_u(T) = 2 \ln 2D'(0^+)T$.

At $c = c_0$, we have $\tilde{\Delta} = \min_k \epsilon_+(k) = 0$ and $D(\omega) = D(0) + A|\omega|^{2/3} > 0$ for small ω , thus $C_v(T) = \frac{\pi^2}{3} D(0)T$. Similarly, $\kappa_u(T) = D(0) + 1.1486AT^{5/3}$.

At $c > c_0$, we have $\tilde{\Delta} = \min_k \epsilon_+(k) < 0$ and $D(\omega) = \text{const.}$ for $|\omega| < |\tilde{\Delta}|$, thus $C_v(T) = \frac{\pi^2}{3} D(0)T$. Similarly, $\kappa_u(T) = D(0) + 2[D(\tilde{\Delta}) - D(0)]T e^{-|\tilde{\Delta}|/T}$.

When taking only the leading term in the low-temperature specific heat and compressibility, we have:

When $\Delta \neq 0$: at $c < c_0$, $C_v(T) = 2D(\tilde{\Delta})\tilde{\Delta}^2 T^{-1} e^{-\tilde{\Delta}/T}$ and $\kappa_u(T) = 2D(\tilde{\Delta})T e^{-|\tilde{\Delta}|/T}$; at $c \geq c_0$, $C_v(T) = \frac{\pi^2}{3} D(0)T$ and $\kappa_u(T) = D(0)$.

When $\Delta = 0$: at $c < c_0$, $C_v(T) = 9\zeta(3)D'(0^+)T^2$ and $\kappa_u(T) = 2 \ln 2D'(0^+)T$; at $c \geq c_0$, $C_v(T) = \frac{\pi^2}{3} D(0)T$ and $\kappa_u(T) = D(0)$.

(c). Wilson ratio

The Wilson ratio is defined as $R_W = T\kappa_u/C_v$ which has the following low temperature behaviours:

$\Delta \neq 0$ case

At $c < c_0$, $R_W = (T/\tilde{\Delta})^2$; At $c \geq c_0$, $R_W = 3/\pi^2$.

$\Delta = 0$ case

At $c < c_0$, $R_W = 2 \ln 2 / (9\zeta(3)) \approx 0.1281$; At $c \geq c_0$, $R_W = 3/\pi^2$.

These results are consistent with those achieved directly on the lattice in Sec.II-C-3 and also listed in the last line of Table-I.

B. The bulk topological phase transitions near $|h/t| \sim 0$ (the $\alpha_x\alpha_y < 0$ case).

When $h \sim 0$ and near the two valleys $K_1 = (\pi, 0)$ and $K_2 = (0, \pi)$, we have

$$\begin{aligned} H_1 &= [\Delta - \alpha(k_x^2 - k_y^2)]\sigma_z - vk_x\sigma_x + vk_y\sigma_y - ck_y\sigma_0 \\ H_2 &= [\Delta + \alpha(k_x^2 - k_y^2)]\sigma_z + vk_x\sigma_x - vk_y\sigma_y + ck_y\sigma_0 \end{aligned} \quad (60)$$

where $\Delta = -h$ and other parameters are the same as the $h \sim 4t$ case discussed in Sec.III-A. Note the opposite sign of the velocities v between k_x and k_y and opposite sign of α between k_x^2 and k_y^2 indicating $\alpha_x\alpha_y < 0$.

Due to the two valleys, we obtain four bands

$$\epsilon_{i,\pm} = \pm \sqrt{v^2k^2 + [\Delta + \eta_i\alpha(k_x^2 - k_y^2)]^2} + \eta_i ck_y, \quad (61)$$

where $\eta_i = (-1)^i$ and $i = 1, 2$. It can be compared to Eq.35 in the $\alpha_x\alpha_y > 0$ case. So the two cases should have quite different physical properties.

When $\alpha\Delta < 0$, the two critical velocities $c_1 = |v| < c_2 = \sqrt{v^2 - 4\alpha\Delta}$. When $\sqrt{v^2 - 4\alpha\Delta} > c > |v|$, Thus only H_1 becomes metal. When $c > \max(c_1, c_2)$, both H_1 and H_2 become metal.

When $\alpha\Delta > 0$, the two critical velocities $c_1 = \sqrt{v^2 + 4\alpha\Delta} > c_2 = |v|$. When $\sqrt{v^2 + 4\alpha\Delta} > c > |v|$, Thus only H_2 becomes metal. When $c > \max(c_1, c_2)$, then both H_1 and H_2 become metal.

Another new feature of $\alpha_x\alpha_y < 0$ is that the FS extends to infinity when $c \geq \sqrt{2}|v|$. The divergent k_F suggests a FS collision between the two valleys, which is consistent with the existence of phase C1 or C2 in the global lattice phase diagram Fig.3. Below, we will not discuss the C- phase, so restrict $c < \sqrt{2}|v|$. If $c > \sqrt{2}|v|$, it leads to the class-3 TPT discussed in [30] and reviewed in Sec.II.

1. Hall conductance at zero and finite temperatures

(a). Zero temperature

When $c < \min(c_1, c_2)$, the Hall conductance σ_H of each valleys gives $\sigma_H^{(i)} = -\text{sgn}(\Delta)/2$, adding the two contributions together leads to

$$\sigma_H = \sigma_H^{(1)} + \sigma_H^{(2)} = -\text{sgn}(\Delta) \quad (62)$$

which indicates $\sigma_H = -1$ for $\Delta > 0$ and $\sigma_H = +1$ for $\Delta < 0$.

If $c > \min(c_1, c_2)$, then we need to discuss $\alpha\Delta > 0$ or $\alpha\Delta < 0$ separately.

Case $\alpha\Delta < 0$:

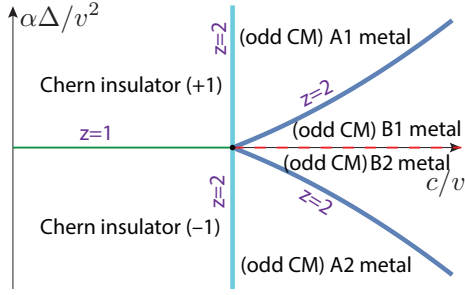


FIG. 16. The phase diagram of Eq.(60). It is the part near $h/t \sim \pm 0$ in the global phase diagram in Fig.3. Similar to Fig.12, Thick/thin/dashed line are 2nd/3rd/infinite order Topological phase transitions (TPTs) respectively. The consecutive Chern insulator to A1 Odd Chern metal, then to B1 Odd Chern metal transitions can be read from Fig.17. The dashed line from the B1 Odd Chern metal to the B2 Odd Chern metal can be read from the B1 box and B1/B2 box on the right in Fig.3. Similar to A1 Odd Chern metal to band metal transition in Fig.12, it is also induced by the conic touching of the P- and H- FS and also infinite order.

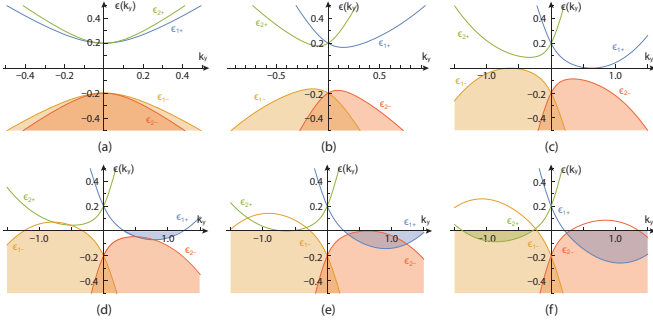


FIG. 17. The dispersion $\epsilon_{i,\pm}(k)$ as function of k_y with fixed $k_x = 0$ and $v = 1$, $\Delta = 1/5$, $\alpha = -1/2 < 0$, $c = 0, 0.5, 1.0, \sqrt{1.4}, 1.3$. (a) both H_1 and H_2 has a direct gap at $k_y = 0$; in Chern insulator phase. (b) Due to the opposite boost velocity in Eq.61, the dispersion at K_1 and K_2 shift to the opposite directions. both H_1 and H_2 has an indirect gap at $k_y \neq 0$; (c) H_1 becomes gapless and shows two Fermi points at $k_y = \pm k_0$ with $z = 2$, but H_2 still has an indirect gap. It corresponds to A1/B1 in Fig.3. (d) H_1 becomes gapless and show two finite Fermi pockets, but H_2 becomes gapless and shows two Fermi points still at $k_y = \pm k_0$ also with $z = 2$ after subtracting the non-critical H_1 part; (e) both H_1 and H_2 are gapless and show finite Fermi pockets [35]. It corresponds to B1 in Fig.3.

If $c_2 > c > c_1 = |v|$, H_1 first develops an instability while H_2 remains gapped.

$$\begin{aligned}\sigma_H^{(1)} &= -\text{sgn}(\Delta)/2 + \text{sgn}(\Delta)\frac{c-v}{c}\Theta(v-c), \\ \sigma_H^{(2)} &= -\text{sgn}(\Delta)/2\end{aligned}\quad (63)$$

If $c > c_2$, both H_1 and H_2 are gapless, however, $\sigma_{xy}^{(2)}$ remains the same as $c = 0$ as dictated by Eq.33. Thus,

we arrive at

$$\sigma_H = \text{sgn}(\Delta) \min(1, v/c) \quad (64)$$

Case $\alpha\Delta > 0$:

If $c_1 > c > c_2 = |v|$, H_2 first develops an instability while H_1 remains gapped.

$$\begin{aligned}\sigma_H^{(1)} &= -\text{sgn}(\Delta)/2, \\ \sigma_H^{(2)} &= -\text{sgn}(\Delta)/2 + \text{sgn}(\Delta)\frac{c-v}{c}\Theta(v-c)\end{aligned}\quad (65)$$

If $c > c_1$, both H_1 and H_2 are gapless, however, $\sigma_{xy}^{(1)}$ remains the same as $c = 0$ as also dictated by Eq.33. Thus, we also arrive at Eq.64.

So we always have the Hall conductance Eq.64, no matter in the insulating phase or the metallic phase which is independent of many microscopic details.

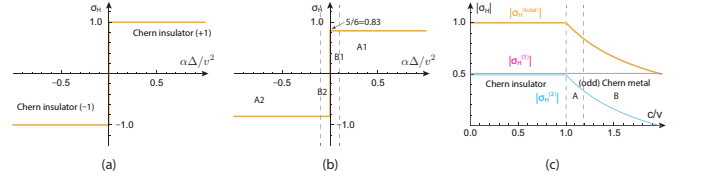


FIG. 18. The Hall conductance of Eq.60 at different $\alpha\Delta/v^2$ or c/v values: varying $\alpha\Delta/v^2$ in (a) and (b): (a) fix $c/v = 0.5$ (b) fix $c/v = 1.2$. There is a jump from B2 to B1 with the magnitude $2 \times v/c = 2 \times 5/6$, but no change from B1 to A1 Odd Chern metal phase. However, as indicated in Fig.16, the former is infinite order, the latter is 2nd order with $z = 2$. See also Fig.4b on a lattice. Varying c/v in (c) fix $\alpha\Delta/v^2 = -0.1$, σ_H^1 stays as a constant. But $\sigma_H = \sigma_H^1 + \sigma_H^2 = v/c$.

(b). Finite temperature Hall conductance

Similar to the $\alpha_x\alpha_y > 0$ case in Eq.43, the finite temperature Hall conductance at the valley i is

$$\begin{aligned}\sigma_H^{(i)}(T) &= \sigma_H^{(i)}(T=0) + \frac{1}{\pi} \int_{\mathbb{R}^2} d^2\mathbf{k} \Omega_{i,+}(\mathbf{k}) \\ &\times [f(\epsilon_{i,+}(\mathbf{k})) - \Theta(-\epsilon_{i,+}(\mathbf{k}))] \\ &= \text{Ch}_{i,-} + \frac{1}{\pi} \int_{\mathbb{R}^2} d^2\mathbf{k} \Omega_{i,+}(\mathbf{k}) f(\epsilon_{i,+}(\mathbf{k}))\end{aligned}\quad (66)$$

Thus, the total Hall conductance is:

$$\begin{aligned}\sigma_H(T) &= \sigma_H^{(1)}(T) + \sigma_H^{(2)}(T) \\ &= \text{Ch}_{1,-} + \text{Ch}_{2,-} + \nu_1(T) + \nu_2(T)\end{aligned}\quad (67)$$

where $\text{Ch}_{i,-}$ and $\nu_i(T=0)$ has been studied in Sec.III-A-1.

At a low temperature T which is the lowest energy scale, one can get a low temperature expansion of $\nu_i(T)$. Without loss of generality, we choose $\alpha\Delta < 0$ case, the two critical velocities $c_1 = |v| < c_2 = \sqrt{v^2 - 4\alpha\Delta} = \sqrt{v^2 + 4|\alpha\Delta|}$. By keeping the leading low T dependence and assuming $|\alpha\Delta/v^2| \ll 1/2$, we have

At $c < c_1$, H_1 has a gap $2\tilde{\Delta}_1$ and H_2 has a bigger gap $2\tilde{\Delta}_2 > 2\tilde{\Delta}_1$. Thus, $\nu_1(T) - \nu_1(T=0) \propto -\text{sgn}(\Delta)Te^{-|\tilde{\Delta}_1|/T}$ and $\nu_2(T) - \nu_2(T=0) \propto -\text{sgn}(\Delta)Te^{-|\tilde{\Delta}_2|/T}$;

At $c = c_1$, H_1 is critical with $\tilde{\Delta}_1 = 0$ and H_2 still has a gap $2\tilde{\Delta}_2$. Thus, $\nu_1(T) - \nu_1(T=0) \propto -\text{sgn}(\Delta)T$ and $\nu_2(T) - \nu_2(T=0) \propto -\text{sgn}(\Delta)Te^{-|\tilde{\Delta}_2|/T}$;

At $c_2 > c > c_1$, H_1 is gapless and H_2 still has a gap $2\tilde{\Delta}_2$. Thus, $\nu_1(T) - \nu_1(T=0) \propto -\text{sgn}(\Delta)T^2$ and $\nu_2(T) - \nu_2(T=0) \propto -\text{sgn}(\Delta)Te^{-|\tilde{\Delta}_2|/T}$;

At $c = c_2$, H_1 is gapless and H_2 is also critical with $\tilde{\Delta}_2 = 0$. Thus, $\nu_1(T) - \nu_1(T=0) \propto -\text{sgn}(\Delta)T^2$ and $\nu_2(T) - \nu_2(T=0) \propto -\text{sgn}(\Delta)T$;

At $c > c_2$, both H_1 and H_2 are gapless. Thus, $\nu_1(T) - \nu_1(T=0) \propto -\text{sgn}(\Delta)T^2$ and $\nu_2(T) - \nu_2(T=0) \propto -\text{sgn}(\Delta)T^2$.

In summary, if we only need the leading behaviors of $\nu(T) = \nu_1(T) + \nu_2(T)$, then we have:

At $c < c_1$, $\nu(T) - \nu(T=0) \propto -\text{sgn}(\Delta)Te^{-|\tilde{\Delta}_1|/T}$; at $c = c_1$, $\nu(T) - \nu(T=0) \propto -\text{sgn}(\Delta)T$; at $c_2 > c > c_1$, $\nu(T) - \nu(T=0) \propto -\text{sgn}(\Delta)T^2$; at $c = c_2$, $\nu(T) - \nu(T=0) \propto -\text{sgn}(\Delta)T$; at $c > c_2$, $\nu(T) - \nu(T=0) \propto -\text{sgn}(\Delta)T^2$.

2. Ground-state energy density and topological phase transitions

When $c < \min(c_1, c_2)$, $\min \epsilon_{i,+} \geq 0 \geq \max \epsilon_{i,-}$, both valley 1&2's lower band is full occupied and 1&2's upper band is complete empty, thus the ground-state energy density is $E_{\text{GS}} = (4\pi^2)^{-1} \int_{\mathbb{R}^2} d^2\mathbf{k} [\epsilon_{1-}(\mathbf{k}) + \epsilon_{2-}(\mathbf{k})]$. The integral is divergent, we need a cut-off Λ for k . Due to its odd property, the ck_y part in Eq.61 drops off, one obtain:

$$E_0 = -\frac{|\Delta|^3}{3\pi v^2} + E_\Lambda \quad (68)$$

where E_Λ is Λ , $\alpha\Delta$ and v dependent C^3 function. Note that E_Λ in the $\alpha_x\alpha_y < 0$ case is dramatically different from that in the $\alpha_x\alpha_y > 0$ case listed in Eq.44.

When $\max(c_1, c_2) > c > \min(c_1, c_2)$, one of $\epsilon_{1,-}$ and $\epsilon_{2,-}$ are partially filled, then there is another parts E_1 and $E_{\text{GS}} = E_0 + E_1$; When $c > \max(c_1, c_2)$, both $\epsilon_{1,-}$ and $\epsilon_{2,-}$ are partially filled, then there is also one more part E_2 and $E_{\text{GS}} = E_0 + E_1 + E_2$, where E_1 and E_2 are slightly more complicated than that in the $\alpha_x\alpha_y > 0$ case listed in Eq.45:

$$\begin{aligned} E_1 &= \frac{-\pi}{32|\alpha|^3} [8\alpha\Delta v^2 + 2v^4(\arcsin \frac{c}{\sqrt{2}v} - \frac{\pi}{4}) \\ &\quad + c\sqrt{2v^2 - c^2}(v^2 - 8\alpha\Delta - c^2)] \\ E_2 &= \frac{-\pi}{32|\alpha|^3} [4\alpha\Delta\sqrt{v^4 - 16\alpha^2\Delta^2} \\ &\quad + 2v^4(\arcsin \frac{c}{\sqrt{2}v} - \frac{1}{2}\arccos \frac{4\alpha\Delta}{v^2}) \\ &\quad + c(v^2 - 8\alpha\Delta - c^2)\sqrt{2v^2 - c^2}] \quad (69) \end{aligned}$$

(a). *Chern insulator (+1) to Chern insulator (-1) transition:*

In the range $c < v$ and tuned by Δ , one only have the E_0 part which has a third-order non-analytical behaviour at $\Delta = 0$,

$$E_{\text{GS}} = -\frac{|\Delta|^3}{3\pi v^2} + \dots \quad (70)$$

which has the dynamic exponent $z = 1$.

(b). *B1 Odd Chern metal to B2 Odd Chern metal transition:*

In the range $c > v$ and the driven parameter is Δ . Now we have both E_0 and $E_1 + E_2$ part, the third-order non-analytical term at $\Delta = 0$ from the two parts gets canceled,

$$E_{\text{GS}} = -\frac{|\Delta|^3}{3\pi v^2} + \frac{|\Delta|^3}{3\pi v^2} + \dots \quad (71)$$

which explains why the 3rd order TPT across the green line changes to infinite order across the red dashed line in Fig.16. Even so, as shown in Fig.17b, there is still a universal jump $\Delta\sigma_H = 2v/c$, so it is still a TPT.

(c). *Odd Chern A metal to Odd Chern B metal transition*

In the range $\alpha\Delta > 0$ and tuned by either Δ or c , one finds a second-order non-analytical behaviour at $\Delta = (c^2 - v^2)/(4\alpha)$ tuned by Δ ,

$$\begin{aligned} E_{\text{GS}} &= \frac{v^2 - c^2}{4\pi\alpha\sqrt{c^2(2v^2 - c^2)}} [\Delta - (c^2 - v^2)/(4\alpha)]^2 \\ &\quad \times \Theta(c^2 - v^2 - 4\alpha\Delta) + \dots \quad (72) \end{aligned}$$

and also a second-order non-analytical behaviour at $c = \sqrt{v^2 + 4\alpha\Delta}$ tuned by c ,

$$\begin{aligned} E_{\text{GS}} &= -\frac{\Delta\sqrt{v^2 + 4\alpha\Delta}}{4\pi\alpha\sqrt{v^2 - 4\alpha\Delta}} (c - \sqrt{v^2 + 4\alpha\Delta})^2 \\ &\quad \times \Theta(c^2 - v^2 - 4\alpha\Delta) + \dots \quad (73) \end{aligned}$$

which has the dynamic exponent $z = 2$.

(d). *Chern insulator to A Odd Chern metal transition:*

In the range $\alpha\Delta > 0$ and tuned by c , one finds a second-order non-analytical behaviour at $c = v$,

$$E_{\text{GS}} = E_0 - \frac{(c - v)^2\Delta}{4\pi\alpha^2} \Theta(c - v) + \dots \quad (74)$$

which has the dynamic exponent $z = 2$.

In summary, (c) and (d) are 2nd-order with $z = 2$; (a) is 3rd-order with $z = 1$; (b) is infinite-order.

3. Thermodynamic quantities

(a). *The density of states*

From the Hamiltonian (25), the Matsubara Green's function

$$G_i(\mathbf{k}, i\omega_n) = \frac{P_{i,+}(\mathbf{k})}{i\omega_n - \epsilon_{i,+}(\mathbf{k})} + \frac{P_{i,-}(\mathbf{k})}{i\omega_n - \epsilon_{i,-}(\mathbf{k})} \quad (75)$$

where $P_{i,s}$ are the projection operators onto $s = \pm$ bands.

The total DOS for each flavor is

$$D_i(\omega) = \int \frac{d^2q}{(2\pi)^2} [\delta(\omega - \epsilon_{i,+}(k)) + \delta(\omega - \epsilon_{i,-}(k))] \quad (76)$$

It would be convenient to introduce the DOS for each band $D_i(\omega) = D_{i,+}(\omega) + D_{i,-}(\omega)$:

$$D_{i,\pm}(\omega) = \int \frac{d^2\mathbf{k}}{4\pi^2} \delta(\omega - \epsilon_{i,\pm}(\mathbf{k})), \quad (77)$$

Due to the C-symmetry, $D_{i,+}(\omega) = D_{i,-}(-\omega)$. Similar to Eq.54, we also have

$$D_{i,+}(\omega) = \frac{1}{4\pi|\alpha|} \sqrt{\frac{c^2}{2v^2 - c^2}} [1 + \rho_i(\omega)] \Theta(\omega - \min \epsilon_{i,+}) \quad (78)$$

where $\rho_i(\omega) = -\rho_i(-\omega)$ is an odd function. When $\min \epsilon_{i,+} < 0 < \max \epsilon_{i,-}$, the odd property leads to the flat feature of total DOS $D(\omega) = D_1(\omega) + D_2(\omega)$ for H_i near $\omega = 0$ (Fig.19):

$$D_i(\omega) = \frac{1}{2\pi|\alpha|} \sqrt{\frac{c^2}{2v^2 - c^2}}, \min \epsilon_{i,+} < \omega < \max \epsilon_{i,-} \quad (79)$$

where as alerted below Eq.61, we restrict $c < \sqrt{2}v$, so that the DOS remain finite. Otherwise, one must resort to the lattice calculations in Sec.II.

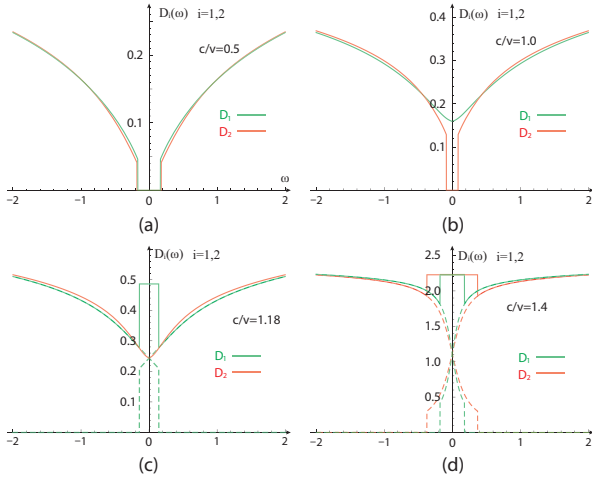


FIG. 19. The Density of states $D_1(\omega)$ and $D_2(\omega)$ of Eq.(60) at different c/v values: (a) $c/v = 0.5$, (b) $c/v = 1.0$, (c) $c/v = \sqrt{1.4} \approx 1.18$, (d) $c/v = 1.4$. Here, we fixed $v = 1$, $\alpha = 1/2$, $\Delta = 1/5$. In (c) and (d), the central plateau DOS value is given in Eq.79. Again, similar to Fig.15, the flat feature of total DOS near $\omega = 0$ is a result of truncation of $H(k)$ at k^2 order, and the lattice DOS shown in Fig.10 is not a constant anymore. The total DOS $D(\omega) = D_1(\omega) + D_2(\omega)$ is just the sum of the two.

(b). The specific heat and compressibility

The Helmholtz free energy density $F(T) = F_1(T) + F_2(T)$:

$$F_i(T) = E_{i,\text{GS}} + \int \frac{d^2\mathbf{k}}{(2\pi)^2} \left(|\epsilon_{i,+}(\mathbf{k})| - T \ln[2(1 + \cosh(\epsilon_{i,+}(\mathbf{k})/T))] \right) \quad (80)$$

where the zero temperature part of $F(T)$ is nothing but the ground-state energy density E_{GS} calculated in Sec.III-B-2. The specific heat (at constant volume) is given by $C_v(T) = C_{v,1}(T) + C_{v,2}(T)$:

$$C_v(T) = \int \frac{d^2\mathbf{k}}{(2\pi)^2} \sum_{i=1,2} \frac{[\epsilon_{i,+}(\mathbf{k})]^2}{T^2[1 + \cosh(\epsilon_{i,+}(\mathbf{k})/T)]} \quad (81)$$

Similarly, the (isothermal) uniform compressibility $\kappa_u(T) = \kappa_{u,1}(T) + \kappa_{u,2}(T)$ is

$$\kappa_u(T) = \sum_{i,s} \int \frac{d^2k}{(2\pi)^2} \frac{\partial f(\epsilon_{i,s}(k))}{\partial \epsilon_{i,s}(k)} = \int \frac{d\omega D(\omega)}{2T(1 + \cosh(\omega/T))} \quad (82)$$

where $D_i(\omega)$, $D(\omega)$ are listed in Eq.79.

Its zero temperature limit $\frac{\partial f(\epsilon)}{\partial \epsilon} = \delta(\epsilon)$ recovers the well-known relation between the compressibility and the DOS $\kappa_u(T) = D(0)$.

At low temperature T which is the lowest energy scale, one can get a low temperature expansion of $C_v(T)$ and $\kappa_u(T)$. Without loss of generality, we choose $\alpha\Delta < 0$ case in Fig.16, the two critical velocities $c_1 = |v| < c_2 = \sqrt{v^2 - 4\alpha\Delta} = \sqrt{v^2 + 4|\alpha\Delta|}$. By keeping the leading low T dependence and assuming $|\alpha\Delta/v^2| < 1/2$, we have

$\Delta \neq 0$ cases:

At $c < c_1$, H_1 has a gap $2\tilde{\Delta}_1 > 0$ and H_2 has a bigger gap $2\tilde{\Delta}_2 > 2\tilde{\Delta}_1$, $D_i(\omega) = 0$ for $|\omega| < \tilde{\Delta}_i$ (Fig.19a). Thus, $C_{v,i}(T) = 2D_i(\tilde{\Delta}_i)\tilde{\Delta}_i^2 T^{-1} e^{-\tilde{\Delta}_i/T}$, so $C_v(T) = 2D_1(\tilde{\Delta}_1)\tilde{\Delta}_1^2 T^{-1} e^{-\tilde{\Delta}_1/T}$. Similarly, $\kappa_{u,i}(T) = 2D_i(\tilde{\Delta}_i)T e^{-\tilde{\Delta}_i/T}$, so $\kappa_u(T) = 2D_1(\tilde{\Delta}_1)T e^{-\tilde{\Delta}_1/T}$. Both $C_v(T)$ and $\kappa_u(T)$ are dominated by the node 1.

At $c = c_1$, H_1 is critical with $\tilde{\Delta}_1 = 0$ and H_2 still has a gap $2\tilde{\Delta}_2 > 0$, $D_1(\omega) = D_1(0) + D_1'(0^+)|\omega|$ for small $|\omega|$, $D_2(\omega) = 0$ for $|\omega| < \tilde{\Delta}_2$ (Fig.19b). Thus, $C_{v,1}(T) = \frac{\pi^2}{3} D_1(0)T$ and $C_{v,2}(T) = 2D_2(\tilde{\Delta}_2)\tilde{\Delta}_2^2 T^{-1} e^{-\tilde{\Delta}_2/T}$, so $C_v(T) = \frac{\pi^2}{3} D_1(0)T$. Similarly, $\kappa_{u,1}(T) = D_1(0) + 2 \ln 2D_1'(0^+)T$ and $\kappa_{u,2}(T) = 2D_2(\tilde{\Delta}_2)T e^{-\tilde{\Delta}_2/T}$, so $\kappa_u(T) = D_1(0) + 2 \ln 2D_1'(0^+)T$. Both $C_v(T)$ and $\kappa_u(T)$ are still dominated by the node 1.

At $c_2 > c > c_1$, H_1 is gapless with $\tilde{\Delta}_1 < 0$ and H_2 still has a gap $2\tilde{\Delta}_2 > 0$, $D_1(\omega) = \frac{1}{2\pi|\alpha|} \sqrt{\frac{c^2}{2v^2 - c^2}}$ in Eq.79 for $|\omega| < |\tilde{\Delta}_1|$, $D_2(\omega) = 0$ for $|\omega| < \tilde{\Delta}_2$. Thus, $C_{v,1}(T) = \frac{\pi^2}{3} D_1(0)T$ and $C_{v,2}(T) = 2D_2(\tilde{\Delta}_2)\tilde{\Delta}_2^2 T^{-1} e^{-|\tilde{\Delta}_2|/T}$, so $C_v(T) = \frac{\pi^2}{3} D_1(0)T$. Similarly, $\kappa_{u,1}(T) = D_1(0) + 2[D_1(\tilde{\Delta}_1) - D_1(0)]T e^{-|\tilde{\Delta}_1|/T}$ and $\kappa_{u,2}(T) = 2D_2(\tilde{\Delta}_2)T e^{-|\tilde{\Delta}_2|/T}$, so $\kappa_u(T) = D_1(0) +$

$2[D_1(\tilde{\Delta}_1) - D_1(0)]Te^{-|\tilde{\Delta}_1|/T} + 2D_2(\tilde{\Delta}_2)Te^{-|\tilde{\Delta}_2|/T}$. However, the relative magnitude of $|\tilde{\Delta}_1|$ and $|\tilde{\Delta}_2|$ depends on c , so one can not tell which is smaller in general.

At $c = c_2$, H_1 is gapless with $\tilde{\Delta}_1 < 0$ and H_2 becomes critical with $\tilde{\Delta}_2 = 0$, $D_1(\omega) = \frac{1}{2\pi|\alpha|}\sqrt{\frac{c^2}{2v^2-c^2}}$ in Eq.79 for $|\omega| < |\tilde{\Delta}_1|$, $D_2(\omega) = D_2(0) + D_2'(0^+)|\omega|$ for small $|\omega|$ (Fig.19c). Thus, $C_{v,1}(T) = \frac{\pi^2}{3}D_1(0)T$ and $C_{v,2}(T) = \frac{\pi^2}{3}D_2(0)T$, so $C_v(T) = \frac{\pi^2}{3}D(0)T$. Similarly, $\kappa_{u,1}(T) = D_1(0) + 2[D_1(\tilde{\Delta}_1) - D_1(0)]Te^{-|\tilde{\Delta}_1|/T}$ and $\kappa_{u,2}(T) = D_2(0) + 2\ln 2D_2'(0)T$, so $\kappa_u(T) = D(0) + 2\ln 2D_2'(0)T$.

At $c > c_2$, H_1 is gapless with $\tilde{\Delta}_1 < 0$ and H_2 is also gapless with $\tilde{\Delta}_2 < 0$, $D_1(\omega) = \frac{1}{2\pi|\alpha|}\sqrt{\frac{c^2}{2v^2-c^2}}$ in Eq.79 for small $|\omega| < |\tilde{\Delta}_1|$, $D_2(\omega) = \frac{1}{2\pi|\alpha|}\sqrt{\frac{c^2}{2v^2-c^2}}$ in Eq.79 for small $|\omega| < |\tilde{\Delta}_2|$ (Fig.19d). Thus, $C_{v,1}(T) = \frac{\pi^2}{3}D_1(0)T$ and $C_{v,2}(T) = \frac{\pi^2}{3}D_2(0)T$, so $C_v(T) = \frac{\pi^2}{3}D(0)T$. Similarly, $\kappa_{u,1}(T) = D_1(0) + 2[D_1(\tilde{\Delta}_1) - D_1(0)]Te^{-|\tilde{\Delta}_1|/T}$ and $\kappa_{u,2}(T) = D_2(0) + 2[D_2(\tilde{\Delta}_1) - D_2(0)]Te^{-|\tilde{\Delta}_2|/T}$. so $\kappa_u(T) = D(0) + 2[D_2(\tilde{\Delta}_1) - D_2(0)]Te^{-|\tilde{\Delta}_2|/T}$.

$\Delta = 0$ cases:

In this case, $c_1 = c_2 = c$ and H_1 and H_2 have exactly the same spectrum.

At $c < v$, $D_i(\omega) = D_i'(0)|\omega|$ for small $|\omega|$, thus $C_{v,1}(T) = C_{v,2}(T) = 9\zeta(3)D_i'(0^+)T^2$ and $C_v(T) = 9\zeta(3)D'(0^+)T^2$. Similarly, $\kappa_{u,1}(T) = \kappa_{u,2}(T) = 2\ln 2D_i'(0)T$ and $\kappa_u(T) = 2\ln 2D'(0)T$.

At $c = v$ and $\Delta = 0$, $D_i(\omega) = D_i(0) + A_i(0)|\omega|^{2/3}$ for small $|\omega|$, thus $C_{v,1}(T) = C_{v,2}(T) = \frac{\pi^2}{3}D_i(0)T$ and $C_v(T) = \frac{\pi^2}{3}D(0)T$. Similarly, $\kappa_{u,1}(T) = \kappa_{u,2}(T) = D_i(0) + 1.1486A_iT^{5/3}$ and $\kappa_u(T) = D(0) + 1.1486AT^{5/3}$.

At $c > v$ and $\Delta = 0$, $D_i(\omega) = D_i(0)$ for small $|\omega|$, $C_{v,1}(T) = C_{v,2}(T) = \frac{\pi^2}{3}D_i(0)T$ and $C_v(T) = \frac{\pi^2}{3}D(0)T$. Similarly, $\kappa_{u,1}(T) = \kappa_{u,2}(T) = D_i(0) + 2[D_i(\tilde{\Delta}_i) - D_i(0)]Te^{-|\tilde{\Delta}_i|/T}$ and $\kappa_u(T) = D(0) + 2[D(\tilde{\Delta}) - D(0)]Te^{-|\tilde{\Delta}|/T}$.

If we only consider the leading low temperature behaviors of $C_v(T) = C_{v,1}(T) + C_{v,2}(T)$ and $\kappa_u(T) = \kappa_{u,1}(T) + \kappa_{u,2}(T)$, one can summarize these results as:

When $\Delta \neq 0$: at $c < c_1$, $C_v(T) = 2D_1(\tilde{\Delta}_1)\tilde{\Delta}_1^2T^{-1}e^{-|\tilde{\Delta}_1|/T}$ and $\kappa_u(T) = 2D_1(\tilde{\Delta}_1)Te^{-\tilde{\Delta}_1/T}$; at $c \geq c_1$, $C_v(T) = \frac{\pi^2}{3}D(0)T$ and $\kappa_u(T) = D(0)$.

When $\Delta = 0$: at $c < v$, $C_v(T) = 9\zeta(3)D'(0^+)T$ and $\kappa_u(T) = 2\ln 2D'(0)T$; at $c \geq v$, $C_v(T) = \frac{\pi^2}{3}D(0)T^2$ and $\kappa_u(T) = D(0)$.

(c). *The Wilson ratio*

The Wilson ratio is defined as $R_W = T\kappa_u/C_v$ which has the following low temperature behaviours.

$\Delta \neq 0$ case:

When $c < c_0$, $R_W = (T/\tilde{\Delta})^2$; when $c \geq c_0$, $R_W = 3/\pi^2$.

$\Delta = 0$ case:

When $c < c_0$, $R_W = 2\ln 2/(9\zeta(3)) \approx 0.1281$; when $c \geq c_0$, $R_W = 3/\pi^2$.

These results are consistent with those achieved directly on the lattice in Sec.II-C-3 and also listed in the last line of Table-I.

IV. THE CHIRAL EDGE PROPERTIES IN A STRIP GEOMETRY

Following the approach used in the bulk properties, we will first study the edge properties from the lattice system, then investigate them from the continuum effective theory, then contrast the two complementary approaches.

A. Edge states from the microscopic lattice theory

For the periodic boundary condition in the y -direction and open boundary condition in the x -direction, k_y is a good quantum number, the Hamiltonian in the mixed (i, k_y) representation becomes

$$H = \sum_{k_y, i, j} c_{i, k_y}^\dagger \{ [-(h + 2t \cos k_y)\sigma_z + 2t_s \sin k_y \sigma_y + 2t_b \sin k_y \sigma_0] \delta_{i, j} + (t\sigma_z - it_s \sigma_y) \delta_{i, j+1} + (t\sigma_z + it_s \sigma_y) \delta_{i, j-1} \} c_{j, k_y} \quad (83)$$

For the periodic boundary condition in the x -direction and open boundary condition in the y -direction, k_x is a good quantum number, the Hamiltonian in the mixed (k_x, i) representation becomes:

$$H = \sum_{k_x, i, j} c_{k_x, i}^\dagger \{ [-(h + 2t \cos k_x)\sigma_z + t_s \sin k_x \sigma_x] \delta_{i, j} + (t\sigma_z - it_s \sigma_y - it_b \sigma_0) \delta_{i, j+1} + (t\sigma_z + it_s \sigma_y + it_b \sigma_0) \delta_{i, j-1} \} c_{k_x, j} \quad (84)$$

In the Fig.20 and 21, we show the numerical results on the lattice edge states.

1. Interpretation of the Hall conductance in terms of the edge states, enriched bulk-edge and new L/edge-T/edge correspondences

The bulk-edge correspondence in a static frame is also enriched under the injection or in a moving sample: Relative to the injection or boost, there is a longitudinal or transverse edge, so the original bulk-edge correspondence is enriched to the bulk to longitudinal/or transverse edge correspondence, then the longitudinal edge to transverse edge correspondence.

In the longitudinal injecting case, the edge state always exist, so its contribution to σ_H remains quantized as $\sigma_H = Ch_- = 1$ throughout the TPT at (c1). However, there is no bulk contributions in the Chern insulator, but the bulk starts to contribute $\sigma_H = \nu_b = v/c - 1$ in the

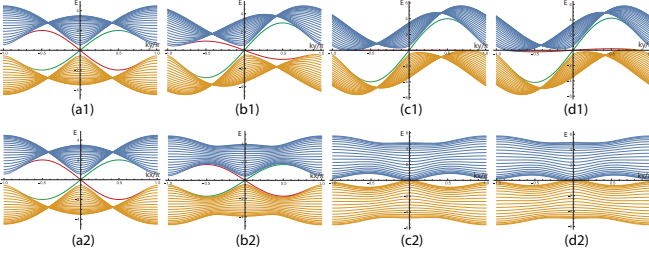


FIG. 20. The edge states of the lattice Hamiltonian in a strip geometry. We fixed $h = -0.5$. From left to right, the parameter t_b/t_s is 0, 0.5, 1.0, 1.1, respectively. (Top) Longitudinal injection: With the periodic boundary condition in the y -direction and the open boundary condition in the x -direction. The edge modes always exist, but undergoes the edge reconstruction at $t_s/t = 1$. The two edges move along the opposite directions when $t_s/t < 1$ in (a1) and (b1) in the CI, then one edge becomes flat at $t_s/t = 1$ in (c1), then two edges move along the *same* direction when $t_s/t > 1$ in (d1) in the odd CM, (Bottom) Transverse injection: Exchanging the role of x and y direction. The edge modes exist only when $t_s/t < 1$ in (a2) and (b2), but squeezed out at $t_s/t = 1$ in (c2) where the direct bulk gap closes, completely disappear when $t_s/t > 1$ in (d2) in the odd CM. Although the edge modes show quite different behaviours in the line 1 and the line 2, there seems a one to one Longitudinal/Transverse edge-edge correspondence between them. In both figures, one can shift $k \rightarrow k + \pi$ to reach $h = +0.5$ results. See also Fig.22 and Fig.23 for the continuum calculations. See also Fig.S1 for the expanded figure.

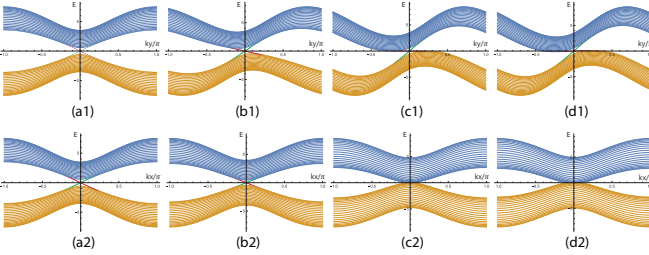


FIG. 21. The same situation as in Fig.20 except at a fixed $h = -3.5$. In both figures, one can shift $k \rightarrow k + \pi$ to reach $h = +3.5$ results. It shows qualitatively the same edge TPTs as those in Fig.20. See also Fig.S2 for the expanded figure.

Odd Chern metal phase. The two parts lead back to Eq.32 evaluated in the bulk:

$$\sigma_H = \frac{1}{2\pi} \int_{\mathbb{R}^2} \Omega_-(\mathbf{k}) d^2\mathbf{k} + \frac{1}{\pi} \int_{\mathbb{R}^2} \Omega_+(\mathbf{k}) \Theta(-\epsilon_+(\mathbf{k})) d^2\mathbf{k} = \text{Ch}_- + \nu_b \quad (85)$$

In the transverse injecting case, the edge states exist only before the TPT at (c2), so its contribution to σ_H remains quantized as $\sigma_H = \text{Ch}_-$ only before the TPT at (c2). There is no bulk contributions in the Chern insulator before (c2). However, after (c2), the edge states emerge into the bulk and disappear. All the contributions come from the bulk as $\sigma_H = v/c < 1$.

B. Solving the edge states from the effective theory in the continuum

We will solve the edge states with the periodic boundary condition in the y -direction and the open boundary condition in the x -direction, then vice versa.

1. Solving the edge states in the longitudinal injection

We will solve the model in a strip geometry [31] with the periodic boundary condition in the y -direction and open boundary condition in the x -direction. The continuum Hamiltonian in the mixed (∂_x, k_y) representation:

$$H(\partial_x, k_y) = (\Delta - \alpha_x \partial_x^2) \sigma_z - i v_x \partial_x \sigma_x + \alpha_y k_y^2 \sigma_z + v_y k_y \sigma_y - c k_y \sigma_0 \quad (86)$$

The problem will first be studied in the $k_y = 0$ limit where $H_{1D} = (\Delta - \alpha_x \partial_x^2) \sigma_z - i v_x \partial_x \sigma_x$, and then extended to finite $k_y \neq 0$. Due to the C-symmetry, the edge mode $\psi(x, k_y = 0)$ is expected to exist at zero energy, therefore $H_{1D} \psi = 0$. Multiplying both side by σ_z gives $[(\Delta - \alpha_x \partial_x^2) + v_x \partial_x \sigma_y] \psi = 0$. Choosing $\sigma_y \psi_{\pm} = \pm \psi_{\pm}$ with $\psi_{\pm} = \frac{1}{\sqrt{2}}(\phi, \pm i\phi)^T$, or $\psi_{\pm} = \phi \chi_{\pm}$ with

$$\chi_{\pm} = \frac{1}{\sqrt{2}} \begin{pmatrix} 1 \\ \pm i \end{pmatrix} \quad (87)$$

then the coupled differential equations can be reduced to a second order homogeneous ordinary differential equation

$$[(\Delta - \alpha_x \partial_x^2) \pm v_x \partial_x] \phi = 0. \quad (88)$$

Substituting the ansatz $\phi \propto e^{-\lambda x}$ leads to a character equation $\alpha_x \lambda^2 \pm v_x \lambda - \Delta = 0$ with the solutions:

$$\lambda_{1,2}^{(s)} = \frac{-s v_x \pm \sqrt{v_x^2 + 4\alpha_x \Delta}}{2\alpha_x}, \quad (89)$$

where $s = \pm$ corresponding to the choice of \pm in Eq.88. Thus, the general solution can be written as

$$\phi = c_1 e^{-\lambda_1 x} + c_2 e^{-\lambda_2 x}. \quad (90)$$

Due to the C-symmetry, one only need to consider one edge. Choosing the left edge and imposing the wave function to vanish at $x = 0$ and $x = +\infty$ requires $c_1 = -c_2$ and $\Re \epsilon \lambda_{1,2} > 0$. Thus, we have $\phi_L(x) \propto (e^{-\lambda_1 x} - e^{-\lambda_2 x})$, where $\lambda_{1,2}$ denote either $\lambda_{1,2}^{(+)}$ or $\lambda_{1,2}^{(-)}$ in Eq.89 whichever have positive real parts.

The condition for $\Re \epsilon \lambda_{1,2} > 0$ is analyzed as:

If $v_x > 0$, $\alpha_x > 0$, $\Delta < 0$, the localized edge state is $\psi_L(x) \propto (e^{-\lambda_1^{(-)} x} - e^{-\lambda_2^{(-)} x}) \chi_-$.

If $v_x > 0$, $\alpha_x < 0$, $\Delta > 0$, the localized edge state is $\psi_L(x) \propto (e^{-\lambda_1^{(+)} x} - e^{-\lambda_2^{(+)} x}) \chi_+$.

If $v_x < 0$, $\alpha_x > 0$, $\Delta < 0$, the localized edge state is $\psi_L(x) \propto (e^{-\lambda_1^{(+)} x} - e^{-\lambda_2^{(+)} x}) \chi_+$.

If $v_x < 0$, $\alpha_x < 0$, $\Delta > 0$, the localized edge state is $\psi_L(x) \propto (e^{-\lambda_1^{(-)}x} - e^{-\lambda_2^{(-)}x})\chi_-$.

Otherwise, there is not any localized edge state.

In short, the left localized edge state exists when $\alpha_x\Delta < 0$ and $\psi_L = +\text{sgn}(v_x\Delta)\psi_L$. The C-symmetry indicates that the right localized edge state also exists when $\alpha_x\Delta < 0$ and $\sigma_y\psi_R = -\text{sgn}(v_x\Delta)\psi_R$.

When extending the results at $k_y = 0$ to finite k_y case, one can just replace $\Delta \rightarrow \Delta + \alpha k_y^2$ in Eq.89, and then $\psi_L(x, y) \propto \psi_L(x)e^{ik_y y}$ is an eigenstate of $H(\partial_x, k_y)$. [It is obvious to see that the exact spectrum is the same as that achieved by treating k_y -dependent part perturbatively. Note that χ_{\pm} is not eigenstate of $\alpha_x k_x^2 \sigma_z$.] Therefore, we get the edge effective Hamiltonian including both left ψ_L and right ψ_R edge:

$$H_{\text{edge}}(k_y) = \text{sgn}(v_x\Delta)[(v_y - c)k_y\psi_L^\dagger\psi_L - (v_y + c)k_y\psi_R^\dagger\psi_R] \quad (91)$$

which shows the dispersion relations for the edge states at the open x -boundary are

$$\begin{aligned} \epsilon_L(k_y) &= +\text{sgn}(v_x\Delta)(v_y - c)k_y, \\ \epsilon_R(k_y) &= -\text{sgn}(v_x\Delta)(v_y + c)k_y \end{aligned} \quad (92)$$

Meanwhile, the bulk spectrum is continuous, which is given by

$$\epsilon_{\text{bulk}}^\pm(k_y) = \pm\sqrt{(\Delta + \alpha_x k_x^2 + \alpha_y k_y^2)^2 + v_x^2 k_x^2 + v_y^2 k_y^2} - ck_y \quad (93)$$

where k_x is a continuous real parameter.

The edge state extends in a finite regime around $k_y = 0$ which can be estimated by when the energy of edge state first enter into the bulk spectrum. Solving $\min_{k_x} \epsilon_{\text{bulk}}^\pm(k_y) = \epsilon_L(k_y)$ gives the max k_x . Thus when $\alpha\Delta < 0$, the edge state survives in the regime $|k_y| < \sqrt{-\Delta/\alpha}$ which is also independent of boost c .

Which shows one edge state becomes zero slope at the QPT, then reverses its slope after. We plot bulk states and edge states in Fig.22.

Putting $c = 0$ in Eq.91 recovers the edge theory without the injection. Then directly performing a Galileo boost along the edge leads to Eq.91.

2. Solving the edge states in the transverse injection

Similarly, we can also consider the model in a strip geometry [31] with the periodic boundary condition in the x -direction and open boundary condition in the y -direction. The continuum Hamiltonian in the mixed (k_x, ∂_y) representation:

$$\begin{aligned} H(k_x, \partial_y) &= (\Delta - \alpha_y \partial_y^2)\sigma_z - iv_y \partial_y \sigma_y + ic \partial_y \sigma_0 \\ &\quad + \alpha_x k_x^2 \sigma_z + v_x k_x \sigma_x \end{aligned} \quad (94)$$

The problem will first be studied in the $k_x = 0$ limit where $H_{1D} = (\Delta - \alpha_y \partial_y^2)\sigma_z - iv_y \partial_y \sigma_y + ic \partial_y \sigma_0$, and

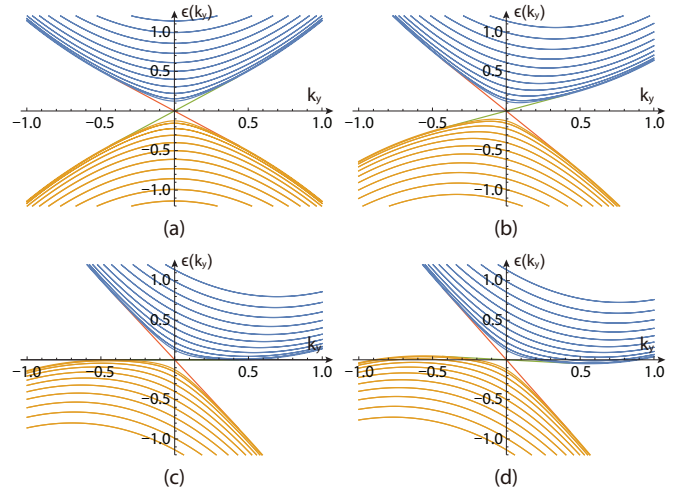


FIG. 22. Longitudinal (L-) edge: The spectrum of the Hamiltonian $H_{1D}(\partial_x, k_y)$ in Eq.86 with periodic boundary condition in the y -direction and open boundary condition in the x -direction. From left to right, the parameter c is 0, 0.5, 1.0, 1.1, respectively. Other parameters are fixed as $v_x = v_y = 1$, $\alpha_{x,y} = 1$, $\Delta = -0.1$. The left/right edge mode is highlighted in the red/green color. The results are consistent with those on the lattice in Fig.20, 21 with the same boundary conditions.

then extended to finite $k_x \neq 0$. Due to the C-symmetry, the edge mode $\psi(k_x = 0, y)$ is expected to exist at zero energy, thus $H_{1D}\psi = 0$. Multiplying both side by σ_z gives $[\Delta + (ic\sigma_z - v_y\sigma_x)\partial_y - \alpha\partial_y^2]\psi = 0$. Choosing $(ic\sigma_z - v_y\sigma_x)\psi_{\pm} = \pm\sqrt{v_y^2 - c^2}\psi_{\pm}$ with $\psi_{\pm} = \phi\chi_{\pm}$ where the two-component spinor is

$$\chi_{\pm} = \frac{1}{\sqrt{2}}\begin{pmatrix} 1 \\ \xi_{\pm} \end{pmatrix}, \quad \xi_{\pm} = (ic \mp \sqrt{v_y^2 - c^2})/v_y \quad (95)$$

which depends on the transverse boost c explicitly. Then the coupled differential equation also can be reduced to a second order ordinary differential equation

$$(\Delta \pm \sqrt{v_y^2 - c^2}\partial_y - \alpha_y \partial_y^2)\phi = 0, \quad (96)$$

where \pm corresponding to the choice of ψ_{\pm} . Substituting the ansatz $\phi = e^{-\lambda y}$ leads to $\alpha_y \lambda^2 \pm \sqrt{v_y^2 - c^2}\lambda - \Delta = 0$ with the roots:

$$\lambda_{1,2}^{(s)} = \frac{-s\sqrt{v_y^2 - c^2} \pm \sqrt{v_y^2 - c^2 + 4\alpha_y \Delta}}{2\alpha_y}, \quad (97)$$

where $s = \pm$ corresponds to the choice of \pm in Eq.96. Thus, the general solution can be written as

$$\phi = c_1 e^{-\lambda_1 y} + c_2 e^{-\lambda_2 y} \quad (98)$$

Due to the C-symmetry, one only need consider one edge. Choosing the bottom edge, imposing the wave function to vanish at $y = 0$ and $y = +\infty$ requires $c_1 = -c_2$ and $\Re\lambda_{1,2} > 0$. Thus, we have $\phi_B(y) \propto$

($e^{-\lambda_1 y} - e^{-\lambda_2 y}$) where $\lambda_{1,2}$ denote $\lambda_{1,2}^{(+)}$ or $\lambda_{1,2}^{(-)}$ in Eq.97 whichever have positive real parts.

The condition for $\Re\epsilon\lambda_{1,2} > 0$ is analyzed as:

If $v_y^2 > c^2$, $\alpha_y > 0$, $\Delta < 0$, the localized edge state is

$$\psi_B(y) \propto (e^{-\lambda_1^{(-)} y} - e^{-\lambda_2^{(-)} y})\chi_-;$$

If $v_y^2 > c^2$, $\alpha_y < 0$, $\Delta > 0$, the localized edge state is

$$\psi_B(y) \propto (e^{-\lambda_1^{(+)} y} - e^{-\lambda_2^{(+)} y})\chi_+;$$

Otherwise, there is not any localized edge state.

In short, the Bottom localized edge state exists when $\alpha_y \Delta < 0$ and $c^2 < v_y^2$, and $(ic\sigma_z - v_y\sigma_x)\psi_B = +\text{sgn}(\Delta)\sqrt{v_y^2 - c^2}\psi_B$. The C-symmetry indicates that the Top localized edge state exists when $\alpha_y \Delta < 0$ and $c^2 < v_y^2$, and $(ic\sigma_z - v_y\sigma_x)\psi_T = -\text{sgn}(\Delta)\sqrt{v_y^2 - c^2}\psi_T$.

When extending to finite k_x case, one need replace $\lambda_{1,2} \rightarrow \lambda_{1,2}(k_x)$ and $\chi_{\pm} \rightarrow \chi_{\pm}(k_x)$, then redo the eigenvalue problem. [After tedious algebra, we find it gives the same spectrum as treated the k_x -dependent part as perturbation.] Alternatively, one may just take $\psi_B(x, y) = \psi_B(y)e^{ik_x x}$ and use the first order perturbation theory. Due to $\langle \chi_{\pm} | \sigma_x | \chi_{\pm} \rangle = \mp\sqrt{v_y^2 - c^2}/v_y$ and $\langle \chi_{\pm} | \sigma_z | \chi_{\pm} \rangle = 0$, we find the edge effective Hamiltonian including both the bottom ψ_B and the top ψ_T edge state

$$H_{\text{edge}}(k_x) = -\text{sgn}(v_y \Delta) v_x \sqrt{1 - c^2/v_y^2} k_x [\psi_B^\dagger \psi_B - \psi_T^\dagger \psi_T] \quad (99)$$

which indicates the dispersion relations for the edge states at the y -boundary:

$$\begin{aligned} \epsilon_B(k_x) &= -\text{sgn}(v_y \Delta) v_x \sqrt{1 - c^2/v_y^2} k_x, \\ \epsilon_T(k_x) &= +\text{sgn}(v_y \Delta) v_x \sqrt{1 - c^2/v_y^2} k_x \end{aligned} \quad (100)$$

Meanwhile, the bulk spectrum is continuous, which is given by

$$\epsilon_{\text{bulk}}^{\pm}(k_x) = \pm \sqrt{(\Delta + \alpha_x k_x^2 + \alpha_y k_y^2)^2 + v_x^2 k_x^2 + v_y^2 k_y^2} - c k_y \quad (101)$$

where k_y is a continuous real parameter. The edge state usual extent in a finite regime around $k_x = 0$, which can be estimated by when the energy of edge state first enter into the bulk spectrum. Solving $\min_{k_y} \epsilon_{\text{bulk}}^+(k_x) = \epsilon_B(k_x)$ gives the max k_x . Thus when $\alpha\Delta < 0$ and $|v_y| > |c|$, the edge state survives in the regime $|k_x| < \sqrt{(c^2/v_y^2 - 1)\Delta/\alpha}$, and the regime is decrease as increasing the boost c .

Which shows edge states do not exist anymore after the bulk QPT. We plot bulk states and edge states in Fig.23.

Putting $c = 0$ in Eq.99 recovers the edge theory without the injection. However, in contrast to Eq.91, one may not achieve Eq.99 by directly performing a Galileo boost. Naively, a direct boost may lead to $\sqrt{v^2 + c^2}$ instead of $\sqrt{v^2 - c^2}$. To achieve Eq.99, one may still need to solve the bulk + the transverse boundary condition

as done here and find that one must substitute $c \rightarrow ic$ in the naive Galileo boost results to reach the correct transverse boost result. While the i in the substitution in $c \rightarrow ic$ stands for the decay of edge mode along the boost direction. Eq.99 indicates that the two perpendicular motions: the spinor edge wave propagation along the x -edge and the boost along the y -axis are coupled to each other through the SOC which breaks the GI explicitly. Indeed, its 2-component spinor χ_{\pm} does depend on the transverse boost sensitively.

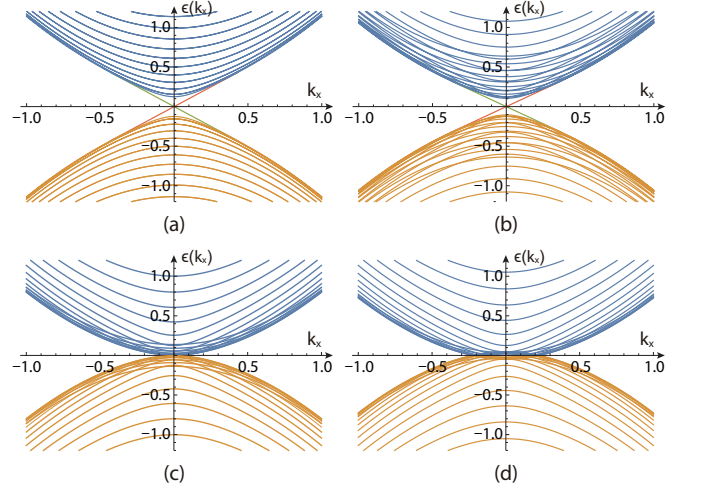


FIG. 23. The transverse (T-) edge: spectrum of the Hamiltonian $H_{1D}(k_x, \partial_y)$ in Eq.94. with periodic boundary condition in the x -direction and open boundary condition in the y -direction. From left to right, the parameter c is 0, 0.5, 1.0, 1.1, respectively. The T-edge disappears at the same time as the bulk TPT with its velocity vanishing as $\sqrt{v^2 - c^2}$. Other parameters are fixed as $v_x = v_y = 1$, $\alpha_{x,y} = 1$, $\Delta = -0.1$. The Top/Bottom edge mode is highlighted in the red/green color. The results are consistent with those on the lattice in Fig.20, 21 with the same boundary conditions.

C. The bulk-edge correspondence from the continuum edge theory

We will discuss the bulk-edge correspondence near $h \sim -4t$ and $h \sim 0$ respectively.

1. The bulk-edge correspondence near $h \sim -4t$ case

In the $h \sim -4t$ case, there is only one valley at $K_0 = (0, 0)$, the bulk effective Hamiltonian is:

$$H_0 = [\Delta + \alpha(k_x^2 + k_y^2)]\sigma_z + v k_x \sigma_x + v k_y \sigma_y - c k_y \sigma_0, \quad (102)$$

where $\Delta = -4t - h$, $\alpha = t$, $v = 2t_s$, $c = 2t_b$,

Since we choose $t, t_s, t_b > 0$, thus $h < -4t$ leads to $\Delta > 0$ and $\alpha\Delta > 0$, no edge states. $h > -4t$ leads to $\Delta < 0$ and $\alpha\Delta < 0$. Edge state is possible.

(a) *Open boundary condition in the x-direction: longitudinal injection*

When $h < -4t$, there is no edge state;

When $h > -4t$, there is always one localized edge state which is given by the continuum theory near $K_0 = (0, 0)$ and exists near $K_{0y} = 0$.

(b) *Open boundary condition in the y-direction: transverse injection*

If $\alpha\Delta < 0$ and $v^2 > c^2$, then H_0 has one localized edge state.

Thus, $h < -4t$, there is no edge state;

When $h > -4t$, if $c^2 < v^2$, there is one localized edge state which is given by the continuum theory near $K_0 = (0, 0)$ and exists near $K_{0x} = 0$. If $c^2 > v^2$, there is still no edge state.

These results in (a) and (b) are consistent with those on a lattice reached in Sec.IV-A.

2. The bulk-edge correspondence near $h \sim 0$ case

In the $h \sim 0$ case, there are two valleys at K_1, K_2 , the bulk effective Hamiltonian are:

$$\begin{aligned} H_1 &= [\Delta - \alpha(k_x^2 - k_y^2)]\sigma_z - vk_x\sigma_x + vk_y\sigma_y - ck_y\sigma_0 \\ H_2 &= [\Delta + \alpha(k_x^2 - k_y^2)]\sigma_z + vk_x\sigma_x - vk_y\sigma_y + ck_y\sigma_0 \end{aligned} \quad (103)$$

where $\Delta = -h$, $\alpha = t$, $v = 2t_s$, $c = 2t_b$, written in the generic form of Eq.25:

$$\begin{aligned} H_1 &= (\Delta + \alpha_{1x}k_x^2 + \alpha_{1y}k_y^2)\sigma_z + v_{1x}k_x\sigma_x + v_{1y}k_y\sigma_y + c_1k_y\sigma_0 \\ H_2 &= (\Delta + \alpha_{2x}k_x^2 + \alpha_{2y}k_y^2)\sigma_z + v_{2x}k_x\sigma_x + v_{2y}k_y\sigma_y + c_2k_y\sigma_0 \end{aligned} \quad (104)$$

which leads to the relations:

$$\begin{aligned} \alpha_{1x} &= -\alpha, \alpha_{1y} = +\alpha, v_{1x} = -v, v_{1y} = +v, c_1 = -c \\ \alpha_{2x} &= +\alpha, \alpha_{2y} = -\alpha, v_{2x} = +v, v_{2y} = -v, c_2 = +c \end{aligned} \quad (105)$$

If $\alpha_{1x}\Delta > 0$, then $\alpha_{2x}\Delta < 0$, $\alpha_{1y}\Delta < 0$, $\alpha_{2y}\Delta > 0$, which means only one valley may have one edge state for a given type of boundary. Since we choose $t, t_s, t_b > 0$, thus $h > 0$ leads to $\Delta < 0$ and $\alpha\Delta < 0$; $h < 0$ leads to $\Delta > 0$ and $\alpha\Delta > 0$.

(a) *Open boundary condition in the x-direction: longitudinal injection*

If $\alpha\Delta > 0$, then $\alpha_{1x}\Delta < 0$ which means H_1 has one localized edge state;

If $\alpha\Delta < 0$, then $\alpha_{2x}\Delta < 0$ which means H_2 has one localized edge state.

Thus, there is always one edge state. When $h > 0$, there is one edge state given by the continuum theory near $K_2 = (0, \pi)$ and exists near $K_{2y} = \pi$. This is expected, because it is smoothly connected to the edge state near $h < 4t$ where there is only one valley at $K_3 = (\pi, \pi)$ and one edge states exists near $K_{3y} = \pi$.

When $h < 0$, there is one edge state given by the continuum theory near $K_1 = (\pi, 0)$ and exists near $K_{1y} = 0$.

This is expected, because it is smoothly connected to the edge state near $h > -4t$ where there is only one valley at $K_0 = (0, 0)$ and one edge states exists near $K_{0y} = 0$.

(b) *Open boundary condition in the y-direction: transverse injection*

If $c^2 > v^2$, then there is not any localized edge state. If $c^2 < v^2$ and $\alpha\Delta > 0$, then $\alpha_{2y}\Delta < 0$ which means H_2 has one localized edge state; if $c^2 < v^2$ and $\alpha\Delta < 0$, then $\alpha_{1y}\Delta < 0$ which means H_1 has one localized edge state.

Thus, there is one edge state only if $t_b < t_s$.

When $h > 0$, there is one edge state given by the continuum theory near $K_1 = (\pi, 0)$ and exists near $K_{1x} = \pi$. This is expected, because it is smoothly connected to the edge state near $h < 4t$ where there is only one valley at $K_3 = (\pi, \pi)$ and one edge states exists near $K_{3x} = \pi$.

When $h < 0$, there is one edge state given by the continuum theory near $K_2 = (0, \pi)$ and exists near $K_{2x} = 0$. This is expected, because it is smoothly connected to the edge state near $h > -4t$ where there is only one valley at $K_0 = (0, 0)$ and one edge states exists near $K_{0x} = 0$.

These results in (a) and (b) are consistent with those on a lattice reached in Sec.IV-A.

V. GAUGE INVARIANT CURRENT: BULK PROPERTIES

Injecting currents into the system could result in the following form:

$$H_{inj,x} = -[\kappa_{b1} \sum_i J_{ix} + i \sum_{n=2}^{\infty} (t_{bn}/n) c_i^\dagger c_{i+nx}] + h.c. \quad (106)$$

where J_{ix} is the NN gauge-invariant current, the other terms $n = 2, 3, \dots$ are NNN, NNNN,.... κ_{b1} is dimensionless and t_{bn} , $n \geq 2$ carry the same dimension as the hopping.

To capture the physics, one only need to include the NN and the $n = 2$ NNN term (which can also be called higher order current). We still take the ‘‘divide and conquer’’ strategy to treat the two terms separately and differently. As shown in Fig.19-22, for the $n = 1$ case, the bulk TPT and the edge reconstruction happens at the same time. But this coincidence could be due to the $n = 1$ case which maybe a fine tuning phase. It is not protected by any symmetry. So they can split in a more general case. If so, the edge reconstruction must happen earlier than the bulk TPT, not the other way around. Then, there must be an intermediate phase between the bulk TPT and the edge reconstruction, we call such a phase an odd Chern insulator phase which has the same bulk properties as the ordinary Chern insulator, but different edge properties: Its longitudinal edge modes satisfy the exotic relation $v_L v_R > 0$, its transverse edge modes satisfy the conventional relation $v_L v_R < 0$. In the longitudinal edge, the edge mode undergoes its own edge TPT with an longitudinal edge dynamic exponent $z_L = 3$ instead of being exactly flat for the $n = 1$ even

inside the Chern insulator before the bulk TPT. So there is an even enriched surface TPT before the bulk TPT. As to be shown in Sec.VII and Sec.VIII, this case also provide another example of odd Chern metal. The BM also leads to a non-vanishing AHE. Remarkably, the σ_H jump from the odd Chern metal to the BM remains the same universal non-integer number as $n = 1$.

A. The NN gauge-invariant current and the NNN current term

Due to the commutation relation

$$[c_{i,\sigma}^\dagger c_{i,\sigma}, \sum_j c_{j,\alpha}^\dagger T_{\alpha\beta} c_{j+\delta,\beta}] = c_{i,\alpha}^\dagger T_{\alpha\beta} c_{i+\delta,\beta} - c_{i-\delta,\alpha}^\dagger T_{\alpha\beta} c_{i,\beta} \quad (107)$$

where the summation over spin indices σ, α, β is implied.

Given a general Hubbard Hamiltonian with SOC on a square lattice

$$H_0 = \sum_{j\delta} [c_{j,\alpha}^\dagger T_{\alpha\beta}^\delta c_{j+\delta,\beta} + h.c.] + \sum_j U n_j^2 - \mu \sum_j n_j - h \sum_j (n_{j\uparrow} - n_{j\downarrow}) \quad (108)$$

where $\delta = \hat{x}, \hat{y}$ and U is Hubbard interaction. The quantum anomalous Hall model Eq.1 is just a special case of the general Hamiltonian in Eq.(108), with $T^x = -t_0\sigma_z + it_{s0}\sigma^x$ and $T^y = -t_0\sigma_z + it_{s0}\sigma^y$.

Combining the Heisenberg equation of motion and the continuity equation

$$\begin{aligned} \frac{d}{dt} n_i &= i[H_0, n_i] = -\nabla \cdot \mathbf{J}_i \\ i[H_0, n_i] &= \sum_{\alpha\beta\delta} [i(c_{i,\alpha}^\dagger T_{\alpha\beta}^\delta c_{i+\delta,\beta} - c_{i-\delta,\alpha}^\dagger T_{\alpha\beta}^\delta c_{i,\beta}) + h.c.] \\ \nabla \cdot \mathbf{J}_i &= J_i^x - J_{i-x}^x + J_i^y - J_{i-y}^y \end{aligned} \quad (109)$$

Thus one can identify the gauge-invariant current as

$$\begin{aligned} J_i^x &= -ic_{i,\alpha}^\dagger T_{\alpha\beta}^x c_{i+x,\beta} + h.c. \\ J_i^y &= -ic_{i,\alpha}^\dagger T_{\alpha\beta}^y c_{i+y,\beta} + h.c. \end{aligned} \quad (110)$$

which is different from the injecting current Eq.2.

The total number conservation follows:

$$\frac{d}{dt} \sum_i n_i = \sum_i (J_i^x - J_{i-x}^x + J_i^y - J_{i-y}^y) = 0 \quad (111)$$

However, $\sum_i J_i^x \neq 0$ and $\sum_i J_i^y \neq 0$.

Consider a new Hamiltonian $H_{inj} = H_0 - \sum_i (\kappa_{b1,x} J_i^x + \kappa_{b1,y} J_i^y)$,

$$\begin{aligned} H_{inj} &= \sum_{j\delta} [\kappa_\delta e^{i\phi_\delta} c_{j,\alpha}^\dagger T_{\alpha\beta}^\delta c_{j+\delta,\beta} + h.c.] + \sum_j U n_j^2 \\ &\quad - \mu \sum_j n_j - h \sum_j (n_{j\uparrow} - n_{j\downarrow}) \end{aligned} \quad (112)$$

where $\kappa_\delta = \sqrt{1 + \kappa_{b1,\delta}^2}$ and $\phi_\delta = \arg(1 + i\kappa_{b1,\delta})$, $\tan\phi_\delta = \kappa_{b1,\delta}$. The phase factor $e^{i\phi_\delta}$ can be transformed away via:

$$\tilde{c}_j = e^{-i(j_x\phi_x + j_y\phi_y)} c_j \quad (113)$$

This is expected based on the fact that the gauge-invariant current has the same structure as the hopping and the SOC term, so can be absorbed by a transformation like Eq.113, but leave the interaction U and the chemical potential μ un-touched. This absorption does not happen for the injecting current Eq.2.

Now we study the Hamiltonian in the \tilde{c}_j basis and incorporate the NNN $n = 2$ boost term

$$H_{inj} = \tilde{H}_0 + \sum_i [i(t_b/n) \tilde{c}_i^\dagger \tilde{c}_{i+ny} + h.c.] \quad (114)$$

where $t = t_0\sqrt{1 + \kappa_{b1}^2}$, $t_s = t_{s0}\sqrt{1 + \kappa_{b1}^2}$. For simplicity, we assume $t_0 = t_{s0}$, so

$$t = t_s = t_0\sqrt{1 + \kappa_{b1}^2} \quad (115)$$

Then in the \tilde{c}_j basis, the $n = 2$ term t_b becomes effectively as:

$$t_b = \frac{1 - \kappa_{b1}^2}{1 + \kappa_{b1}^2} t_{b2} \quad (116)$$

where t_b has the same sign as t_{b2} only when $0 \leq \kappa_{b1} < 1$, vanishes at $\kappa_{b1} = 1$, but becomes opposite to t_{b2} after $\kappa_{b1} > 1$. This sign change reflects the underlying lattice effects. Setting $\kappa_{b1} = 0$ reduces to the pure t_{b2} case without any NN current term.

In the following, we set $U = 0$ and $\mu = 0$ and study the effects of this NNN boost term. We treat t_b/t as an independent parameters to tune various TPTs in Fig.24.

B. The lattice theory

In the momentum space, the Hamiltonian Eq.114 becomes (dropping \sim for notational simplicity)

$$\begin{aligned} H_{inj} &= \sum_k c_k^\dagger \{ -[h + 2t(\cos k_x + \cos k_y)]\sigma_z + 2t_s \sin k_x \sigma_x \\ &\quad + 2t_s \sin k_y \sigma_y - 2(t_b/n) \sin(nk_y)\sigma_0 \} c_k \end{aligned} \quad (117)$$

where the two competing scales are listed in Eq.116 and Eq.115 respectively.

Diagonalization of Eq.(117) leads to two bands

$$\begin{aligned} E_\pm(\mathbf{k}) &= -2(t_b/n) \sin(nk_y) \\ &\quad \pm \sqrt{[h + 2t(\cos k_x + \cos k_y)]^2 + 4t_s^2(\sin^2 k_x + \sin^2 k_y)} \end{aligned} \quad (118)$$

Since $E_+(\mathbf{k}) \geq E_-(\mathbf{k})$ always holds for a fixed \mathbf{k} , we will call the E_+ the upper band and the E_- the lower band. When t_b is sufficiently small, it is in an insulating phase;

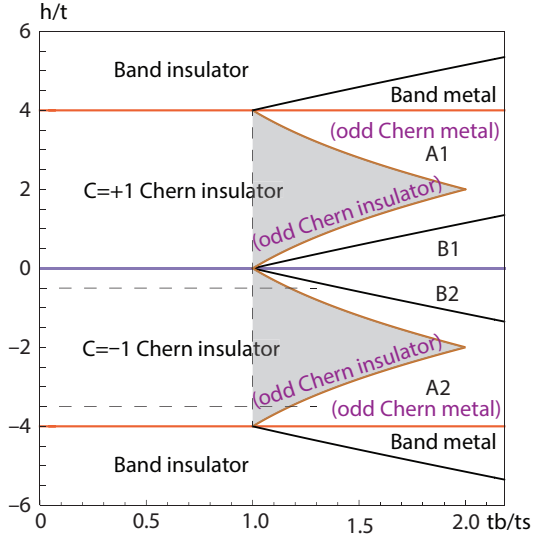


FIG. 24. The global phase diagram of the Lattice Hamiltonian (117) with $n = 2$ and $t = t_s$ under the $n = 1$ gauge-invariant injecting current. Setting $t_b = 0$ recovers dropping the $n = 2$ term. The horizontal dashed line $h = -0.5$ corresponds to the edge mode in Fig.27. The new phase is the odd Chern insulator phase in the shaded lobe. The vertical dashed line indicates the edge TPT with the parallel edge dynamic exponent $z_L = 3$. It happens earlier than the orange solid line which is the bulk TPT with the bulk dynamic exponent $z = 2$ from the bulk Chern insulator to Odd Chern metal also shown in Fig.27b1. Now the band metal has a nonzero Hall conductance, A1(A2) phase has one electronic/hole Fermi surface (FS) with positive(negative) Hall conductance. B1(B2) phase has two electronic/hole FSs with positive(negative) Hall conductance in Fig.26. While the C1 and C2 phases in Fig.3 do not exist anymore when $n > 1$. The phase boundary is related by the Mirror reflection with respect to $h \leftrightarrow \pm 4 - h$ with the mirror symmetric (MS) point at $h = \pm 2$. However, the MS only holds at the phase boundary when $t = t_s$. Compared to Fig.3.

When t_b is sufficiently large, it is in a metallic phase, with hole FS given by $E_-(\mathbf{k}) = 0$ and electronic FS given by $E_+(\mathbf{k}) = 0$.

In fact, Sec.II-IV correspond to the $n = 1$ case. Here we will briefly explore the $n = 2$ cases. The first critical t_b (let us call it $t_{b,c1}$) are determined by the global minimization problem $\min_{\mathbf{k}} E_+(\mathbf{k}; t_b) = 0$. When $t_b > t_{b,c1}$, the energy bands overlap and Fermi surface (FS) start to appear. It was shown in Sec.II that when $n = 1$, the critical $t_{b,c1} = t_s$ for $4t > h > 0$ (Fig.3). However, when $n > 1$, $t_{b,c1}$ is more complicated. For example, when $n = 2$, the critical $t_{b,c1} > t_s$ for $4t > h > 0$. When $h \sim 0$, the second critical t_b (let us call it $t_{b,c2}$) are determined by the local minimization problem $\min_{\mathbf{k}} E_+(\mathbf{k}; t_b) = 0$ with k near $(0, \pi)$ and $(\pi, 0)$. When $t_b > t_{b,c2}$, the energy bands overlap and two FSs start to appear. Unlike the $n = 1$ case, if $t > t_{b,c2}$ these two Fermi surfaces do not collide with each other, so no C phases in Fig.3 exist here. But when $t_b > t_{b,c2}$, the FS can collide with

itself, namely become extensive in k_x to cover the entire $k_x \in [-\pi, \pi]$. The extensive FS is signaled by the divergence of k_F in continuum theory. The global phase diagram of the Lattice Hamiltonian (117) with $n = 2$ is shown in Fig.24

1. The universal conductance jump of zero temperature Hall conductance

On the lattice scale, the value of Hall conductance σ_H of the insulator phases of $n > 1$ case is the same as those in the $n = 1$ case; but its value in the metal phase of $n > 1$ case is different from that in the $n = 1$ case at least in the following ways: 1) The σ_H in the band metal phase is not zero anymore in the former, but it is identically zero in the latter. 2) The σ_H in the Odd Chern metal phase is not $\pm t_s/t_b$ anymore in the former, but it is $\pm t_s/t_b$ in the latter. We show an example of Hall conductance as a function of h in Fig.25.

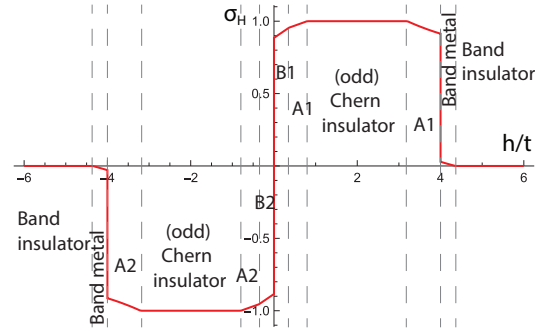


FIG. 25. The Hall conductance σ_H with a higher order boost $n = 2$ as a function of h with fixed $t = 1$, $t_s = 1$, and $t_b/t_s = 1.3$. There is an intermediate odd Chern insulator. The σ_H of band metal is not zero, and σ_H of the odd Chern metal A1 or B1 is not $\pm t_s/t_b$. However, the jump in σ_H from A1 odd Chern metal to the band metal remains t_s/t_b , that from B2 to B1 odd Chern metal remains $2t_s/t_b$. Compared to Fig.4b, σ_H is no longer a simple step function when $n > 1$. However, all the jumps stay the same as the $n = 1$ case, indicating its universal feature.

C. The continuum limit

In the momentum space, Eq.(117) becomes

$$H(\mathbf{k}) = -[h + 2t(\cos k_x + \cos k_y)]\sigma_z + 2t_s \sin k_x \sigma_x + 2t_s \sin k_y \sigma_y - 2(t_b/n) \sin(nk_y)\sigma_0 \quad (119)$$

when $h \sim 4t$, low-energy excitations exist near $\mathbf{K}_3 = (\pi, \pi)$

$$H_3(\mathbf{K}_3 + k) = -[h - 4t + t(k_x^2 + k_y^2)]\sigma_z - 2t_s k_x \sigma_x - 2t_s k_y \sigma_y - (-1)^n 2t_b k_y \sigma_0 \quad (120)$$

when $h \sim 0$, low-energy excitations exist near both $\mathbf{K}_1 = (\pi, 0)$ and $\mathbf{K}_2 = (0, \pi)$

$$\begin{aligned} H_1(\mathbf{K}_1 + \mathbf{k}) &= -[h + t(k_x^2 - k_y^2)]\sigma_z - 2t_s k_x \sigma_x + 2t_s k_y \sigma_y \\ &\quad - 2t_b k_y \sigma_0 \\ H_2(\mathbf{K}_2 + \mathbf{k}) &= -[h - t(k_x^2 - k_y^2)]\sigma_z + 2t_s k_x \sigma_x - 2t_s k_y \sigma_y \\ &\quad - (-1)^n 2t_b k_y \sigma_0 \end{aligned} \quad (121)$$

when $h \sim -4t$, low-energy excitations exist near $\mathbf{K}_0 = (0, 0)$

$$\begin{aligned} H_0(\mathbf{k}) &= -[h + 4t - t(k_x^2 + k_y^2)]\sigma_z \\ &\quad + 2t_s k_x \sigma_x + 2t_s k_y \sigma_y - 2t_b k_y \sigma_0 \end{aligned} \quad (122)$$

Thus only even or odd nature of n is important.

The continuum theory with just one valley is identical to that in the injecting case with $n = 1$. So we only need to look at the continuum theory near the two valleys K_1 and K_2 :

$$\begin{aligned} H_1 &= [\Delta - \alpha(k_x^2 - k_y^2)]\sigma_z - vk_x \sigma_x + vk_y \sigma_y - ck_y \sigma_0 \\ H_2 &= [\Delta + \alpha(k_x^2 - k_y^2)]\sigma_z + vk_x \sigma_x - vk_y \sigma_y - ck_y \sigma_0 \end{aligned} \quad (123)$$

where $\Delta = -h, \alpha = -t, v = 2t_s$ and $c = 2t_b$. Note the different sign of velocities v between k_x and k_y and different sign of α between k_x^2 and k_y^2 . Most importantly, the Doppler shifts are identical in the two nodes, in contrast to Eq.61 where they are opposite in the two nodes.

Due to the extra two degree of freedom, we obtain the four bands

$$\epsilon_{i,\pm} = \pm \sqrt{v^2 k^2 + [\Delta + (-1)^i \alpha(k_x^2 - k_y^2)]^2} + ck_y, \quad (124)$$

where $i = 1, 2$. Due to $c_1 = c_2$, the electron Fermi momentum of $\epsilon_{1,2}$ will have the same sign. We show the evolution of the FS of H_1 and H_2 in Fig.26.

Another important feature of $\alpha_x \alpha_y < 0$ is that the FS extends to infinity when $c \geq \sqrt{2}|v|$. The divergent k_F hints the FS is extensive in k_x , which covers the entire $k_x \in [-\pi, \pi]$.

VI. THE TOPOLOGICAL PHASES IN THE GAUGE INVARIANT CURRENT: EDGE PROPERTIES

Following the approach used in the Sec.IV for the $n = 1$ case, we will first study the edge properties from the lattice system, then investigate them from the continuum effective theory, then contrast the two complementary approaches.

A. New bulk-edge correspondence from the lattice theory

For the periodic boundary condition in the y -direction and open boundary condition in the x -direction, k_y is

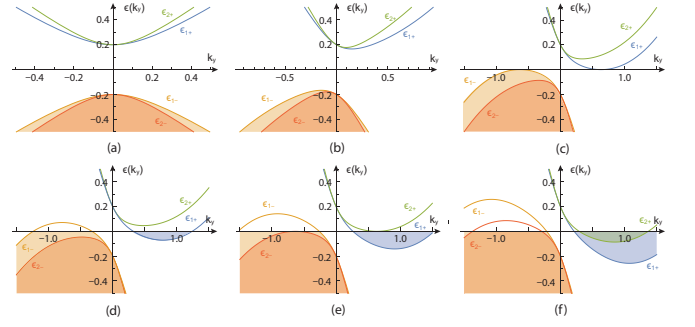


FIG. 26. $\epsilon_{i,\pm}(k)$ with even n as function of k_y with fixed $k_x = 0$ and $v = 1, \Delta = 1/5, \alpha = -1/2, c = 0, 0.5, 1.0, \sqrt{1.4}, 1.3$. (a) both H_1 and H_2 has a direct gap at $k_y = 0$; in the Chern Insulator phase (b) Due to the same sign of the boost velocity in Eq.124, H_1 and H_2 shift to the same direction, so has an indirect gap at $k_y \neq 0$; (c) H_1 becomes gapless and shows two Fermi points at $k_y = \pm k_0$ with $z = 2$, but H_2 still has an indirect gap. This is in the A1 phase in Fig.24. (d) H_1 becomes gapless and show finite Fermi pockets, H_2 also becomes gapless and shows two Fermi points still at $k_y = \pm k_0$ with $z = 2$ after subtracting the non-critical contributions from H_1 ; (e) both H_1 and H_2 are gapless and show finite Fermi pockets. This is in the B1 phase in Fig.24. Compared to Fig.17. H_1 and H_2 may collide with each other (namely, hit the BZ boundary, not shown in Fig.23) instead of colliding with each other as in Fig.17.

a good quantum number, the Hamiltonian in the mixed (i, k_y) representation becomes

$$\begin{aligned} H &= \sum_{k_y, i, j} c_{i, k_y}^\dagger \{[-(h + 2t \cos k_y)\sigma_z \\ &\quad + 2t_s \sin k_y \sigma_y + t_b \sin 2k_y \sigma_0] \delta_{i, j} \\ &\quad + (t\sigma_z - it_s \sigma_y) \delta_{i, j+1} + (t\sigma_z + it_s \sigma_y) \delta_{i, j-1}\} c_{j, k_y} \end{aligned} \quad (125)$$

For the periodic boundary condition in the x -direction and open boundary condition in the y -direction, k_x is a good quantum number, the Hamiltonian in the mixed (k_x, i) representation becomes:

$$\begin{aligned} H &= \sum_{k_x, i, j} c_{k_x, i}^\dagger \{[-(h + 2t \cos k_x)\sigma_z + t_s \sin k_x \sigma_x] \delta_{i, j} \\ &\quad + (t\sigma_z - it_s \sigma_y) \delta_{i, j+1} + (t\sigma_z + it_s \sigma_y) \delta_{i, j-1} \\ &\quad - it_b \sigma_0 (\delta_{i, j+2} - \delta_{i, j-2})/2\} c_{k_x, j} \end{aligned} \quad (126)$$

We show the numerical results on the lattice edge states in the Fig.27 and 28.

When comparing the $n = 2$ case with previous $n = 1$ case, We discover several new surface TPT and novel bulk-edge correspondence:

(a) Longitudinal injection

We first choose periodic boundary condition in the y -direction and open boundary condition in the x -direction. For $n = 1$ case and $t_b/t_s = 1$, the bulk is critical. The $n = 1$ edge mode is almost flat due to the cancelation of $\omega \sim t_s \sin k_y - t_b \sin k_y = 0$. So the TPT happens in the edge and the bulk at the same time. However, for $n = 2$,

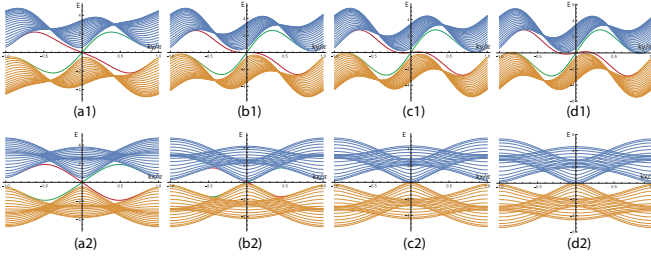


FIG. 27. The edge state of the lattice Hamiltonian Eq. (117). From (a) to (d), the parameter t_b/t_s is 0.5, 1.0, 1.17, 1.3, respectively. We fixed $h = -0.5$. (Top) Longitudinal boost: With periodic boundary condition in the y -direction and open boundary condition in the x -direction. The edge modes always exist in this case. The two edge mods move in the opposite direction near $k_y = 0$ in (a1) Chern Insulator where $t_b/t_s < 1$, then one edge mode's slope vanishes in (b1) where $t_b/t_s = 1$ with the edge dispersion $\omega \sim k_y^3$, namely the longitudinal edge dynamic exponent $z_L = 3$. then the two edge modes move along the same direction near $k_y = 0$ in (c1) odd Chern insulator where $t_b/t_s = 1.17 > 1$. At the same time, the system's (in-direct) gap vanishes which corresponds to the $z = 2$ bulk TPT from the $C = -1$ odd Chern insulator to A2 Odd Chern metal in Fig.24. It gets to the Odd Chern metal phase in (d1) where $t_b/t_s = 1.3 > 1.17$, the two edge modes still move along the same direction. (Bottom) Transverse boost: Exchanging the role of x - and y - direction. The edge mode exists upto (c2) where $t_b/t_s = 1.17 > 1$. So the odd CI between (b2) and (c2) still has the transverse edge mode. At (c2), the system's direct gap vanishes which corresponds to the TPT from the $C = -1$ odd Chern insulator to A2 Odd Chern metal in the bulk in Fig.24. It is in the Odd Chern metal phase in (d2) where $t_b/t_s = 1.3 > 1.17$, no edge mode. The T-edge disappears at the same time as the bulk TPT with its velocity still vanishing $\sqrt{v^2 - c^2}$ as in Fig.23. One can shift $k \rightarrow k + \pi$ to reach $h = +0.5$ results. See also Fig.S3 for the expanded figure.

the TPT splits into two with the odd Chern insulator intervening between: the reconstruction in the edge always happens earlier than in the bulk. When $t_b/t_s < 1$, the two edge modes in the Left and Right move along the opposite direction. When $t_b/t_s > 1$, the two edge modes in the Left and Right move along the same direction. At the QCP $t_b/t_s = 1$, the $n = 2$ edge mode is not flat, due to the edge dispersion relation

$$\begin{aligned} \omega &\sim t_s \sin k_y - (t_b/2) \sin 2k_y \\ &= (t_s - t_b \cos k_y) \sin k_y \sim k_y^3 \end{aligned} \quad (127)$$

which is shown in Fig.27b1. So the CI to odd CI transition indeed happens at $t_b/t_s = 1$ with the dynamic exponent $z_L = 3$ due to the longitudinal edge reconstruction. The bulk remains gapped despite the edge mode reconstruction at the QCP. Then as t_b/t_s increase further, the bulk gap closes and also undergoes a TPT at $t_b/t_s = 1.17$ in Fig.27c. It corresponds to nothing but the bulk TPT from the $C = 1$ odd Chern insulator to the A1 Odd Chern metal in Fig.24 and Fig.26c.

(b) *Transverse injection:*

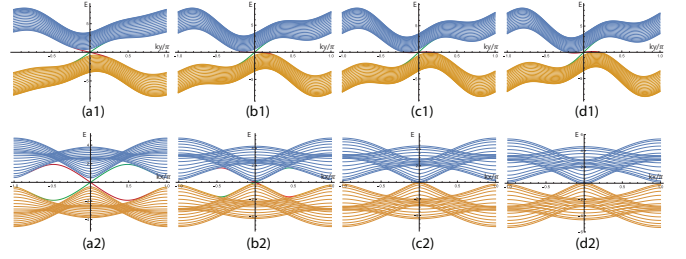


FIG. 28. The same situation as Fig.27 except $h = -3.5$ which is Mirror reflected image of $h = -0.5$. As alerted in Fig.24, despite the bulk phase boundary in Fig.24 has such a Mirror symmetry at $t = t_s$, it is not persevered in the presence of the strip boundaries. One can shift $k \rightarrow k + \pi$ to reach $h = +3.5$ results which is Mirror reflected image of $h = 0.5$. It shows qualitatively the same edge TPTs, odd CI and odd CM as those in Fig.27. See also Fig.S4 for the expanded figure.

Then we choose the periodic boundary condition in the x -direction and open boundary condition in the y -direction. For $n = 1$ case and $t_b/t_s = 1$, the bulk is critical. The $n = 1$ edge mode is also squeezed away. So the TPT happens in the edge and the bulk at the same time. However, for $n = 2$, one can find the edge mode of the odd CI still exists at $t_b/t_s = 1$ in Fig.27-b2. So the transverse edge mode of the odd CI survives always before the bulk gap closing. So we conclude that the odd CI has the longitudinal edge modes satisfying the exotic $v_L v_R > 0$, but the transverse edge modes satisfying the conventional $v_L v_R < 0$. Eq.99. break down and need to be replaced by more refined edge theory by incorporating high order derivatives in the continuum theory.

B. New bulk-edge correspondence from the continuum theory

Because $h/t \sim -4$ case with only one valley is similar to the injecting case with $n = 1$ on the long-wave length limit, so we only need to focus on the $h \sim 0$ case with two valleys when $n = 2$.

When $h \sim 0$, the effective Hamiltonians near the two valleys K_1, K_2 are:

$$\begin{aligned} H_1 &= [\Delta - \alpha(k_x^2 - k_y^2)]\sigma_z - vk_x\sigma_x + vk_y\sigma_y - ck_y\sigma_0 \\ H_2 &= [\Delta + \alpha(k_x^2 - k_y^2)]\sigma_z + vk_x\sigma_x - vk_y\sigma_y - ck_y\sigma_0 \end{aligned} \quad (128)$$

where $\Delta = -h$, $\alpha = t$, $v = 2t_s$, $c = 2t_b$. In fact, all the 4 nodes suffer the same sign of Doppler shifts when $n = 2$ case.

It can be rewritten in the generic form of Eq.104

$$\begin{aligned} H_1 &= (\Delta + \alpha_{1x}k_x^2 + \alpha_{1y}k_y^2)\sigma_z + v_{1x}k_x\sigma_x + v_{1y}k_y\sigma_y \\ &\quad - c_1k_y\sigma_0 \\ H_2 &= (\Delta + \alpha_{2x}k_x^2 + \alpha_{2y}k_y^2)\sigma_z + v_{2x}k_x\sigma_x + v_{2y}k_y\sigma_y \\ &\quad - c_2k_y\sigma_0 \end{aligned} \quad (129)$$

which leads to the relations

$$\begin{aligned} \alpha_{1x} &= -\alpha, \quad \alpha_{1y} = +\alpha, \quad v_{1x} = -v, \quad v_{1y} = +v, \quad c_1 = +c \\ \alpha_{2x} &= +\alpha, \quad \alpha_{2y} = -\alpha, \quad v_{2x} = +v, \quad v_{2y} = -v, \quad c_2 = +c \end{aligned} \quad (130)$$

If $\alpha_{1x}\Delta > 0$, then $\alpha_{2x}\Delta < 0$, $\alpha_{1y}\Delta < 0$, and $\alpha_{2y}\Delta > 0$, which means only one of the valleys may have one edge state for a given type of boundary. Further discussions on the long-wavelength limit to the quadratic order are the same as Sec.IV-C-2. For example, if one keeps only up to the quadratic order, then both $n = 1$ and $n = 2$ gives zero slope when $t_b/t_s = 1$.

However, to check against the new bulk-edge correspondence discovered on the lattice theory in Sec.VI-A, one may need to go to higher order derivatives in the continuum edge theory. For example, to find the dynamic exponent $z_L = 3$ in the longitudinal boost, one needs to go to at least the cubic order in Eq.127. Similarly, one need to push Eq.99 to higher order derivatives to describe the edge states evolution in Fig.27 and 28 under the transverse boost. More works need here to discern the fine structures of the edge states by going to high order in the momentum.

VII. THE CLASSIFICATION OF EVEN/ODD CHERN METAL AND BAND METAL

So far, we only consider the case where the Hamiltonian respects the \mathcal{C} -symmetry, but breaks the \mathcal{P} -symmetry, namely, odd under the \mathcal{P} . We call it the odd Chern metal. In the Appendix A and B, we discuss the complimentary cases: respects the \mathcal{P} -symmetry, but breaks the \mathcal{C} -symmetry. We call it the even Chern metal which will be shown to show dramatically different behaviours than the odd Chern metals. In this section, we classify Chern metals as even and odd. In the next section, we discuss the general case which breaks both the \mathcal{C} -symmetry and \mathcal{P} -symmetry.

The generic Hamiltonian in a material consists of two parts

$$H(k) = \epsilon_0(k)\sigma_0 + H_{\text{QAH}}(k), \quad (131)$$

where the $H_{\text{QAH}}(k)$ part respects both \mathcal{C} -symmetry in Eq.3 and \mathcal{P} -symmetry. An even function $\epsilon_0(k)$ breaks the \mathcal{C} -symmetry, but keeps the \mathcal{P} -symmetry, In the appendix A and B, we consider the two typical even cases respectively: (I) $\epsilon_0(k) = -\mu = -t_b$ and (II) $\epsilon_0(k) = -2t_b(1 - \cos k_y)$. More general case $\epsilon_0(k) = -2t_b(1 - \cos k_x + 1 - \cos k_y)$ can be straightforwardly extended to. To break both the \mathcal{C} -symmetry and \mathcal{P} -symmetry, we choose $\epsilon_0(k) = -2t_b(\sin k_y + 1 - \cos k_y)$ as a concrete example to discuss in Sec.VIII.

Varying the strength of $\epsilon_0(k)$ drives an Chern insulator to a Chern metal with Fermi surfaces. Both carry non-vanishing Chern number. If keeping \mathcal{C} -symmetry, tentatively, we name the Chern metal as ‘‘odd’’ Chern

metal; If keeping \mathcal{P} -symmetry, tentatively, we name the Chern metal as ‘‘even’’ Chern metal. If no symmetries is kept, then it could be either odd-like or even-like Chern metal.

In the following, we will only focus on exploring the differences between odd and even Chern metal in the phase diagram and the Hall conductance from both the bulk and edge picture.

A. Phase diagram: TPT from (odd) Chern Insulator to odd/even Chern metal due to the competition between the P-even and P-odd component

In the global phase diagram, due to its topological protection, the Chern insulator remains the same in both P-breaking and P-preserving deformation. Even the band insulator remains the same. However, the metallic phases may differ. The big differences between odd and even Chern metals can be best seen around the critical points at $h = \pm 4t, 0$. In the odd Chern metal, as shown in Fig.2 (also Fig.11 and Fig.15) and Fig.23, the QPTs at $h = \pm 4t$ and 0 (Dirac theory) with $z = 1$ is stable, which means the TPT from the CI to the odd CM needs a sufficiently large enough t_b even near $h = \pm 4t$ and 0. The energy scale of the critical t_b is comparable to the Fermi velocity of the Dirac cone, which is of the energy scale t_s . As demonstrated in the previous sections, there is a universal non-integer jump from the odd Chern metal to the band metal. The longitudinal edge modes in the odd CI and odd CM on the two opposite side of a sample move along the same direction. These salient bulk and edge properties make it very easy to distinguish an odd CM from the BM.

In the even Chern metal, as shown in Fig.37a, the critical points at $h = 4t$ with the Dirac point at (π, π) and $h = 0$ (with the two Dirac points at $(\pi, 0)$ and $(0, \pi)$) with $z = 1$ is not stable, even a small t_b drives a TPT from the CI to even CM near $h = 4t$ and 0. Then the energy scale of transition t_b is comparable with the gap of the Dirac cone, which is of the energy scale t or $h \pm 4t$. This has been demonstrated in the appendix B. However, the critical points at $h = -4t$ with the Dirac point at $(0, 0)$ remains stable. So due to C- symmetry breaking by the P- preserving energy dispersion, the CM at $0 < h/t < 4$ behave very differently than that at $-4 < h/t < 0$: the former is essentially the same as BM, the latter is the true CM with edge modes well separated from the bulk. So the naively thought even Chern metal at $0 < h/t < 4$ turns out to be the same phase as BM (Table II).

B. Universal Hall conductance jump: bulk picture

It was well-known that there is an integer (quantized) Hall conductance jump between Chern insulator and

band insulator, or different Chern insulators (see also Fig.2). As shown in the previous sections and elucidated further in the appendix C, a non-integer (unquantized but universal v/c) Hall conductance jump from odd or odd-like Chern metal to itself or to a band metal. As shown in the appendix A, B and Sec.VIII, there may be an integer (quantized) Hall conductance jump from even or even-like Chern metal to itself or to a band metal.

In the bulk picture, the Universal Hall conductance jump across the two metallic phases (either even/odd Chern metal or a band metal) at $h = h_c$ can be understood as follows: it is the sum of the upper and lower bands $\Delta\sigma = \Delta\sigma_- + \Delta\sigma_+$, where

$$\Delta\sigma_s(h_c) = \lim_{h \rightarrow h_c^+} \frac{1}{2\pi} \int_{k \text{ filled}} d^2k \Omega_s(k; h) - \lim_{h \rightarrow h_c^-} \frac{1}{2\pi} \int_{k \text{ filled}} d^2k \Omega_s(k; h) \quad (132)$$

where $s = \pm$ stands for the upper/lower band respectively.

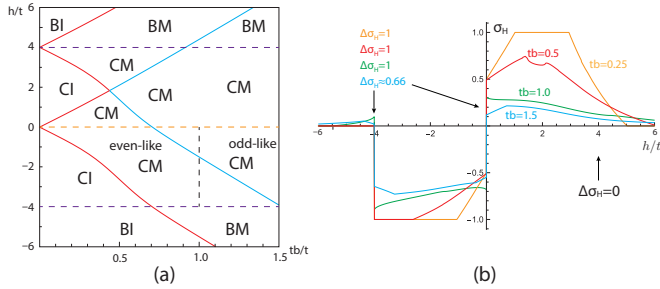


FIG. 29. (a) The global phase diagram of the Lattice Hamiltonian (135) of the even-odd mixing Chern metal. The even-like CM or odd-like CM exist when $-4 < h/t < 0$ with an edge reconstruction between the two with the dynamic longitudinal exponent $z_L = 2$ in Eq.134. In the even CM $v_L v_R < 0$, in the odd CM $v_L v_R > 0$. At the $z_L = 2$ edge reconstruction point, $v_L v_R = 0$. While all the CM at $0 < h/t < 4$ are essentially the same as the BM despite superficially their bands have a non-vanishing Chern number, practically also larger AHE. Due to this superficial and practical difference, we still keep the symbol CM in the figure, but they really belong to the same phase. (b) The Hall conductance as a function of h/t for various fixed values of $t_b/t = 0.25, 0.50, 1.00, 1.50$. The other parameters are $t = t_s = 1$. The Hall conductance only shows a jump at $h/t = -4$ and $h/t = 0$. For example, the $t_b/t = 0.25$ curve shows a unit jump near $h/t = 0$ from the even-like CM to a BM and also a unit jump near $h/t = -4$ from the CI to a BI which always has $\sigma_H = 0$; On the other hand, $t_b/t = 1.5$ curve shows a universal non-integer jump near $h/t = 0$ and also near $h/t = -4$ from the odd-like CM to a BM. Note that due to the absence of even CM to even CM transition here, the factor of 2 in the odd CM to odd CM transition in Fig.25 does not appear here. Near $h/t \sim 0^-$, it is easy to reach the even-like CM from the CI due to $t_b/t \rightarrow 0^-$, but it still need $t_b/t = 1$ to reach the odd-like CM.

As shown in the appendix D, When $h \rightarrow h_c$, $\Omega_s(k; h)$ will show a singularity or a Berry phase at the corre-

sponding Dirac points.

$$\begin{aligned} h \rightarrow +4|t|, & \frac{1}{2\pi} \Omega_s(\mathbf{k}; h) \rightarrow +(s/2) \text{sgn}(4|t| - h) \delta(\mathbf{k} - \mathbf{K}_3) \\ & + F(\mathbf{k}), \\ h \rightarrow 0, & \frac{1}{2\pi} \Omega_s(\mathbf{k}; h) \rightarrow (s/2) \text{sgn}(h) [\delta(\mathbf{k} - \mathbf{K}_1) \\ & + \delta(\mathbf{k} - \mathbf{K}_2)] + F(\mathbf{k}), \\ h \rightarrow -4|t|, & \frac{1}{2\pi} \Omega_s(\mathbf{k}; h) \rightarrow -(s/2) \text{sgn}(4|t| + h) \delta(\mathbf{k} - \mathbf{K}_0) \\ & + F(\mathbf{k}), \end{aligned} \quad (133)$$

where $\mathbf{K}_3 = (\pi, \pi)$, $\mathbf{K}_1 = (\pi, 0)$, $\mathbf{K}_2 = (0, \pi)$ and $\mathbf{K}_0 = (0, 0)$ as listed in Sec.III.

Note that the limit of $\Omega_s(\mathbf{k}; h)$ has both a discontinuous δ -function and a continuous part $F(\mathbf{k})$. The latter is a non-universal function which depends on the microscopic details, but it has no contribution to the Universal Hall conductance jump. When tuning h across h_c , there are three situations:

- 1) The FS includes the singularity of $\Omega_s(k; h)$;
- 2) The FS excludes the singularity of $\Omega_s(k; h)$;
- 3) The FS does not include (or exclude) the singularity of $\Omega_s(k; h)$ when $h \neq h_c$, but approaches it as $h \rightarrow h_c$.

In the case 1) and 2) which belongs to the even Chern metal case, one can interchange the limit with the integral in Eq.132 which is an integration over the δ -functions. Then a simple counting tells the Universal Hall conductance jump is zero or an integer which is in the same class after modula an integer Z .

For the case 3) which belongs to the odd Chern metal case, one can not interchange limit with the integral in Eq.132, so one must do the integral first, then take the limit. This order gives a non-integer number which is found to be a universal number $v/(2c)$ with $c > v$ for each singularity point, where c and v are the two parameters of the boosted continuum Dirac theory in Eq.24. For the specific lattice Hamiltonian Eq.131 $v/(2c) = t_s/(2t_b)$.

C. Universal Hall conductance jump: the edge picture and the bulk-edge correspondence in the even/odd Chern metal

Because as the transverse edge mode behave similarly (see Fig.26 and Fig.27) in all the cases: it disappears at the same time as the bulk TPT with the edge velocity vanishing as $\sqrt{v^2 - c^2}$. So we only consider the longitudinal case in the edge mode. Near the QPTs $h = \pm 4t$ or 0 and $t_b = 0$, there might be edge states near the momentum where the direct band gap closes at $\mathbf{K}_3 = (\pi, \pi)$, $\mathbf{K}_1 = (\pi, 0)$, $\mathbf{K}_2 = (0, \pi)$, $\mathbf{K}_0 = (0, 0)$. When $h/t < -4$, there is no edge states; when $-4 < h/t < 0$, there is an edge state near $k_y = 0$; when $0 < h/t < +4$, there is an edge states near $k_y = \pi$; when $h/t > +4$, there is no edge states. To judge the Universal Hall conductance jump from the edge picture, one need to identify

the relation between the Fermi energy and the edge states near the two minima $k_y = 0$ and $k_y = \pi$.

We reach the following conclusion: When tuning h across the critical points $h = \pm 4t$ or 0 , If the Fermi energy cuts edge states near the two minima in one phase, but not the other, then there is a Universal Hall conductance jump. Otherwise the Hall conductance jump is zero. As $-4 < h/t < 0$ goes to $0 < h/t < +4$, because the change near the minimum $k_y = 0$ to near the minimum $k_y = \pi$

in the momentum space, one may need to keep track of the changing of edge states near both minima.

One may also tell the difference between an integer jump in the even Chern metal and a non-integer jump in the odd Chern metal by the following criterion: In the even $v_L v_R < 0$, in the odd $v_L v_R > 0$ when $h \rightarrow \pm 4t$ or 0 (Table II), where v_L and v_R denote the velocities of the left and right edge modes respectively. Recall that $v = \partial \epsilon_{k_y} / \partial k_y |_{\epsilon_{k_y} = \epsilon_F = 0}$.

TABLE II. The classification of unquantized Anomalous Hall effect. The Bulk σ_H jump is defined across the TPT from the corresponding phase to the band metal phase. As shown in Table III, the integer jump from the BM to the even Chern metal is equal to that of Chern number near $h = -4t$, but only one half of that of Chern number near $h = 0$.

AHE metal	Band metal	Even Chern metal	Odd Chern metal
Symmetry	No	C - No, P -Yes	C -Yes, P -No
Chern number	0 or ± 1	± 1	± 1
Bulk σ_H jump	0	Integer	non-integer
Longitudinal Edge	no edge or floating edge	edge velocities $v_L v_R < 0$	edge velocities $v_L v_R > 0$

Where we did not list the quantized AHE phases: CI and odd CI which has the L/T edge $v_L v_R < 0$ and L/T edge $v_L v_R > / < 0$ respectively. The trivial BI is not listed either. For the bulk TPT or edge TPT between any of the two phases, see the Table I.

The Time reversal symmetry is always spontaneously broken. The bulk jump σ_H is from the BM to the even or odd CM. Note that (1) All the three metals have no transverse edges. (2) Even or odd CM must have a non-vanishing Chern number for the relevant energy bands, but the band metal may or may not have a non-vanishing Chern number. So Chern number becomes an irrelevant topological number in this classification of gapless metallic phases.

We did not list the even-like CM or Odd-like CM to be examined in the next section which breaks both C - and P -, because they qualitatively belong to either even or odd CM. At the edge QCP $t_b/t_s = 1$ from the even-like to odd-like Chern metal, the edge mode is not flat, due to the edge dispersion relation

$$\begin{aligned} \omega &\sim t_s \sin k_y - t_b (\sin k_y + 1 - \cos k_y) \\ &= -t_b (1 - \cos k_y) \sim -k_y^2 < 0 \end{aligned} \quad (134)$$

which leads to the dynamic longitudinal edge exponent $z_L = 2$ from the even-like CM to the odd-like CM (Fig.31 and Fig.33). It can be contrasted to the longitudinal edge exponent $z_L = 3$ from the Chern insulator to the odd Chern insulator in Fig.26 and Fig.27. The former is inside the gapless metallic phase, the latter is inside the gapped insulating phase. However, both have the same bulk, but different edges. At both QCPs, $v_L v_R = 0$ which dictates the boundary.

The BM in this table is nothing but the previously well studied one contributing to the un-quantized AHE [2–4]. The even CM with the conventional edge modes $v_L v_R < 0$ may probably have appeared in the context of bilayer Kagome metals [39] or twisted bilayer graphene [40]. Unfortunately, neither bulk nor edge properties of this possible even Chern metal, its distinctions with the band metal have been discussed in any depth in these *ab initio* density functional theory calculations. The odd CM with the exotic edge modes $v_L v_R > 0$ for $n = 1$ in Sec.II-IV and for $n = 2$ in Sec. V-VI are discovered and investigated systematically here. While the itinerant metal contributing the AHE due to the Berry phase acquired by electrons moving in the non-coplanar spin texture from the monopoles in the real space in a Ferromagnet [1] does not fall into this Table which is only for non-interacting fermions.

In the appendix A and B, we demonstrate the above general statements and Table II for two specific examples of the even Chern metal. In the next section, we do it for a concrete example of the generic case in any material which is a mixing of even-odd Chern metal, but still show either even-like or odd-like Chern metal features.

VIII. THE EVEN-LIKE AND ODD-LIKE CHERN METALS

In any real material, there exist both the even and odd component. So in this section, we study the even-odd mixing case $\epsilon_0(k) = -2t_b (\sin k_y + 1 - \cos k_y)$ which break both the C -symmetry and P -symmetry.

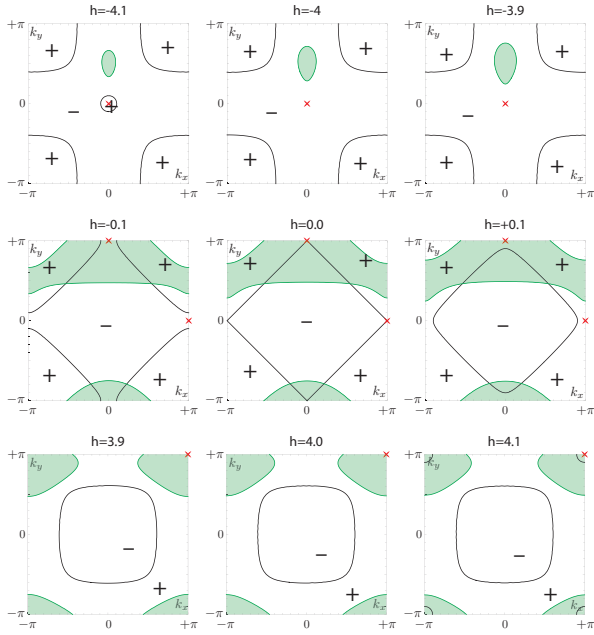


FIG. 30. The Berry curvature $\Omega_+(\mathbf{k})$ and the Fermi surfaces (FS) of the even-like Chern metal, it leads to $\Delta\sigma_+$ in the Table III. Other parameters are $t = 1$, $t_s = 1$, $t_b = 0.75 < 1$. The black curve is the contour of $\Omega_+(\mathbf{k}) = 0$, which separates the positive part denoted by “+” from the negative part denoted by “-”. The red \times denotes the singular part of $\Omega_+(\mathbf{k})$ listed below Eq.132. The green line denotes the electron FS. Top: near $h/t = -4$, the upper band FS always excludes the singularity of $\Omega_+(\mathbf{k})$ leading to $\Delta\sigma_+ = 0$, thus the Universal Hall conductance jump is 1; Middle: near $h/t = 0$: the upper band FS only encloses one of the two singularities of $\Omega_+(\mathbf{k})$ leading to $\Delta\sigma_+ = -1$, thus the Universal Hall conductance jump is also 1; Bottom: near $h/t = +4$, the upper band FS always enclose the singularity of $\Omega_+(\mathbf{k})$ leading to $\Delta\sigma_+ = 1$, thus the Universal Hall conductance jump is 0 (Table III). The lower band is always occupied, so always encloses the singularity of $\Omega_-(\mathbf{k})$, it leads to $\Delta\sigma_-$ in the Table III. These features are essentially the same as those in the even Chern metal case shown in Fig.38, so the metallic phase in $-4t < h < 0$ can be called even-like Chern metal.

The total Hamiltonian takes the form:

$$H(k) = -2t_b(\sin k_y + 1 - \cos k_y) + H_{\text{QAH}}(k) \quad (135)$$

The two energy bands are:

$$E_{\pm}(k) = \pm E_{\text{QAH}}(k) - 2t_b(\sin k_y + 1 - \cos k_y) \quad (136)$$

At the QPT from the Chern metal phase to the band metal, there is no Hall conductance jump at $h/t = 4$, but a Hall conductance jump at $h/t = -4$ and 0. To exam the Hall conductance jump, by tracing the location of the FS, we find it can still be classified into the even-like or odd-like Chern metals.

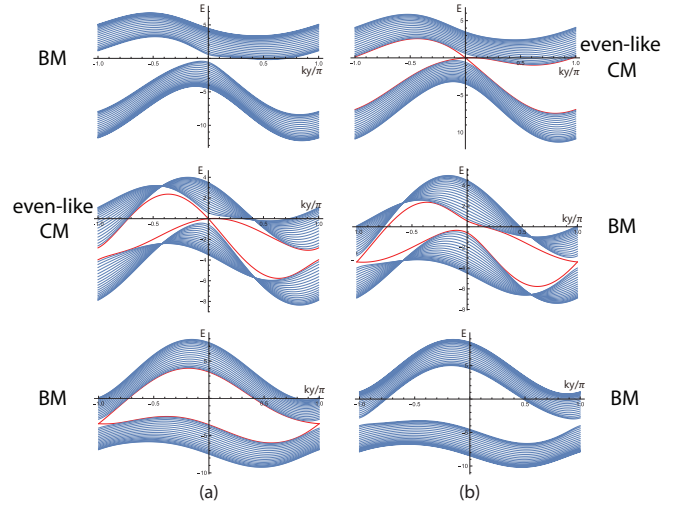


FIG. 31. The longitudinal edge structure of the even-like Chern metal at different h/t values. Other parameters are $t = 1$, $t_s = 1$, $t_b = 0.85 < 1$. Top (a) $h/t = -4.5$, no edge state, bulk FS, just a band metal (b) $h/t = -3.5$, an edge state at Fermi energy near $k_y = 0$, bulk FS, even-like Chern metal. There is TPT from (a) to (b) and an associated unit Hall conductance jump due to the useful edge mode in (b). Middle (a) $h/t = -0.5$, an edge state at Fermi energy near $k_y = 0$, even-like Chern metal (b) $h/t = +0.5$, there is an edge state near $k_y = \pi$, but it is well below the Fermi energy. So despite there is an edge mode floating around the vast majority of bulk states. It is a BM. There is a TPT from (a) to (b) and an associated unit Hall conductance jump due to the useful edge mode in (a). Bottom (a) $h/t = +3.5$, there is an edge state near $k_y = \pi$, but it is well below the Fermi energy, a BM (b) $h/t = +4.5$, no edge state, a BM. There is no Hall conductance jump. Inside the even-like Chern metal, the edge modes at the Fermi energy near $k_y = 0$ satisfy $v_L v_R < 0$, thus the Hall conductance jump is an integer. These features are essentially the same as those in the even Chern metal shown in Fig.39, so can be called even-like Chern metal.

A. The even-like Chern metal

When $t_b \leq t_s$, the situation is similar to the even case II presented in the appendix B, thus there is no Hall conductance jump at $h/t = 4$, but a unit Hall conductance jump at $h/t = -4$ and 0. It is shown in Table III which is identical as the Table V for the even Chern metal, so the metallic phase in $-4t < h < 0$ can be called even-like Chern metal. The change of Chern number ΔCh_- can be read from Fig.1, which is independent of σ_0 term.

TABLE III. The Universal Hall conductance jump from the even-like Chern metal to BM extracted from Fig.30. It is defined as that of BM subtracts that of the even CM.

h	$\Delta\sigma_-$	$\Delta\sigma_+$	$\Delta\sigma$	ΔCh_-
$-4 t $	+1	0	1	1
0	+2	-1	1	2
$+4 t $	-1	+1	0	-1

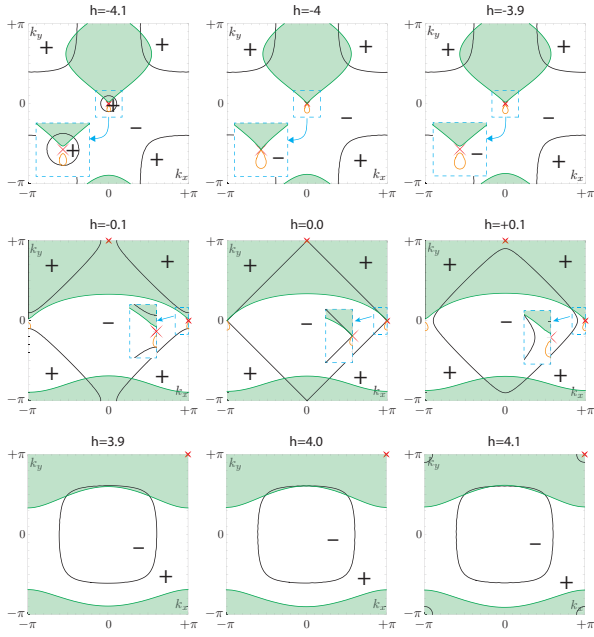


FIG. 32. Berry curvature $\Omega_+(\mathbf{k})$ and the FS of the odd-like Chern metal: Other parameters are $t = 1$, $t_s = 1$, $t_b = 1.25 > 1$. The black curve, the red \times and the green line denote the same information as Fig.36. However, the main difference than Fig.30 is that the lower band is not always occupied, then the orange line denotes the hole FS of the lower band which is small and magnified in the figure. Top: near $h/t = -4$: the upper band FS inclined to enclose the singularity of $\Omega_+(\mathbf{k})$, it leads to $\Delta\sigma_+$ in the first line in Table III. the lower band FS inclined to exclude the singularity of $\Omega_-(\mathbf{k})$, it leads to $\Delta\sigma_-$ in the first line in the Table III. thus the Universal Hall conductance jump is a non-integer; Middle: near $h/t = 0$: the upper band FS inclined to enclose one of the two singularities of $\Omega_+(\mathbf{k})$, the lower band FS inclined to exclude one of the two singularities of $\Omega_-(\mathbf{k})$, thus the Universal Hall conductance jump is a non-integer; Bottom: near $h/t = +4$: the upper band FS always enclose the singularity of $\Omega_+(\mathbf{k})$, the lower band is full occupied, thus the Hall conductance jump is 0. As shown in Table IV, Fig.33 and appendix C, the metallic phase in $-4t < h < 0$ can be called odd-like Chern metal.

B. The odd-like Chern metal

When $t_b > t_s$, the situation is similar to the main text “odd” case. thus there is no Hall conductance jump at $h/t = 4$ and non-integer Hall conductance jump at $h/t = -4$ and 0. The value of non-integer is nothing but t_s/t_b .

TABLE IV. The Universal Hall conductance jump of the odd-like Chern metal to BM. The change of Chern number ΔCh_- is the same as that in Table-III.

h	$\Delta\sigma_-$	$\Delta\sigma_+$	$\Delta\sigma$
$-4 t $	$t_s/(2t_b)$	$t_s/(2t_b)$	t_s/t_b
0	$+1 + t_s/(2t_b)$	$-1 + t_s/(2t_b)$	t_s/t_b
$+4 t $	-1	+1	0

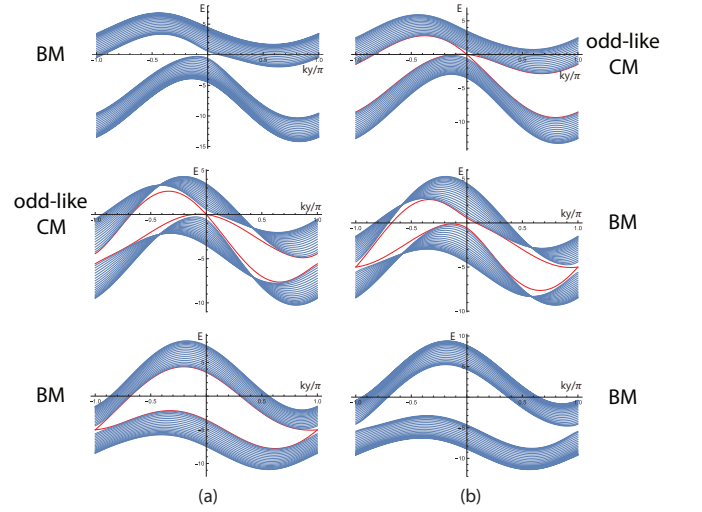


FIG. 33. The longitudinal edge of the odd-like Chern metal in a stripe geometry at different h/t values. Other parameters are $t = 1$, $t_s = 1$, $t_b = 1.25 > 1$. Top (a) $h/t = -4.5$, no edge state, a bulk FS, a BM. (b) $h/t = -3.5$, an edge state at Fermi energy near $k_y = 0$, a bulk FS, an odd-like Chern metal. Due to the useful exotic edge mode in (b), there is a universal non-integer Universal Hall conductance jump across the TPT from the BM to the odd-like CM. Middle (a) $h/t = -0.5$, an edge state at Fermi energy near $k_y = 0$, a bulk FS, an odd-like Chern metal. (b) $h/t = +0.5$, there is an edge state near $k_y = \pi$, but it is well below the Fermi energy. despite an edge mode floating around the vast majority of bulk modes. Due to the useful exotic edge mode in (a), there is a universal non-integer Universal Hall conductance jump across the TPT from (a) to (b). Bottom (a) $h/t = +3.5$, there is an edge state near $k_y = \pi$, but it is well below the Fermi energy, a BM. (b) $h/t = +4.5$, no edge state, a BM. There is no Hall conductance jump. Inside the odd-like CM, the exotic edge modes at the Fermi energy near $k_y = 0$ satisfy $v_L v_R > 0$, thus the Universal Hall conductance jump is a universal non-integer.

which is identical to the odd-Chern metal presented in Secs.II-VI, so the metallic phase below $-4t < h < 0$ can be called odd-like Chern metal. Note that due to the C- symmetry, the jump from one odd Chern metal to another odd Chern metal near $h = 0$ is “twice” that from the odd CM to BM (Fig.24). Here, due to the absence of the C- symmetry, there is only TPT from an odd CM to a BM, the TPT from one odd CM to another odd CM is absent, so does the “doubling”.

IX. “TOPOLOGICAL INVARIANTS” AND BULK-EDGE CORRESPONDENCE IN GAPLESS FERMIONIC SYSTEMS WITH EXTENDED FERMION SURFACE

Table I shows that the Chern number (or Chern number jump) may not be an effective way to distinguish even/odd Chern metal from the band metal. Because as shown in the appendix A and B, the band metal could

also have non-vanishing Chern number. There could also be Chern number jump across two band metals which are essentially the same quantum phase. The band metal and even/odd CM themselves all have non-vanishing Hall conductances (Only in the fine tuning case addressed in Sec.II and Sec.III, the band metal itself has zero Hall conductance). It is the Universal Hall conductance jump which plays the role of the "topological invariant " to distinguish phases with different topological properties. However, they may not be an integer anymore: it remains an integer at the TPT from ECM to band metal. However, it becomes any number at the TPT from OCM to band metal. Chern number or its jump are not experimentally measurable, but the Hall conductance jumps are. There are also corresponding TPT in the L-edge mode. However, as shown in Table 1, these TPTs are not QPT. So far, they present the very first example of TPT which is not a QPT. These salient features describe completely the unique properties of "topological invariants" and bulk/edge correspondence in gapless topological phases with extended FS. Of course, the topological gapless phases studied in this manuscript have no indirect gaps, but still direct gaps which give the room for bulk "topological invariants" and the associated L-edge modes.

A. Chern number (jump) versus the Hall conductance (jump)

It was known that the topological invariant can not be experimentally measured directly. What can be experimentally measured directly is the Hall conductance σ_H . As shown in the introduction, there are intricate relations between the two [34]: in the gapped insulating phases such as the even Chern insulator, odd Chern insulator and band insulator, they are the same, but in the gapless metal phases such as Band metal, even CM and odd CM, they maybe different: the Chern number Ch_- is evaluated over a given band, independent of the fillings of the band, so can only be an integer [47]. But the Hall conductance σ_H depends sensitively on the filling of the band, so need not to be quantized and can be any number even at $T = 0$. One can also evaluate $\sigma_H(T)$ at a finite T by incorporating the Fermi distribution functions on the fillings of the band at a finite T . Most importantly, there are enriched bulk-edge correspondences across the bulk TPT from the even Chern insulators to odd Chern Insulator, then to Odd Chern metals or an alternative path from the even CI to even CM, then to Odd CM shown in Fig.2. The differences between Ch_- and σ_H , especially their jumps in the Odd/Even Chern metal phases can be fully appreciated in both longitudinal edge and transverse edge.

B. A first example of TPT without a QPT

It is interesting to dig further from Sec.II-D on the universal unit conductance jump from the even CM to the BM listed in Table III and the universal non-integer conductance jump from the odd CM to the BM listed in Table IV. Just from the change in the ground state energy which reflects the quantum fluctuations, it is not a QPT. As demonstrated in the last section, both odd and even CM have a non-vanishing Chern number and associated edge modes near the Fermi energy inside the gap. But some BM also has non-vanishing Chern number and some floating L-edge modes near the Fermi energy only.

However, from the change in the bulk Berry curvature, especially near the Dirac points, which reflects the global topological features, it does show the universal Hall conductance jump. So it is clearly a TPT.

From the change in the edge modes which also reflects the global topological features, it does show the change in the edge mode: the even CM has edge modes at the Fermi energy near the projection of the Dirac points on the edge satisfying $v_L v_R < 0$. the odd CM has edge modes at the Fermi energy near the projection of the Dirac points on the edge satisfying $v_L v_R > 0$. These Dirac points are also the bulk singularities in the bulk Berry curvature. The even CM and odd CM have the same bulk, but different edge with an edge reconstruction dynamic exponent $z_L = 2$. While the BM does not have such edge modes except some floating edge modes away from these projection points.

It is also instructive to compare this universal Hall conductance jump to the universal jump in the superfluid density across the KT transition $\Delta\rho_s/k_B T = \pi/2$. It is a topological phase transition driven by vortex binding-unbinding, no order parameters, no symmetry breaking, has an essential singularity in free energy and also an infinite order transition. Numerically, we are not able to tell if there is also such a essential singularity in the ground state energy across the even/odd CM to BM transition.

In summary, this maybe the very first example of a TPT with the corresponding edge reconstruction, but not a QPT. So far, all the previous known examples are TPT is always accompanied by a QPT [30]. Namely, any changes in topology and topological invariants is also accompanied by the change in the ground state energy. Of course, a QPT need not necessarily a TPT. This very first example maybe contrasted to the bosonic 2d KT which is in its own class in 2d classical and 1+1 d quantum critical phenomena.

X. EXPERIMENTAL DETECTIONS BY INJECTING CURRENT OR IN A MOVING SAMPLE

This work consists of two parts. In the first part, we explore the QAH in a NN injecting current. In the sec-

ond part, we examine the QAH subject to a NN gauge invariant current plus a NNN current. As shown in [23] and reviewed in the appendix E, the second part may also apply to the QAH in cold atom systems where the SOC is generated artificially, therefore non-relativistic. In this section, we discuss the experimental detections in the following three different and complementary set-ups respectively.

1. In a NN injecting current

The first experiment to do is to directly inject current into the QAH systems shown in Fig.1a,b. In fact, the injecting current is nothing but the $d_0(k)$ term in Eq.6 in the momentum space which breaks the Parity. Of course, as alerted at the very beginning, a parity-even component $\epsilon_0(k) = -2t_e(2 - \cos k_x - \cos k_y)$ may also exist in any real material in the first place. Its effects can be addressed similarly as in Sec.VII-VIII. Injecting currents maybe just the most effective way to tune this P- breaking term to drive the TPTs in Fig.3 or Fig.29. As shown in Fig.3, it needs $t_b/t = 1$ to reach the odd CM directly from the even CI. As shown in Fig.29. Near $h/t \sim 0^-$, it is easy to reach the even-like CM from the even CI due to $t_b/t \rightarrow 0^-$, but it still needs $t_b/t = 1$ to reach the odd-like CM.

All the measurements can be routinely performed in a static sample. The whole global phase diagram Fig.3 and Fig.29 can be explored by just tuning the strength of the injecting current t_b . For example, various light [32, 33], atom, X-ray (or ARPES) and neutron scattering can be used to detect the bulk FS geometry, the bulk excitation spectrum and the associated edge reconstructions in all the phases in Fig.24 and Fig.29. The conventional 2-terminal or 4- terminal transport measurements can be applied to measure the Hall conductance σ_H and its jump $\Delta\sigma_H$ from even/odd CM to the band metal. The specific heat C_v , the compressibility κ_u and the Wilson ratio R_w can be separately measured by various established thermodynamic measurements in both materials and cold atom systems.

2. In a NN gauge invariant current plus NNN current

The injecting current term could also be the gauge-invariant current in Eq.106. We assume the NN dimensionless ratio κ_{b1} and the NNN hopping t_{b2} in Eq.106 can be controlled independently. Then the full phase diagram Fig.24, especially the odd CI phase and its associated edge modes can be explored.

From Eq.115, one can see that the band insulator with $Ch_- = 0$ in the absence of the current near the phase boundary $h/t \sim \pm 4$ can be transformed to the Chern insulator with $Ch_- = \pm 1$ by injecting the current Eq.106. This is because the gauge-invariant current effectively increases the hopping t and the SOC strength t_s accord-

ing to Eq.115, therefore reduces the critical value of h/t . This qualitative change of ground state can be detected by measuring the Hall conductance σ_H and also detecting the edge modes by ARPES. t_b term Eq.116 leads to the Doppler effect in the electronic spectrum which changes sign when $\kappa_{b1} = 1$. This sign change can be captured by the various light scattering detections. By keeping $\kappa_{b1} \ll 1$, increasing the NNN t_{b2} current will drive the even CI to odd CI, then the odd CI to odd CM in Fig.24. It needs $t_b/t = 1$ to reach the odd CI, then a even larger $t_b/t > 1$ to reach the odd CM. The evolution of edge states, the edge reconstruction, the enriched bulk-edge correspondence, especially in the odd CI and odd/even CM can be mapped out by light scattering detections in the longitudinal or transverse moving sample in Fig.27 and 28.

3. In a moving sample for the artificially generated QAH

As discussed in [23], if the SOC is artificially created in cold atom system [12, 13, 28], it is not a relativistic effect. The spin in the SOC is just a pseudo-spin consisting of two hyperfine states. Then the gauge invariant current plus a NNN current in Eq.106 can be generated by a Galileo transformation (GT) as analyzed in the appendix E, except the two terms are not independent anymore. So some of the results achieved in Sec.V and VI can be adopted to this case also with some stringent restrictions.

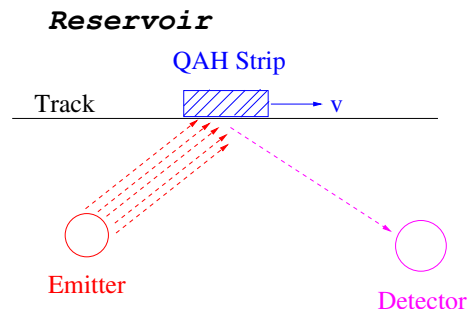


FIG. 34. Light (ARPES), atom or neutron scattering on a moving QAH sample with a strip geometry and a velocity \vec{v} . The longitudinal moving means the sample edge is along the velocity \vec{v} . The transverse moving means the sample edge is normal to the velocity \vec{v} . As shown in Sec.V, VI and appendix E, the edge states show quite different behaviours in the longitudinal or the transverse moving case which can be detected by the scattering cross sections. The multiple irradiating lines from the emitter declinate the irradiation regime where the sample enter and leave, then the scattered beams can be detected by the receiver. In a grand canonical ensemble, the Reservoir shows exchange particles with the sample through the chemical potential μ .

From Eq.E5, one can see that the band insulator with $Ch_- = 0$ in the static frame $v = 0$ near the phase boundary $h/t \sim \pm 4$ can be transformed to the Chern insulator with $Ch_- = \pm 1$, but not the other way around.

This counter-intuitive phenomenon can be best read from Eq.E5: the Galileo boost effectively increases the hopping t and the SOC strength t_s , therefore reduces the critical value of h/t . However, due to $t_b/t \ll 1$, one is not able to even get close to the phase boundaries from the CI to odd CI, let alone the odd CI to odd CM in Fig.24 which all happen when $t_b/t_s > 1$. So the NNN t_b term can only introduce a small Doppler effect in the electronic spectrum.

Even so, we still have the three interesting results accessible to the detection in Fig.34: (1) The band insulator near the 3rd order TPT from the Chern insulator to the band insulator will turn into a Chern insulator (2) There is a Doppler shift term in the fermionic spectrum in the moving sample which changes sign when $v = v_c = t_0/t_{b1}$. For the cold atom systems in an optical lattice, the characteristic velocity can be estimated as $v_c \sim 1cm$ which is easily within experimental reach [23]. (3) The shifted edge dispersions Eq.92 in the longitudinal edge and Eq.100 in the transverse edge. These three predictions can be detected in the moving sample Fig.34 by taking advantages of both bulk and longitudinal or transverse edge properties.

First thing to try is to set the sample static in the lab frame S , but observed in the moving frame S' . In practice, the sample is very small, but the detecting device is usually heavy. Because exchanging the role of the lab and moving frame does not change the results, because both are related by Galileo transformation (GT) anyway. So, in a practical scattering detection experiment shown in Fig.34, it is more convenient to set the emitter and the receiver static and make the sample moving with a constant velocity \vec{v} . Due to the small size of the sample, it is not easy to focus the beam on the sample when it is moving. To overcome this difficulty, one may just continuously shine the emitting beam, only when the sample move into its shadow, it will be scattered and collected by the detector. When it moves out of the shadow, there is no scattered beam anymore.

However, when setting the sample moving with a constant velocity v in Fig.34, some of the measurements such as transports may become hard to implement. The Chern number Ch_- is not experimentally measurable in any inertial frames anyway. Fortunately, all kinds of scattering experiments mentioned in *I* and sketched in Fig.34 remain applicable. One simply perform all the measurements in the lab frame S , so for the light scattering, there is no need to consider the relativistic Doppler shift of the photon. Unfortunately, it seems difficult to measure the free energy, therefore the specific heat in the moving sample. Even more difficult things to measure is the Hall conductance σ_H which can be used to distinguish the Chern insulator from the band insulator, also the Odd Chern metal from the band metal. Fortunately, they can still be detected by the edge states either in longitudinal or transverse moving shown in Fig.34.

XI. CONCLUSIONS AND PERSPECTIVES

The global phase diagram Fig.3 due to the injecting current and Fig.24 due to the gauge invariant current or a moving sample contain several novel TPT/QPT. Several new concepts also emerge from these phase diagrams: enriched bulk/L-edge/T-edge correspondences which lead to intervening new topological phases such as OCI and ECM, the L-edge dynamic exponent such as $z_L = 2, 3$, the T-edge critical behaviour such as $\sim \sqrt{v^2 - c^2}$, the Universal Hall conductance jump replace the Chern number as "topological invariants", especially a TPT which is not a QPT such as the OCM to BM and ECM to BM transition, etc.

It is instructive to compare the non-interacting spin-1/2 SOC fermionic TPTs in Fig.3 with that of the interacting spin-0 bosonic Mott to the superfluid (SF) QPT with $z = 1$ in [23]. One can make the following loose analogy between the two systems: $h/t \sim U/t$, band insulator \sim Mott phase, Chern insulator \sim SF phase, Odd Chern metal/band metal phase \sim Boosted SF (BSF) phase. Here it has no symmetry breaking, the continuous $U(1)$ symmetry and the discrete C-symmetry are never broken, so no order parameters. The change of FS topology and geometry across TPTs can be characterized by the topological invariants such as the Universal Hall conductance jump $\Delta\sigma_H$. There are also corresponding edge-states through the enriched bulk-edge correspondences. However, in the interacting bosonic case, the continuous $U(1)$ symmetry and the discrete C-symmetry can be broken and characterized by various order parameters: the $U(1)$ is broken in the SF, both $U(1)$ and C- are broken in the BSF phase. There are no non-trivial edge modes, let alone any edge reconstructions in such topologically trivial interacting bosonic systems. The boost favors the SF phase in the boson case. Here it favors the Chern insulator. For the interacting bosons, moving away from the C-symmetric point corresponds to $z = 2$. In Sec.II-VI, we focus on the half filling $\mu = 0$ case which respects the C-symmetry. In appendix A, we study the $\mu \neq 0$ case by doping the QAH materials. We also investigate the much more interesting cases of breaking the C-symmetry in the appendix B and Sec.VII-VIII.

The Universal Hall conductance jump $\Delta\sigma_H$ replace the Chern number jump to become the new bulk topological invariant involved in the even/odd CI and the even/odd CM discovered in this work (Fig.2). There is also corresponding new enriched bulk/L-edge/T-edge correspondence. It is these combined features which lead to a likely complete classification of quantized, especially un-quantized AHE metals. It is constructive to compare to the 3d Weyl metals where there is no new topological invariant involved, but a new structure of edge modes called Fermi-arc. It also contributes to a un-quantized 3d AHE $\sigma_{xy} = e^2/h \times (2k_0)$ where $2k_0$ is the momentum distance along \hat{z} between the + and - Weyl point. As mentioned in the introduction, our approach to the classification of gapless AHE metallic phase is complemen-

tary to the traditional one using SPT or SET to classify gapped or gapless topological phases: We start from the known parent Hamiltonian whose topological phases are known, then add various symmetry breaking perturbations to drive the known topological phases to new topological phases through new TPTs. Here, we add the P-breaking currents leading to the odd Chern Insulator or odd Chern-metal. We also add the C- breaking energy dispersion leading to possible even Chern metals. This specific Hamiltonian based classification scheme has the advantages to discover new topological phases through possible novel TPTs, so can be used to classify topological phases and TPTs at the same time. Furthermore it also automatically leads to various deformed Hamiltonians hosting these phases, so may be directly connected to experimental realizations. The disadvantages is that it is hard to prove it is a complete and exhaustive classifications. It remains to show its completeness from a symmetry based approach such as K-theory on the Wannier basis [43]. However, it remains very challenging to clarify completely and exhaustively topological gapless phases with extended FS with $z = 2$ from such an abstract algebraic/topological K-theory approach, and also classify the bulk TPTs and the edge reconstructions among these phases.

Recently, there are also new advances in the classification of 1d gapless interacting topological phases [44–46] where 2d CFT and boundary CFT can be a useful tool. Due to the lack of local CFT, its extension to higher dimensions is more challenging. Here, we attempt a classification of 2d gapped Chern insulators and 2d gapless AHE metals with extended FS and $z = 2$. Obviously, it has no conformal invariance in the first place, so 2d CFT and boundary CFT may not apply. It may also tempting to study the effects of the Hubbard interaction U in both the weak $U/t \ll 1$ and strong coupling $U/t \gg 1$ limit in Eq.1 under an injecting current or in a moving sample. In the strong coupling limit and at integer fillings, both the bosonic and fermionic Hubbard model leads to various quantum spin models. Drawing the insights here achieved on the non-interacting topological phases, we expect that Similar methods may also be applied to study the strongly interacting SPT and SET, an injecting current will also drive SPT/SET to new SPT/SET through some novel TPTs. SPT/SET near a TPT may also depend on sensitively the observer in an inertial frame.

Acknowledgements

We thank Prof. Congjun Wu for helpful discussions and W. M. Liu for consistent encouragements. We also thank Prof. Congjun Wu and Prof. Gang Tian for the hospitality during our visit at the Institute for Theoretical Sciences.

Appendix A: " Even Chern metal " Case I:

$$\epsilon_0(k) = -t_b = -\mu$$

As defined in Sec. VII, a even Chern metal breaks the \mathcal{C} -symmetry, but keeps \mathcal{P} -symmetry. The simplest even case is to choose $\epsilon_0(k) = -t_b = -\mu$ in Eq.131. However, in this appendix, we show that simply doping the Chern insulator only leads to a band metal (BM). The naively thought even Chern metal is nothing but the same phase as the BM. As stressed in Sec.IX, this is also the simplest example to show the Chern number and its jump may not be effective anymore in characterizing gapless fermionic topological phases with extended FS.

This corresponds to the doped case away from the charge neutral point $\mu = 0$. The total Hamiltonian Eq.131 takes the form

$$H(k) = H_{\text{QAH}}(k) - \mu \quad (\text{A1})$$

where the chemical potential μ is tuned by the reservoir in Fig.34.

At the QPT from the even Chern metal phase to the band metal, there is no singularity in the ground-state energy density and no Hall conductance jump. The two energy bands are

$$E_{\pm}(k) = \pm E_{\text{QAH}}(k) - \mu \quad (\text{A2})$$

where $E_{\text{QAH}}(k) = \sqrt{[h + 2t(\cos k_x + \cos k_y)]^2 + 4t_s^2(\sin^2 k_x + \sin^2 k_y)}$. To exam if there is a Universal Hall conductance jump, without loss of generality, we take $\mu > 0$. Near $h/t = -4$, the Berry curvature singularity is located at $K_0 = (0, 0)$, $E_{\pm}(K_0) = -\mu < 0$, both upper band and lower band Fermi Surface (FS) enclose the K_0 . So according to Eq.132, the Universal Hall conductance jump eventually cancels as shown in the Table V. Similar situation happens for $h/t = 0$ and $+4$.

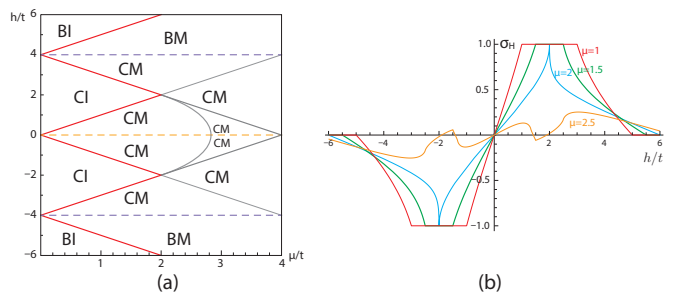


FIG. 35. (a) The global phase diagram of the Lattice Hamiltonian (A1) for the even Chern Metal I. (b) The Hall conductance as a function of h/t for various fixed values of $\mu/t = 1.0, 1.5, 2.0, 2.5$. The Hall conductance shows no jump at $h/t = -4, 0, +4$. As shown in this appendix, the “ even ” Chern metal phase is essentially the same as the band metal phase, except it may just has a larger AHE than the BM. One may simply call all the metallic phase just BM. For a similar analog in the interacting bosonic quantum anomalous Hall system, see [28].

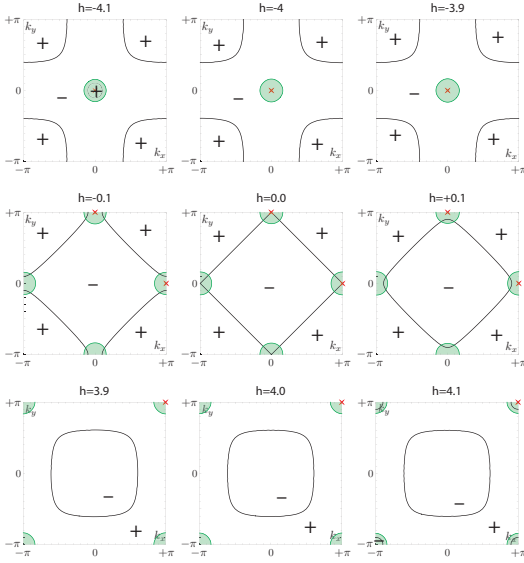


FIG. 36. The Berry curvature $\Omega_+(\mathbf{k})$ and the Fermi surfaces (FS) of the even Chern metal case I: Other parameters are $t = 1$, $t_s = 1$, $\mu = 1$. The black curve is the contour of $\Omega_+(\mathbf{k}) = 0$, which separates the positive part denoted by “+” from the negative part denoted by “-”. The red \times denotes the singularity of $\Omega_+(\mathbf{k})$ listed in Eq.133. The green line denotes the electron FS. Top, near $h/t = -4$, Middle, near $h/t = 0$, Bottom, near $h/t = +4$. The upper band FS always encloses the singularity of $\Omega_+(\mathbf{k})$. They lead to $\Delta\sigma_+$ in the Table V. The lower band is always occupied, so always encloses the singularity of $\Omega_-(\mathbf{k})$, it leads to $\Delta\sigma_-$ in the Table V. Thus there is no Hall conductance jump $\Delta\sigma = \Delta\sigma_+ + \Delta\sigma_-$ as shown in the Table V. One may simply call all the metallic phase just as BM.

TABLE V. The Table of the Universal Hall conductance jump of the even Chern metal case I. The change of Chern number ΔCh_- is the same as that in Table-III.

h	$\Delta\sigma_-$	$\Delta\sigma_+$	$\Delta\sigma$
$-4 t $	+1	-1	0
0	+2	-2	0
$+4 t $	-1	+1	0

which shows there is no difference between the “even” Chern metal here and the BM. So One may simply call all the metallic phase as just BM.

The bulk-edge correspondence in this simplest even-Chern metal case can be extracted from Fig.20 and Fig.21 at $t_b = 0$ by cutting the edge modes at the chemical potential $\mu > 0$ instead of at $\mu = 0$. Because $t_b = 0$, there is no difference between longitudinal and transverse. If the cut remains inside the bulk gap, it is still a Chern insulator phase. When it also cuts some bulk states, it moves into the “even” Chen metal phase. Then it never cuts any edge mode near $k_y = 0$ when $h < 0$ or $k_y = \pi$ when $h > 0$, so there is no jump in the Hall conductance, as indicated in Sec.VII-C. One may still see one edge mode floating above the vast majority of bulk modes, the

edge mode does not play any significant role anymore. In fact, this floating edge mode can be simply absorbed into the vast majority of bulk modes.

In summary, there is no ground state energy singularity, no Hall conductance jump from the tentative “even” Chern metal to the band metal. Despite to so called “even” Chern metal has a non-vanishing Chern number in its whole band structure, there is really no any physical measurable bulk or edge quantities to distinguish the two phases, they are really the same phase which is nothing but the conventional BM phase. So there are only three phases in Fig.35: CI, BI and BM. In fact, similar phenomenon also happens in the interacting bosonic quantum anomalous Hall (QAH) system, see [28].

Appendix B: Even Chern metal Case II:

$$\epsilon_0(k) = -2t_b(1 - \cos k_y).$$

In the last appendix, we show that simply doping the Chern insulator may not lead to a real even Chern metal. Here we discuss a second example by choosing $\epsilon_0(k) = -2t_b(1 - \cos k_y)$ which does lead to a real even Chern metal The total Bloch Hamiltonian takes the form

$$H(k) = -2t_b(1 - \cos k_y) + H_{\text{QAH}}(k) \quad (\text{B1})$$

At the QPT from the even Chern metal phase to the band metal, there is no Hall conductance jump at $h/t = 4$ but a unit Hall conductance jump at $h/t = -4$ and 0. The two energy bands are

$$E_{\pm}(k) = \pm E_{\text{QAH}}(k) - 2t_b(1 - \cos k_y) \quad (\text{B2})$$

To exam the Hall conductance jump, we just examine the FS according to Eq.132. At $h/t = -4$, the Berry curvature singularity is located at $K_0 = (0, 0)$ and $E_{\pm}(K_0) = 0$. For $h/t \approx -4$, $E_+(K_0) > 0$, $E_-(K_0) < 0$, the upper band FS does not enclose the K_0 , but the lower band FS encloses the K_0 . Thus, there is a unit Hall conductance jump. At $h/t = 0$, the Berry curvature singularity is located at $K_1 = (\pi, 0)$ and $K_2 = (0, \pi)$, thus $E_{\pm}(K_1) = 0$ and $E_{\pm}(K_2) \neq 0$. For $h/t \approx 0$, $E_+(K_1) > 0$, $E_-(K_1) < 0$, the upper band FS does not enclose the K_1 , but the lower band FS encloses the K_1 . Meanwhile, $E_{\pm}(K_2)$ always greater than 0 or smaller than 0, the upper band and the lower band FS both enclose or exclude the K_2 . Thus, there is a unit Hall conductance jump contribution from K_1 . At $h/t = +4$, the Berry curvature singularity is located at $K_{\pi} = (\pi, \pi)$ and $E_{\pm}(K_{\pi}) \neq 0$. For $h/t \approx +4$, $E_+(K_{\pi})$ always greater than 0 or smaller than 0, the upper band and the lower band FS both enclose or exclude K_{π} . Thus, there is no Hall conductance jump. In short, only the metallic phase below $h = 0$ can be named as even Chern metal, all the other metallic phases are just BM.

Due to the C- symmetry breaking, $h \rightarrow -h$ is not related by the Time-reversal transformation anymore.

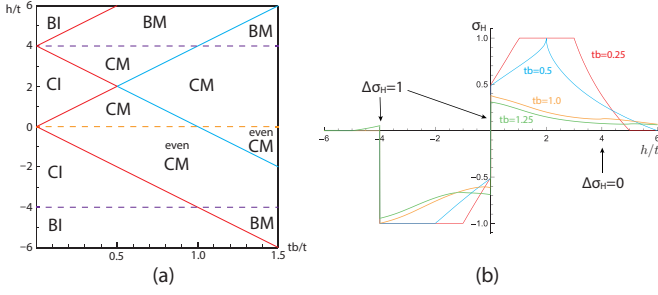


FIG. 37. In both (a) and (b), we also fixed $t = t_s = 1$. (a) The global phase diagram of the Lattice Hamiltonian (B1) for the even Chern metal case II. The even CM exist when $-4 < h/t < 0$. While all the CM at $0 < h/t < 4$ are essentially the same as the BM despite superficially their bands have a non-vanishing Chern number. Due to this superficial difference and its relatively larger AHE, we still keep the symbol CM in the figure. See also Fig.29 which also hosts odd-like CM. (b) The Hall conductance as a function of h/t for various fixed values of $t_b/t = 0.25, 0.50, 1.00, 1.25$. The Hall conductance only shows a unit jump at $h/t = -4, 0$. Especially, the $t_b/t = 0.25$ curve shows a unit jump near $h/t = 0$ from the even CM to a BM, and also a unit jump near $h/t = -4$ from the CI to BI; the $t_b/t = 1.25$ curve shows the even CM to a BM with a unit jump near $h/t = 0$ and $h/t = -4$ (see Table VI and Fig.39). As shown in Table VI and Fig.39, only the metallic phase $-4t < h < 0$ can be named as even Chern metal, all the other metallic phases are just BM. Near $h/t \sim 0^-$, it is easy to reach the even CM from the CI due to $t_b/t \rightarrow 0^-$.

TABLE VI. The Universal Hall conductance jump of the even Chern metal case II to BM in the bulk. It has the same $\Delta\sigma_-$ as those in Table V. But $\Delta\sigma_+$ is different, so the total $\Delta\sigma$ is different. The change of Chern number ΔCh_- is the same as that in Table-III.

h	$\Delta\sigma_-$	$\Delta\sigma_+$	$\Delta\sigma$
$-4 t $	+1	0	1
0	+2	-1	1
$+4 t $	-1	+1	0

Appendix C: The universal non-integer Hall conductance jump of the “odd” Chern metal

We also have a graphics interpretation of the Hall conductance of “odd” Chern metal discussed in the main text. The Hall conductance is an integral of Berry curvature over occupied states. The zero temperature Hall conductance can be evaluated as $\sigma_H = \sigma_- + \sigma_+$:

$$\sigma_s = \frac{1}{2\pi} \int_{\mathbb{R}^2} \Omega_s(\mathbf{k}) \Theta(-\epsilon_s(\mathbf{k})) d^2\mathbf{k} \quad (\text{C1})$$

where we have use the continuum theory to demonstrate the results.

Due to the \mathcal{C} -symmetry in the odd Chern metal, the zero temperature Hall conductance can be also rewritten as

$$\sigma_H = \text{Ch}_- + 2\sigma_+ \quad (\text{C2})$$

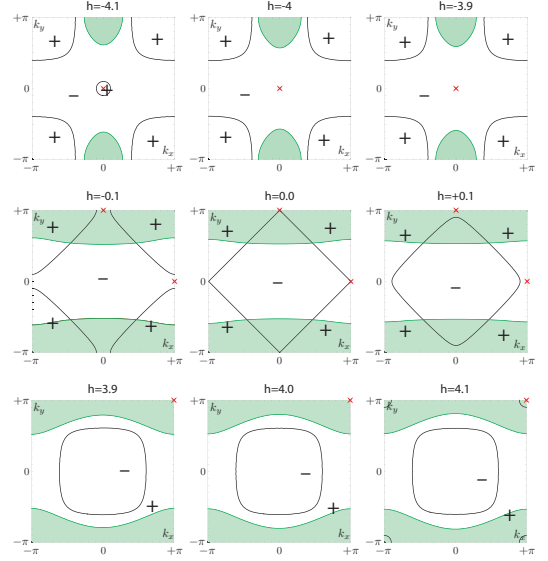


FIG. 38. Berry curvature $\Omega_+(\mathbf{k})$ and the FS of the even Chern metal case II, it leads to $\Delta\sigma_+$ in the Table VI. Other parameters are $t = 1, t_s = 1, t_b = 1.25$. The black curve, the red \times and the green line denote the same information as Fig.36. Top: near $h/t = -4$: the upper band FS always excludes the singularity of $\Omega_+(\mathbf{k})$ leading to $\Delta\sigma_+ = 0$, thus the Hall conductance jump is 1; Middle: near $h/t = 0$: the upper band FS only encloses one of the two singularities of $\Omega_+(\mathbf{k})$ leading to $\Delta\sigma_+ = -1$, thus the Hall conductance jump is also 1; Bottom: near $h/t = +4$: the upper band FS always encloses the singularity of $\Omega_+(\mathbf{k})$ leading to $\Delta\sigma_+ = 1$, thus the Hall conductance jump is 0. The lower band is always occupied, so always encloses the singularity of $\Omega_-(\mathbf{k})$, it leads to $\Delta\sigma_-$ in the Table VI. Only the metallic phase $-4t < h < 0$ can be named as even Chern metal, all the other metallic phases are just BM.

Note that due to the role played by the \mathcal{C} -symmetry, Eq.C2 does not hold in the even Chern metal presented in the appendix A and B or odd-even mixed case studied in Sec.VIII. So it only applies to the odd CM here. of course, the evaluations in the appendix A and B and Sec.VIII also applies here.

Below we will consider the $\alpha_x\alpha_y > 0$ case and $\alpha_x\alpha_y < 0$ case separately.

1. $\alpha_x\alpha_y > 0$ case: from the odd CM to the BM

Without loss of generality, we consider $h/t \sim -4$ cases, which belongs to the $\alpha_x\alpha_y > 0$ case in Eq.34,

$$H_0(\mathbf{k}) = [\Delta + \alpha(k_x^2 + k_y^2)]\sigma_z + vk_x\sigma_x + vk_y\sigma_y - ck_y\sigma_0 \quad (\text{C3})$$

where $\Delta = -(h + 4t)$, $\alpha = t$, $v = 2t_s$, $c = 2t_b$.

The distribution of the Berry curvature $\Omega_+(\mathbf{k})$ and the electron Fermi surface is shown in Fig. 40. Without loss of generality, we have fixed $\alpha_x = \alpha_y = 1$, $v = 1$,

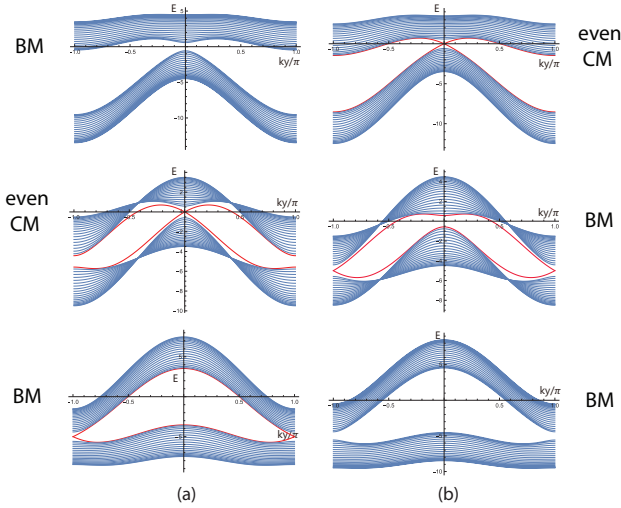


FIG. 39. The longitudinal edge structure in a stripe geometry of the even Chern metal case II at different h/t values. Other parameters are $t = 1$, $t_s = 1$, $t_b = 1.25$. Top (a) $h/t = -4.5$, no edge state, has a bulk FS, it is a BM. (b) $h/t = -3.5$; an edge state at Fermi energy near $k_y = 0$, also a bulk FS. It is a even Chern metal phase. Due to the useful edge state in (b), there is a unit Hall conductance jump across the TPT from the BM to the even Chern metal phase. Middle (a) $h/t = -0.5$, an edge state at Fermi energy near $k_y = 0$, also a bulk FS. It is a even Chern metal phase. (b) $h/t = +0.5$; there is an edge state near $k_y = \pi$, but it is well below the Fermi energy. Despite there is an edge mode floating near the vast majority of bulk modes. It is still a BM. Due to the useful edge state in (a), there is a unit Hall conductance jump across the TPT from the even Chern metal to the BM phase. Bottom (a) $h/t = +3.5$, there is an edge state near $k_y = \pi$, but it is well below the Fermi energy. it is a BM. (b) $h/t = +4.5$, no edge state. It is also a BM. As expected, there is no Hall conductance jump from the BM to the BM. Inside the even Chern metal, the edge modes at the Fermi energy near $k_y = 0$ satisfy $v_L v_R < 0$. The Universal Hall conductance jump from the even Chern metal to the BM is an integer.

$c = 1.3$. When $\Delta > 0$ in the BM, $\Omega_+(\mathbf{k})$ over FS contains positive part and negative part, thus the integral σ_+ is almost get cancelled, (exactly cancelled when $n = 1$), which suggests a negligible Hall conductance contribution from the upper band. Since the $\text{Ch}_- = 0$, thus the total Hall conductance is negligible. When $\Delta < 0$ in the odd CM, $\Omega_+(\mathbf{k})$ over the FS only contains positive part, thus the integral σ_+ is also a positive number. Due to the $\Omega_+(\mathbf{k})$ over entire \mathbf{k} gives $+1$, if c/v is not too large, we also know that $\sigma_+ \ll 1$. Since the $\text{Ch}_- = -1$, thus $\sigma_H = \text{Ch}_- + 2\sigma_+ = -1 + 2\sigma_+$ is still a negative number, and the total Hall conductance takes a non-negligible negative value. As varying Δ from positive to negative values, the Hall conductance has to show a jump in order to connecting a non-negligible value to a negligible value. This is the case for the Hall conductance jump around $h/t = \pm 4$.

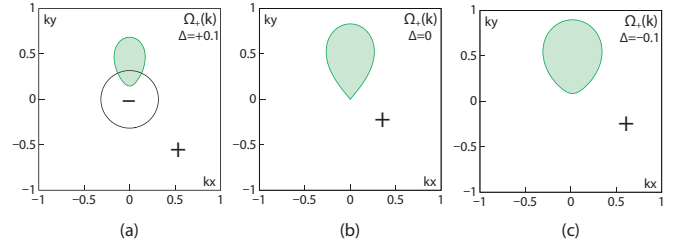


FIG. 40. According to Eq.C2, these pictures explain the universal non-integer Hall conductance jump around $h/t = \pm 4$. The distribution of the Berry curvature $\Omega_+(\mathbf{k})$ and the electron FS at fixed $\alpha_x = \alpha_y = 1$, $v = 1$, $c = 1.2$ and varying (a) $\Delta = +0.1$ in the BM (b) $\Delta = 0$ (c) $\Delta = -0.1$ in the Odd CM. The black curve is the contour of $\Omega_+(\mathbf{k}) = 0$, which separates the positive part denoted by “+” from the negative part denoted by “-”.

2. $\alpha_x \alpha_y < 0$ case: from odd CM to its the time-reversal partner odd CM.

When $h \sim 0$ and near the two valleys K_1 and K_2 , we have

$$\begin{aligned} H_1 &= [\Delta - \alpha(k_x^2 - k_y^2)]\sigma_z - vk_x\sigma_x + vk_y\sigma_y - ck_y\sigma_0 \\ H_2 &= [\Delta + \alpha(k_x^2 - k_y^2)]\sigma_z + vk_x\sigma_x - vk_y\sigma_y + ck_y\sigma_0 \end{aligned} \quad (\text{C4})$$

where $\Delta = -h$ and other parameters are the same as the $h \sim 4t$ case discussed in Sec.III-A. Note the opposite sign of the velocities v between k_x and k_y and opposite sign of α between k_x^2 and k_y^2 indicating $\alpha_x \alpha_y < 0$.

One may also identify the relation between H_1 and H_2 , $\Omega_{1,+}(\mathbf{k}; \Delta) = -\Omega_{2,+}(\mathbf{k}; -\Delta)$, and $\sigma_{1,+}(\Delta) = -\sigma_{2,+}(-\Delta)$. Thus the total Hall conductance is

$$\begin{aligned} \sigma_H &= \text{Ch}_- + 2\sigma_+, \quad \text{Ch}_- = \text{Ch}_{1,-} + \text{Ch}_{2,-}, \\ \sigma_+ &= \sigma_{1,+} + \sigma_{2,+} = \sigma_{2,+}(\Delta) - \sigma_{2,+}(-\Delta) \end{aligned} \quad (\text{C5})$$

The distribution of the Berry curvature $\Omega_{2,+}(\mathbf{k})$ and the electron Fermi surface is shown in Fig. 41. Without loss of generality, we have fixed $\alpha_x = -\alpha_y = 1$, $v = 1$, $c = 1.2$. When $\Delta > 0$ in the odd CM, $\Omega_{2,+}(\mathbf{k})$ over the FS only contains positive part, thus the integral $\sigma_{2,+}$ is also a positive number. When c/v is not too large, we also know that $\sigma_{2,+} \ll 1$. When $\Delta < 0$ in the time-reversal partner of the odd CM, $\Omega_{2,+}(\mathbf{k})$ over the FS contains positive part and negative part, thus the integral $\sigma_{2,+}$ is almost get cancelled, (exactly cancelled when $n = 1$). Combining $\Delta > 0$ and $\Delta < 0$ case, we conclude: if $\Delta > 0$, $\sigma_+(\Delta) = \sigma_{2,+}(\Delta) - \sigma_{2,+}(-\Delta) \approx \sigma_{2,+}(\Delta)$; if $\Delta < 0$, $\sigma_+(\Delta) = \sigma_{2,+}(\Delta) - \sigma_{2,+}(-\Delta) \approx -\sigma_{2,+}(-\Delta)$. We also know $\text{Ch}_- = -\text{sgn}(\Delta)$, so the total Hall conductance is:

$$\begin{aligned} \sigma_H &\approx -\text{sgn}(\Delta) + 2\text{sgn}(\Delta)\sigma_{2,+}(|\Delta|) \\ &= -\text{sgn}(\Delta)[1 - 2\sigma_{2,+}(|\Delta|)] \end{aligned} \quad (\text{C6})$$

When c/v is not too large, $\sigma_{2,+}(|\Delta|)$ is a small quantity, thus the Hall conductance has to show a jump in order

to connecting a positive value to a negative value from the odd CM to its the time-reversal partner. This is the case for the Hall conductance jump around $h/t = 0$ from OCM/OCM which is twice the value of OCM/BM discussed in the last subsection.

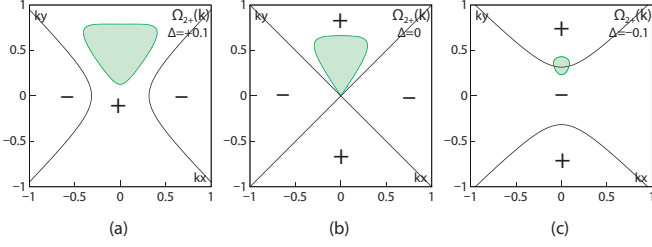


FIG. 41. According Eq.C5, these pictures explain the universal non-integer Hall conductance jump around $h/t = 0$. The distribution of the Berry curvature $\Omega_{2,+}(\mathbf{k})$ and the electron FS at fixed $\alpha_x = -\alpha_y = 1$, $v_x = v_y = 1$, $c = 1.3$ and varying (a) $\Delta = +0.1$, odd CM (b) $\Delta = 0$ (c) $\Delta = -0.1$, the time-reversal partner of the odd CM.

Appendix D: The Berry phase (or singularity) of the $z = 1$ Dirac point

Consider the doped (even) case,

$$H(\mathbf{k}) = (\Delta + \alpha_x k_x^2 + \alpha_y k_y^2)\sigma_z + v_x k_x \sigma_x + v_y k_y \sigma_y - \mu, \quad (\text{D1})$$

For simplicity, we can use the simplified version for $\alpha_x = \alpha_y = 0$:

$$H(\mathbf{k}) = \Delta \sigma_z + v k_x \sigma_x + v k_y \sigma_y - \mu, \quad (\text{D2})$$

For $\mu < |\Delta|$, the Berry curvature takes the form:

$$\Omega_{\pm}(k) = \mp \frac{\Delta}{2(\Delta^2 + k^2)^{3/2}} \quad (\text{D3})$$

Under the limit $\Delta \rightarrow 0$, the $\Omega_{\pm}(k)$ becomes a δ -function. From the definition, we can check that $\lim_{\Delta \rightarrow 0} \Omega_{\pm}(k) = \mp \pi \text{sgn}(\Delta) \delta(\mathbf{k} - 0)$ which is the well known π Berry phase for a Dirac point. In order to see this, we only need to verify two conditions 1) $\lim_{\Delta \rightarrow 0} \Omega_{\pm}(k) = 0$ when $k \neq 0$ and $\lim_{\Delta \rightarrow 0} \Omega_{\pm}(k) = \mp \text{sgn}(\Delta) \infty$ when $k = 0$; 2) $\int d^2 k \Omega_{\pm}(k) = \mp \pi \text{sgn}(\Delta)$. The condition 1) is obvious, the condition 2) is due to the well-known result $\frac{1}{2\pi} \int d^2 k \Omega_{\pm}(k) = \mp \text{sgn}(\Delta)/2$. They were used to evaluate the bulk Universal Hall conductance jump in Sec. VII-B.

Note that if one introduces $\alpha \neq 0$, then $\lim_{\Delta \rightarrow 0} \Omega_{\pm}(k) \neq 0$ when $k \neq 0$, which means $\lim_{\Delta \rightarrow 0} \Omega_{\pm}(k)$ is not just a pure δ -function.

For $\mu > |\Delta|$, we can solve $k_F = \sqrt{\mu^2 - \Delta^2}$ in the upper band. The Berry curvature from the lower band

ϕ_- which is always occupied and the upper band ϕ_+ which has a FS are

$$\phi_+ = \int_0^{k_F} 2\pi k dk \Omega_+(k) = -\pi(1 - |\Delta/\mu|) \text{sgn}(\Delta) \quad (\text{D4})$$

$$\phi_- = \int_0^{\infty} 2\pi k dk \Omega_-(k) = +\pi \text{sgn}(\Delta) \quad (\text{D5})$$

and then:

$$\phi = \phi_+ + \phi_- = \pi|\Delta/\mu| \text{sgn}(\Delta) = \pi\Delta/|\mu| = \pi\Delta/\mu \quad (\text{D6})$$

which leads to the Hall conductance $\sigma_H = \frac{\phi}{2\pi} = \Delta/2\mu$.

Appendix E: Galileo transformation for the artificially generated non-relativistic QAH

As discussed in [23], if the SOC is artificially created in cold atom system [12, 13, 28], it is not a relativistic effect. The spin in the SOC is just a pseudo-spin consisting of two hyperfine states. Then the gauge invariant current plus a NNN current in Eq.106 can be generated by a Galileo transformation (GT). However, the QAH in real materials [9–11] comes from the relativistic effect at the order of $(v/c)^2$. So the conventional GT does not apply anymore, one need to apply a low velocity expansion of the Lorentz transformation (LT) upto the order of $(v/c)^2$ where the time contraction effects of the LT must be taken into account. So here we only focus on the QAH in artificial materials in a moving sample, leave how the QAH in real materials change in a moving sample to a future publication.

To perform a GT on the lattice, the first thing to do is to do it directly on the QAH model Eq.1. The action corresponding to the QAH model Eq.1 is:

$$\mathcal{S}_{QAH} = \int d\tau \sum_i c_i^\dagger \partial_\tau c_i + H_{QAH}[c_i^\dagger, c_i] \quad (\text{E1})$$

In the continuum theory, a Galilean boost with a constant velocity \vec{v}_b will lead to $\partial_\tau \rightarrow \partial_\tau + i\vec{v}_b \cdot \vec{\nabla}$. In the lattice theory, one need replace the spatial derivative $\partial_{\vec{\mu}}$ by its discrete version (lattice derivative) $\Delta_{\vec{\mu}}$ via $\partial_{\vec{\mu}} \phi_i \rightarrow \Delta_{\vec{\mu}} \phi_i = a^{-1}(\phi_{i+\vec{\mu}} - \phi_i) + \dots$ and $\Delta_{\vec{\mu}}^* \phi_i = a^{-1}(\phi_i - \phi_{i-\vec{\mu}}) + \dots$, where a is the lattice constant where \dots means that one should add infinite number of higher order terms which still lead to the same contume limit

Thus, under a Galilean boost, the lattice action can be written as

$$\begin{aligned} \mathcal{L}_{QAH,b} = & \sum_i c_i^\dagger \partial_\tau c_i + i \sum_{n=1}^{\infty} [t_{bn,x} c_i^\dagger c_{i+nx} + t_{bn,y} c_i^\dagger c_{i+ny}] \\ & + h.c. + H_{QAH}[c_i^\dagger, c_i] \end{aligned} \quad (\text{E2})$$

which sets up the form of the Boosted QAH model. In principle, one need to include the infinite sum of

terms. The simplest thing to do is to include only the $n = 1$ NN term $i(t_{b1,x}c_i^\dagger c_{i+x} + t_{b1,y}c_i^\dagger c_{i+y} - h.c.)$ where $t_{b,x} = \hbar v_{b,x}/(2a)$ and $t_{b,y} = \hbar v_{b,y}/(2a)$ has the energy dimension.

For the interacting bosonic system studied in [23], this leading term is proportional to the $U(1)$ conserved current term, so can be absorbed by a unitary transformation into the hopping term in $H_{BH}[b_i^\dagger, b_i]$. So one need also consider also the subleading term $n = 2$ NNN current term in the series. Unfortunately, one can not determine the ratio of t_{b2}/t_{b1} just from the substitution. One need to repeat the derivation from the ionic model to the BH model to determine the whole series in Eq.E2. This was achieved in [23].

For the present non-interacting fermionic QAH, the $n = 1$ term is not proportional to any conserved current term, one can just take it as an injecting current as done in Sec.II which leads to various new phases and TPTs in the main text. However, the Galilean boost in a lattice in the presence of SOC (or Non-Abelian gauge field) should take the different form Eq.E3 where the $n = 1$ term is indeed the NN gauge invariant current. Then it still can be absorbed into the SOC term in H_{QAH} by the unitary transformation Eq.113. Then one must consider the $n = 2$ NNN current term. So under a GT boost with the velocity v relative to the lattice along the \hat{x} direction,

Eq.106 need to be replaced by:

$$H_{bx} = -v \left[\frac{t_{b1}}{t_0} \sum_i J_{ix} + i \sum_{n=2}^{\infty} (t_{bn}/n) c_i^\dagger c_{i+nx} \right] + h.c. \quad (\text{E3})$$

where J_{ix} is the NN gauge-invariant current and t_{b1}, t_{b2} are completely determined by the Wannier functions $\phi(|\vec{x}|)$ of the lattice system:

$$t_{bn} = \hbar \int d^2x \phi(|\vec{x}|) \frac{\partial}{\partial x} \phi(|\vec{x} + n\hat{x}|), \quad n = 1, 2 \quad (\text{E4})$$

where $t_{bn}v$ carry the dimension of the hopping (for notational simplicity, we still use the same symbols as in Eq.E2). So t_{b1}, t_{b2} are not dependent anymore with $t_{b1} \ll t_{b2}$ in the tight-binding limit.

One can adopt the derivation in [23] straightforwardly by identifying:

$$t = t_s = t_{b1} \sqrt{v^2 + v_c^2}, \quad v_c = \frac{t_0}{t_{b1}}$$

$$t_b = \frac{v_c^2 - v^2}{v_c^2 + v^2} v t_{b2} \quad (\text{E5})$$

where v is the velocity of the moving frame, v_c is the characteristic velocity where t_b changes sign. It was used in the main text Sec.IX-3. As shown in Sec.V, t_b cause the same Doppler shift to the 4 nodes as expected for a moving observer.

-
- [1] Jinwu Ye, Yong Baek Kim, A. J. Millis, B. I. Shraiman, P. Majumdar, and Z. Tešanović, Berry Phase Theory of the Anomalous Hall Effect: Application to Colossal Magnetoresistance Manganites, *Phys. Rev. Lett.* **83**, 3737, (1999).
- [2] T. Jungwirth, Qian Niu, and A. H. MacDonald, Anomalous Hall Effect in Ferromagnetic Semiconductors, *Phys. Rev. Lett.* **88**, 207208, (2002).
- [3] F. D. M. Haldane, *Berry Curvature on the Fermi Surface: Anomalous Hall Effect as a Topological Fermi-Liquid Property*, *Phys. Rev. Lett.* **93**, 206602 (2004).
- [4] Naoto Nagaosa, Jairo Sinova, Shigeki Onoda, A. H. MacDonald, and N. P. Ong, Anomalous Hall effect, *Rev. Mod. Phys.* **82**, 1539 (2010).
- [5] F. D. M. Haldane, *Model for a Quantum Hall Effect without Landau Levels: Condensed-Matter Realization of the "Parity Anomaly"*, *Phys. Rev. Lett.* **61**, 2015 (1988).
- [6] X. G. Wen, *Quantum Field Theory of Many-body Systems, From the Origin of Sound to an Origin of Light and Electrons* (Oxford University Press, Oxford, U.K., 2004).
- [7] For a review on different quantum field theory approaches to FQH, see: Ganpathy Murthy and R. Shankar, Hamiltonian theories of the fractional quantum Hall effect, *Rev. Mod. Phys.* **75**, 1101 (2003) - Published 3 October 2003
- [8] Rui Yu, Wei Zhang, Hai-Jun Zhang, Shou-Cheng Zhang, Xi Dai, Zhong Fang, *Quantized Anomalous Hall Effect in Magnetic Topological Insulators*, *Science* **329**, 61 (2010).
- [9] Cui-Zu Chang, Jinsong Zhang, Xiao Feng, Jie Shen, Zuocheng Zhang, Minghua Guo, Kang Li, Yunbo Ou, Pang Wei, Li-Li Wang, Zhong-Qing Ji, Yang Feng, Shuaihua Ji, Xi Chen, Jinfeng Jia, Xi Dai, Zhong Fang, Shou-Cheng Zhang, Ke He, Yayu Wang, Li Lu, Xu-Cun Ma, Qi-Kun Xue, *Experimental Observation of the Quantum Anomalous Hall Effect in a Magnetic Topological Insulator*, *Science* **340**, 167 (2013).
- [10] J. Checkelsky, R. Yoshimi, A. Tsukazaki, K. Takahashi, Y. Kozuka, J. Falson, M. Kawasaki, and Y. Tokura, *Trajectory of Anomalous Hall Effect toward the Quantized State in a Ferromagnetic Topological Insulator*, *Nature Physics* **10**, 731 (2014); X. Kou, S.-T. Guo, Y. Fan, L. Pan, M. Lang, Y. Jiang, Q. Shao, T. Nie, K. Murata, J. Tang, et al., *Scale-Invariant Quantum Anomalous Hall Effect in Magnetic Topological Insulators beyond the Two-Dimensional Limit*, *Phys. Rev. Lett.* **113**, 137201 (2014); A. Bestwick, E. Fox, X. Kou, L. Pan, K. L. Wang, and D. Goldhaber-Gordon, *Precise quantization of anomalous Hall effect near zero magnetic field*, *Phys. Rev. Lett.* **114**, 187201 (2015); X. Kou, L. Pan, J. Wang, Y. Fan, E. S. Choi, W.-L. Lee, T. Nie, K. Murata, Q. Shao, S.-C. Zhang, et al., *Metal-to-Insulator Switching in Quantum Anomalous Hall States*, *Nature Communications* **6**, 8474 (2015). Y. Feng, X. Feng, Y. Ou, J. Wang, C. Liu, L. Zhang, D. Zhao, G. Jiang, S.-C. Zhang, K. He, et al., *Observation of the zero Hall plateau in a quantum anomalous Hall insulator*, *Phys. Rev. Lett.* **115**, 126801

- (2015); C.-Z. Chang, W. Zhao, D. Y. Kim, H. Zhang, B. A. Assaf, D. Heiman, S.-C. Zhang, C. Liu, M. H. Chan, and J. S. Moodera, *High-precision realization of robust quantum anomalous Hall state in a hard ferromagnetic topological insulator*, Nature Materials **14**, 473 (2015).
- [11] M. Serlin, *et.al*, Science, 367, 900(2019); A. L. Sharpe, *et.al*, Science, 365,605(2019); P. Stepanov, *et.al*, Nature, 583, 375 (2020)
- [12] Gregor Jotzu, Michael Messer, Remi Desbuquois, Martin Lebrat, Thomas Uehlinger, Daniel Greif and Tilman Esslinger, *Experimental realization of the topological Haldane model with ultracold fermions*, Nature **515**,237 (2014).
- [13] Zhan Wu, Long Zhang, Wei Sun, Xiao-Tian Xu, Bao-Zong Wang, Si-Cong Ji, Youjin Deng, Shuai Chen, Xiong-Jun Liu, Jian-Wei Pan, Realization of two-Dimensional spin-orbit coupling for Bose-Einstein condensates, Science **354**, 83 (2016).
- [14] M. Z. Hasan and C. L. Kane, *Colloquium: Topological insulators*, Rev. Mod. Phys. **82**, 3045 (2010).
- [15] X. L. Qi and S. C. Zhang, *Topological insulators and superconductors*, Rev. Mod. Phys. **83**, 1057 (2011).
- [16] Ching-Kai Chiu, Jeffrey C. Y. Teo, Andreas P. Schnyder, and Shinsei Ryu, *Classification of topological quantum matter with symmetries*, Rev. Mod. Phys. **88**, 035005 (2016).
- [17] Xiao-Gang Wen, *Colloquium: Zoo of quantum-topological phases of matter*, Rev. Mod. Phys. **89**, 041004 (2017).
- [18] Daniel S. Rokhsar and Steven A. Kivelson, *Superconductivity and the Quantum Hard-Core Dimer Gas*, Phys. Rev. Lett. **61**, 2376 (1988).
- [19] R. Moessner and S. L. Sondhi, *Resonating Valence Bond Phase in the Triangular Lattice Quantum Dimer Model*, Phys. Rev. Lett. **86**, 1881 (2001).
- [20] Hong Yao and Steven A. Kivelson, *Exact Spin Liquid Ground States of the Quantum Dimer Model on the Square and Honeycomb Lattices*, Phys. Rev. Lett. **108**, 247206 (2012).
- [21] A. Yu. Kitaev, *Fault-tolerant quantum computation by anyons*, Ann. Phys. **303**, 2(2003).
- [22] A. Kitaev, *Anyons in an exactly solved model and beyond*, Ann. Phys. **321**, 2 (2006).
- [23] Fadi Sun and Jinwu Ye, *Quantum Phase transitions observed in a moving frame and emergent space-time near Quantum Phase transitions*, Preprint, arXiv:2207.10475 [cond-mat.str-el], 58 PRB pages.
- [24] S. Sachdev, *Quantum Phase transitions*, (2nd edition, Cambridge University Press, 2011).
- [25] Xiao-Liang Qi, Yong-Shi Wu, and Shou-Cheng Zhang, *Topological quantization of the spin Hall effect in two-dimensional paramagnetic semiconductors*, Phys. Rev. B **74**, 085308 (2006).
- [26] Note that Eq.(30) does not holds for the $\alpha_x\alpha_y = 0$ case, a more general form would be $\text{Ch}_- = \frac{1}{2} \text{sgn}(v_x v_y) [\text{sgn}(\Delta) - (1 - \frac{1}{2} \text{sgn}(\alpha_x \alpha_y)) (\text{sgn}(\alpha_x) + \text{sgn}(\alpha_y))]$. But this case does not happen here.
- [27] On the intermediate (intervening) phase, it is instructive to make some analogy to interacting boson systems, there are two possibilities on the transition between two phases breaking different symmetries the SF phase breaking the $U(1)$ symmetry, the solid breaking the translational symmetry. The first one is a direct first order transition. the second is through the intervening phase called supersolid which breaks both the $U(1)$ symmetry and the translational symmetry, so the putative direct first order transition splits into 2 second order ones.
- [28] Fadi Sun and Jinwu Ye, *Nearly order from quantum disorder phenomena: its application and detection in the bosonic quantum anomalous Hall system*, arXiv:1903.11134.
- [29] Fadi Sun, Xiao-Lu Yu, Jinwu Ye, Heng Fan, W. M. Liu, *Topological Quantum Phase Transition in Synthetic Non-Abelian Gauge Potential: Gauge Invariance and Experimental Detections*, Scientific Reports **3**, 2119 (2013).
- [30] Fadi Sun and Jinwu Ye, *Type I and Type II fermions, Topological depletions and sub-leading scalings across topological phase transitions*, Phys. Rev. B **96**, 035113 (2017).
- [31] Yu Yi-Xiang, Fadi, Sun and Jinwu Ye, *New class of topological phase transitions of Rashba spin-orbit coupled fermions on a lattice*, Phys. Rev. B **98**, 174506 (2018)
- [32] J. Ye, J. M. Zhang, W. M. Liu, K. Zhang, Y. Li, and W. Zhang *Light-scattering detection of quantum phases of ultracold atoms in optical lattices*, Phys. Rev. A **83**, 051604 (2011);
- [33] J. Ye, K. Y. Zhang, Y. Li, Y. Chen, and W. P. Zhang, *Optical Bragg, atom Bragg and cavity QED detections of quantum phases and excitation spectra of ultracold atoms in bipartite and frustrated optical lattices*, Ann. Phys. **328**, 103 (2013).
- [34] For a Z_2 topological insulator, there seems no relation between the Z_2 topological invariants and any experimentally measure quantities.
- [35] Note that in the 2d BZ, B1 phase in Fig.2, there is no overlap between any of the P- or H- Fermi pockets near $K_1 = (\pi, 0)$ and near $K_2 = (0, \pi)$. It looks like so in Fig.17 is only because one is expanding around the two different minima, but putting them on the same k_y axis.
- [36] Because the collisions between two FFs takes a saddle point (cone) geometry near a Van Hove singularity (VHS), the dispersion Eq.3 in [30] seems also suggest one may define the dynamic exponent $z = 2$. However, due to its saddle point nature, we feel it may not be suitable to introduce z in this class.
- [37] The following evaluations can be extended to $|\alpha\Delta/v^2| > 1/2$ with more complicated manipulations without changing the results qualitatively.
- [38] Here $T \ll |\Delta|$ should be interpreted as $T \ll |\Delta|$ only when $\Delta \neq 0$. If $\Delta = 0$, then setting $\Delta = 0$, one T remains the lowest energy scale compared to other non-vanishing energy scale.
- [39] Santu Baidya, Aabhaas Vineet Mallik, Subhro Bhat-tacharjee, and Tanusri Saha-Dasgupta, Interplay of Magnetism and Topological Superconductivity in Bilayer Kagome Metals, Phys. Rev. Lett. 125, 026401
- [40] Jianpeng Liu and Xi Dai, Theories for the correlated insulating states and quantum anomalous Hall effect phenomena in twisted bilayer graphene Phys. Rev. B 103, 035427 – Published 25 January 2021
- [41] Fadi Sun and Jinwu Ye, Periodic Table of the Ordinary and Supersymmetric Sachdev-Ye-Kitaev Models, Phys. Rev. Lett. 124, 244101 (2020).
- [42] Wladimir A. Benalcazar, B. Andrei Bernevig, and Taylor L. Hughes, *Electric multipole moments, topological multipole moment pumping, and chiral hinge states in crystalline insulators*, Phys. Rev. B 96, 245115 (2017).
- [43] N. Read, Compactly supported Wannier functions and

- algebraic K-theory, Phys. Rev. B 95, 115309 (2017) - Published 20 March 2017
- [44] Ruben Verresen, Ryan Thorngren, Nick G. Jones, and Frank Pollmann, Gapless Topological Phases and Symmetry-Enriched Quantum Criticality, Phys. Rev. X 11, 041059 – Published 23 December 2021
- [45] Arkya Chatterjee, Xiao-Gang Wen, Holographic theory for the emergence and the symmetry protection of gaplessness and for continuous phase transitions, arXiv:2205.06244.
- [46] Heidar Moradi, Seyed Farooq Moosavian, Apoorv Tiwari, Topological holography: Towards a unification of Landau and beyond-Landau physics arXiv:2207.10712 [cond-mat.str-el]
- [47] As an analogy, for interacting bosonic QAH, because the interacting bosons stay near the minima of a band, so the Chern number defined for a Bogliubov quasi-particle band at the quadratic level only has mathematical sense [28]. At first sight, it may not practically very useful, but it may still be experimentally measured by some non-equilibrium pumping detection.

Supplemental Materials

In the supplemental materials, we provide the enlarged picture for the edge modes in Fig.20, 21 and Fig.27, 28 respectively.

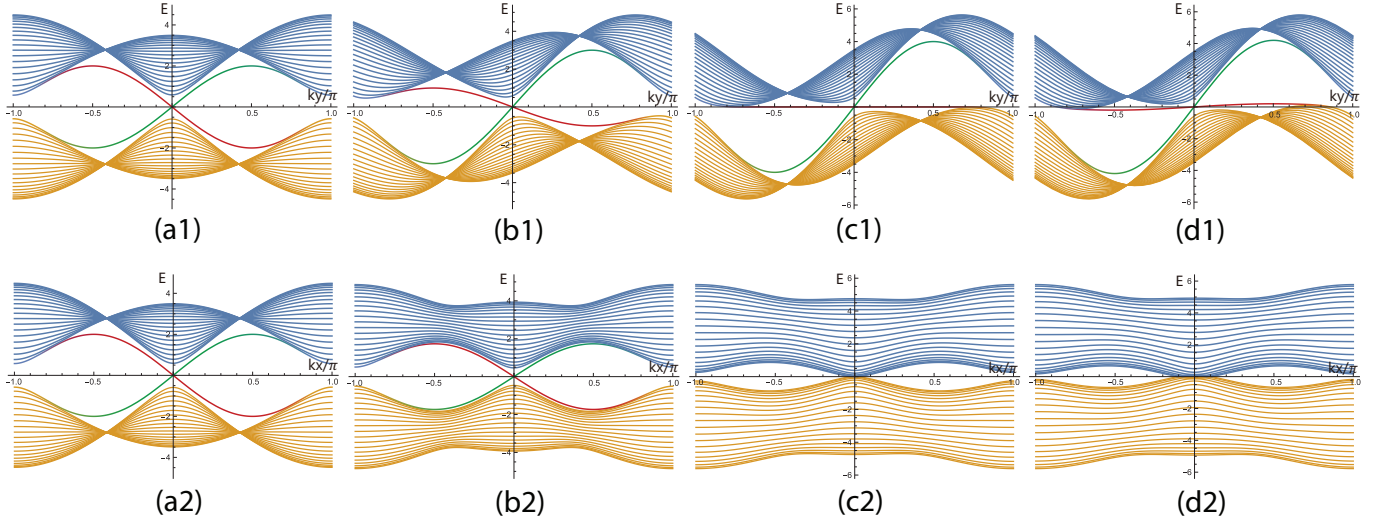


FIG. S1. The edge states of the lattice Hamiltonian in a strip geometry. We fixed $h = -0.5$. From left to right, the parameter t_b/t_s is 0, 0.5, 1.0, 1.1, respectively. (Top) Longitudinal injection: With the periodic boundary condition in the y -direction and the open boundary condition in the x -direction. The edge modes always exist, but undergoes the edge reconstruction at $t_s/t = 1$. The two edges move along the opposite directions when $t_s/t < 1$ in (a1) and (b1) in the CI, then one edge becomes flat at $t_s/t = 1$ in (c1), then two edges move along the *same* direction when $t_s/t > 1$ in (d1) in the odd CM, (Bottom) Transverse injection: Exchanging the role of x and y direction. The edge modes exist only when $t_s/t < 1$ in (a2) and (b2), but squeezed out at $t_s/t = 1$ in (c2) where the direct bulk gap closes, completely disappear when $t_s/t > 1$ in (d2) in the odd CM. Although the edge modes show quite different behaviours in the line 1 and the line 2, there seems a one to one Longitudinal/Transverse edge-edge correspondence between them. In both figures, one can shift $k \rightarrow k + \pi$ to reach $h = +0.5$ results. See also Fig.22 and Fig.23 for the continuum calculations.

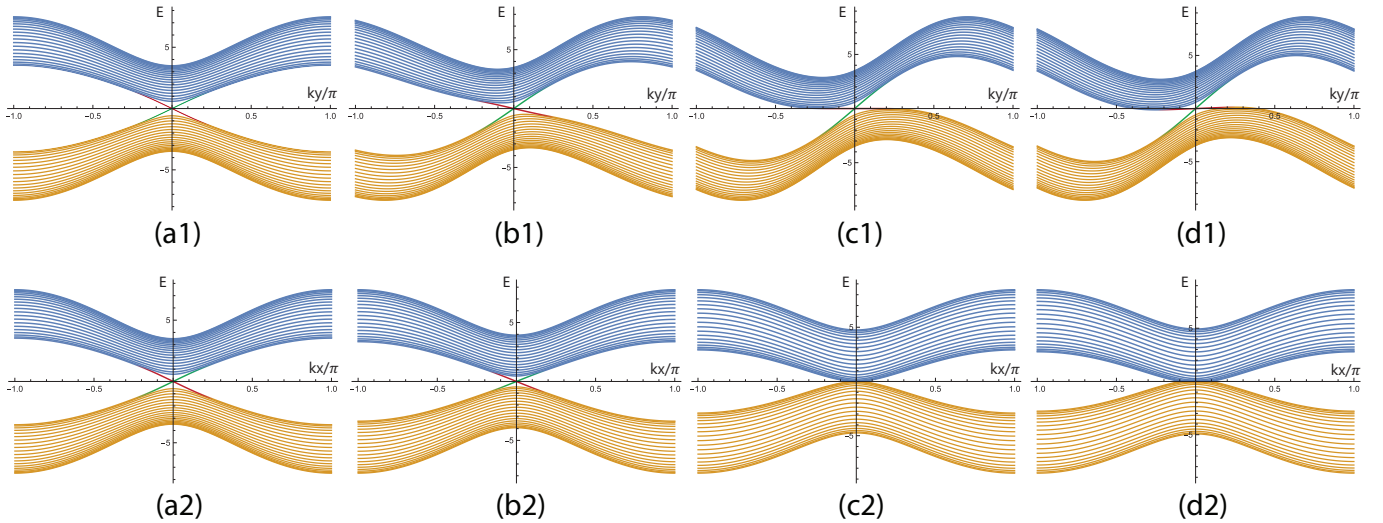


FIG. S2. The same situation as in Fig.20 except at a fixed $h = -3.5$. In both figures, one can shift $k \rightarrow k + \pi$ to reach $h = +3.5$ results. It shows qualitatively the same edge TPTs as those in Fig.20.

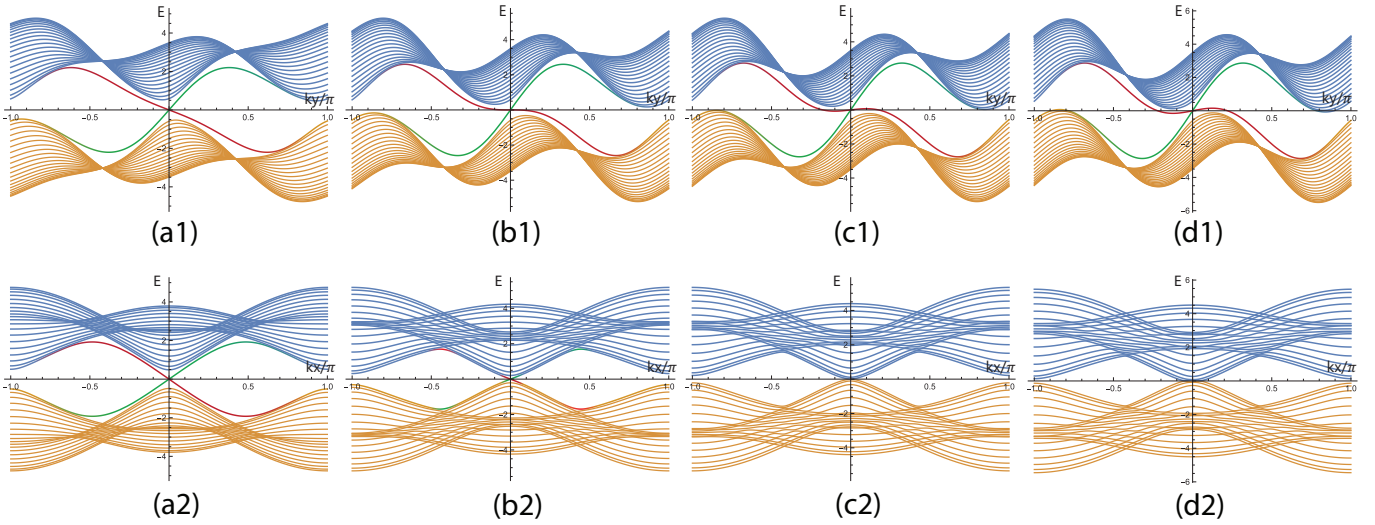


FIG. S3. The edge state of the lattice Hamiltonian Eq. (117). From (a) to (d), the parameter t_b/t_s is 0.5, 1.0, 1.17, 1.3, respectively. We fixed $h = -0.5$. (Top) Longitudinal boost: With periodic boundary condition in the y -direction and open boundary condition in the x -direction. The edge modes always exist in this case. The two edge modes move in the opposite direction near $k_y = 0$ in (a1) Chern Insulator where $t_b/t_s < 1$, then one edge mode's slope vanishes in (b1) where $t_b/t_s = 1$ with the edge dispersion $\omega \sim k_y^3$, namely the longitudinal edge dynamic exponent $z_L = 3$. then the two edge modes move along the same direction near $k_y = 0$ in (c1) odd Chern insulator where $t_b/t_s = 1.17 > 1$. At the same time, the system's (in-direct) gap vanishes which corresponds to the $z = 2$ bulk TPT from the $C = -1$ odd Chern insulator to A2 Odd Chern metal in Fig.24. It gets to the Odd Chern metal phase in (d1) where $t_b/t_s = 1.3 > 1.17$, the two edge modes still move along the same direction. (Bottom) Transverse boost: Exchanging the role of x - and y - direction. The edge mode exists upto (c2) where $t_b/t_s = 1.17 > 1$. So the odd CI between (b2) and (c2) still has the transverse edge mode. At (c2), the system's direct gap vanishes which corresponds to the TPT from the $C = -1$ odd Chern insulator to A2 Odd Chern metal in the bulk in Fig.24. It is in the Odd Chern metal phase in (d2) where $t_b/t_s = 1.3 > 1.17$, no edge mode. The T-edge disappears at the same time as the bulk TPT with its velocity still vanishing $\sqrt{v^2 - c^2}$ as in Fig.23. One can shift $k \rightarrow k + \pi$ to reach $h = +0.5$ results.

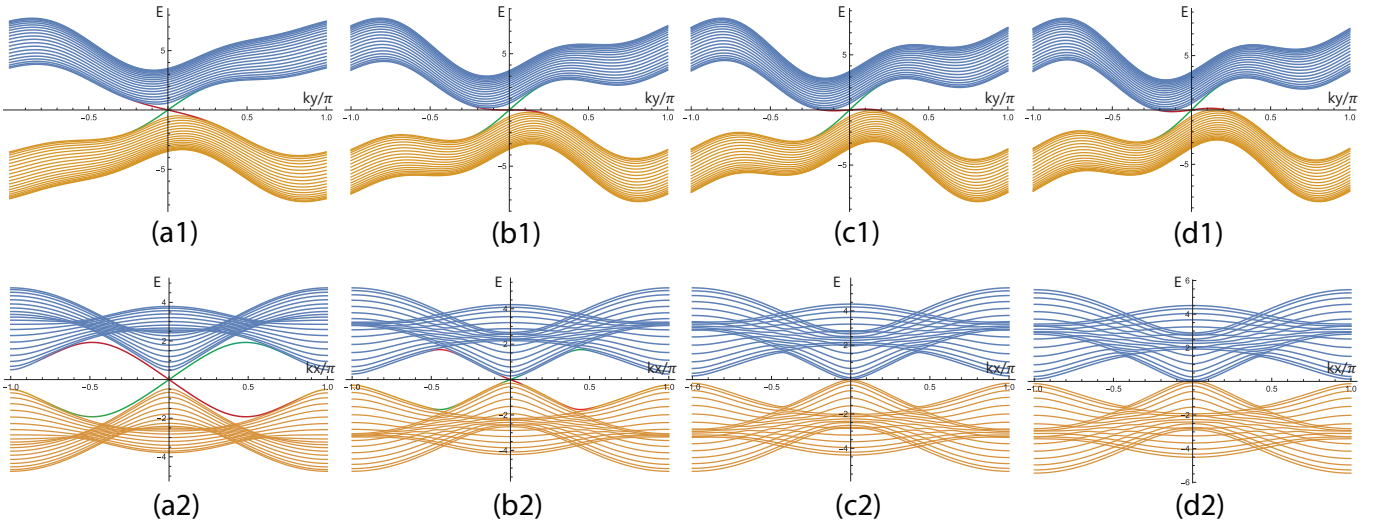


FIG. S4. The same situation as Fig.27 except $h = -3.5$ which is Mirror reflected image of $h = -0.5$. As alerted in Fig.24, despite the bulk phase boundary in Fig.24 has such a Mirror symmetry at $t = t_s$, it is not persevered in the presence of the strip boundaries. One can shift $k \rightarrow k + \pi$ to reach $h = +3.5$ results which is Mirror reflected image of $h = 0.5$. It shows qualitatively the same edge TPTs, odd CI and odd CM as those in Fig.27.